Synthesis of well defined, linear-dendritic, end-functionalised poly N-vinyl pyrrolidone additives via reversible addition-fragmentation transfer polymerisation for use in polymer electrolyte membrane fuel cells

BERGIUS, WILLIAM,NIGEL,ADAM

William N A Bergius

Synthesis of well defined, linear-dendritic, end-functionalised poly *N*-vinyl pyrrolidone additives via reversible addition-fragmentation transfer polymerisation for use in polymer electrolyte membrane fuel cells

Abstract

An ongoing challenge in polymer science is the preparation of materials with specific surface properties that differ from the bulk, whilst retaining the advantageous mechanical properties of the bulk polymer. We have explored the use of multi-end functionalised polymer additives, which undergo rapid spontaneous adsorption to a surface or interface, as an efficient method of modifying surface properties. These materials are of potential use in tailoring the hydrophobicity of the gas diffusion layer (GDL) in a polymer electrolyte membrane fuel cell (PEMFC), and hence optimising fuel cell efficiency.

In this research, reversible addition-fragmentation transfer (RAFT) polymerisation has been used to synthesise a range of well-defined, low molecular weight, end-functionalised poly *N*-vinyl pyrrolidone (PVP) polymer additives bearing aryl-ether end groups containing up to three, low surface energy, C_8F_{17} fluoroalkyl chains. Polymer end-functionality is introduced via the design of functionalised RAFT chain transfer agents (CTAs).

Three novel CTAs have been made in addition to their corresponding end-functionalised PVP additives, in a range of molecular weights. Thin films have been prepared comprised of polymer blends of unfunctionalised PVP and varying percentages of each end-functionalised PVP additive, and these films have been analysed by contact angle measurements, ion beam analysis and atomic force microscopy in order to investigate effects of additive concentration, additive molecular weight, matrix molecular weight, design of functional group and annealing. We have shown that modest amounts of additive (<2.5%) can render the surfaces of bulk PVP hydrophobic and lipophobic.

Synthesis of well defined, linear-dendritic, end-functionalised poly *N*-vinyl pyrrolidone additives via reversible addition-fragmentation transfer polymerisation for use in polymer electrolyte membrane fuel cells

William N A Bergius

University College
Department of Chemistry
Durham University

December 2011

Thesis submitted in fulfillment for the degree of Doctor of Philosophy.

Table of Contents

List of Figures

List of Tables

List of Abbreviations and Symbols

AFM	Atomic Force Microscopy
AIBN	Azobisisobutyronitrile
ATRP	Atom Transfer Radical Polymerisation
BoP	Balance of Plant
CAC	Critical Aggregation Concentration
CDB	Cumyl dithiobenzoate
CMC	Critical Micellisation Concentration
CRP	Controlled Radical Polymerisation
CTA	Chain Transfer Agent
C_{tr}	Chain Transfer Constant
DCM	Dichloromethane
DMFC	Direct Methanol Fuel Cell
DoE	Design of Experiment
DPCM	*S*-malonyl *N*,*N*-diphenyldithiocarbamate
DPFPB-Br	3,5-(di-3-(perfluorooctyl)propyloxy)benzyl bromide
DPFPB-DPCM	*S*-3,5-(di-3-(perfluorooctyl)propyloxy)benzyl *N,N*-diphenyldithiocarbamate
DPFPB-OH	3,5-(di-3-(perfluorooctyl)propyloxy)benzyl alcohol
DPFPB-PNVP	3,5-(di-3-(perfluorooctyl)propyloxy)benzyl poly-*N*-vinyl pyrrolidone
dPS	Deuteriopolystyrene
DMF	Dimethylformamide
DP	Degree of Polymerisation
ERD	Elastic Recoil Detection
FEP	Fluorinated Ethylene Propylene
G-1, G-2 . . .	Dendron Generation
G1-DPCM	*S*-3,5-dibenzyloxybenzyl *N,N*-diphenyldithiocarbamate
GDL	Gas Diffusion Layer
hPS	Unfunctionalised polystyrene (as opposed to dPS)
IBA	Ion Beam Analysis

LCS	Low Cost Substrate
M_n	Number Average Molecular Weight
MWD	Molecular Weight Distribution
NIPAM	*N*-isopropylacrylamide
NMP	Nitroxide Mediated Polymerisation
NMR	Nuclear Magnetic Resonance
NVP	*N*-vinyl pyrrolidone
PDI	Polydispersity Index
PEM	Proton Exchange Membrane
PEMFC	Proton Exchange Membrane Fuel Cell
PFP-Br	1-bromo-3-perfluorooctyl propane
PFP-OH	3-perfluorooctyl-1-propanol
PNVP	Poly-*N*-vinyl pyrrolidone
PS	Polystyrene
PTFE	Polytetrafluoroehtylene
RAFT	Reversible Addition-Fragmentation Transfer
RBS	Rutherford Backscattering
R_G	Root mean square end-to-end distance
RPA	Random Phase Approximation
SANS	Small-Angle Neutron Scattering
SEC	Size Exclusion Chromatography
SOFC	Solid Oxide Fuel Cell
TEM	Transmission Electron Microscopy
TEMPO	(2,2,6,6-tetramethylpiperidin-1-yl)oxyl
T_g	Glass Transition Temperature
TGA	Thermogravimetric Analysis
THB-COOMe	Methyl-3,4,5-trihydroxybenzoate
THF	Tetrahydrofuran
TPFPB-Br	3,4,5(tri-3-(perfluorooctyl)propyloxy)benzyl bromide
TPFPB-COOMe	3,4,5(tri-3-(perfluorooctyl)propyloxy)benzoate
TPFPB-DPCM	*S*-3,4,5(tri-3-(perfluorooctyl)propyloxy)benzyl *N,N*-diphenyldithiocarbamate
TPFPB-OH	3,4,5(tri-3-(perfluorooctyl)propyloxy)benzyl alcohol

TPFPB-PNVP	3,4,5(tri-3-(perfluorooctyl)propyloxy)benzyl poly-*N*-vinyl pyrrolidone
χ	Flory-Huggins interaction parameter

"#K# PVP"

For the purposes of this work, the novel end-functionalised polymer additives presented in this thesis are defined by the end-functionality (either di-functional or tri-functional according to the CTA used) and their number average molecular weight. Throughout the thesis they will be referred to in the format "#K# PVP", where the first digit(s) refers to the number average molecular weight (x1000 g mol^{-1}) of the additive as determined by SEC, and the second digit refers to the specific functionality ("2" for di-functional or "3" for tri-functional). For example, the additive referred to as "6K2 PVP" is a di-functional polyvinyl pyrrolidone polymer additive with a molecular weight of 6000 g mol^{-1}.

"K15", "K17", "K30" and "K90" PVP

These four commercially available polyvinyl pyrrolidone polymers, identical in all but molecular weight, have been used in this research as unfunctionalised polymer matrices with which to blend our novel end-functionalised additives. Their advertised molecular weights, as well as those determined by SEC, are shown in Table 3.1. Throughout this thesis they are referred to by these commercial names.

Statement of Copyright

Acknowledgements

This PhD was joint-funded by the Engineering and Physical Sciences Research Council (EPSRC) and Technical Fibre Products Ltd, Kendal.

I would like to acknowledge, with sincere thanks, the support, encouragement and patience of both my academic supervisor Dr. Lian Hutchings, and my industrial supervisor Dr. Michael Jeschke.

I am also very grateful to Dr. Solomon Kimani for his many hours of help in the lab during both my Masters and PhD research, as well other members of our research group including Dr. Jonathan Dodds and Dr. Norazilawati Muhamad Sarih. Additionally I would like to extend my gratitude to Dr. Richard Thompson for his help and expertise with ion beam analysis, and the use of his lab and equipment for most of my thin film analysis. Also thank you to Rosemary Fisher for her help with the preliminary industrial research.

I have greatly enjoyed my time in the Polymer IRC deskroom and would like to thank all of the occupants of CG156 who have come and gone during my time and who have no doubt helped me with my research at some point. I would especially like to thank Dr. David Johnson, Dr. Barry Dean, Dr. Ben Coombs and Iain Johnson for their invaluable support and friendship over the years.

I am indebted and truly grateful to my parents who have supported me throughout my time at university, and finally I would like to thank my wife who has helped me every step of the way.

Chapter 1
Introduction

Polymer Electrolyte Membrane Fuel Cells, Low Molecular Weight Polymer Additives, Reversible Addition-Fragmentation Transfer Polymerisation and *N*-vinyl pyrrolidone

1.1 Introduction to PEM Fuel Cells and Gas Diffusion Layers

1.1.1 Fuel Cells: basic principles, classifications and applications

Most simply defined, a battery is a device which converts stored chemical energy into electrical energy. While there are many different types suiting a variety of applications, in broad strokes a battery will typically consist of a series of voltaic cells, each cell comprising of an anode and a cathode connected by means of an electrolyte through which charged ions can migrate but electrons cannot. Each electrode is made of a compound comprising one half of a redox pair, typical examples in "primary" (disposable) batteries include zinc-carbon, zinc-chloride, zinc-manganese dioxide ("alkaline" battery) and lithium-manganese dioxide ("lithium" battery). Different materials have different reduction potentials which in turn affect the electromotive force of the resulting cell, and hence material choice is vital when considering the application of the battery as this will affect its operating characteristics. Obviously the type of battery used in a pacemaker has very different requirements to that which might be used in an electric vehicle in terms of electrical output amongst other concerns such as operational lifetime, size and toxicity.

As the electrolyte in a typical battery is ion conducting yet electrically insulating, the redox reaction is able to occur via the migration of ions through the electrolyte, however the terminals of the battery need to be connected in an electrically conducting circuit to allow the passage of electrons from the anode to the cathode and complete the redox reaction. In this way, the chemical reaction within the battery is used to drive electrons around an external circuit where they are used to perform electrical work. In the case of a primary battery when the fuel contained therein is exhausted, the battery is disposed of. However in a so-called "secondary" (rechargeable) battery, the redox reaction is easily reversed by the application of electrical current across the battery terminals thus recharging the battery for further use.[1,2]

In principle, a fuel cell operates in much the same way as an everyday battery. Whereas a battery contains a finite source of fuel which when exhausted renders the battery useless (except in the case of a secondary battery where it is possible for it to be recharged), the main characteristic that differentiates a fuel cell from a battery is that its fuel is fed into the cell continuously from an external source (to the anode, and an oxidant such as air to the cathode). Therefore a fuel cell will in principle continue to generate electricity and heat for as long as its fuel supply is maintained. In reality however, fuel cells do have a maximum working lifetime which varies between the differing types that are under development or in use today.[3,4]

There are several significant advantages that fuel cells in general possess over batteries, predominantly associated with inherent problems with batteries themselves. With many types of battery there is a small risk of explosion which can be caused by malfunction, attempting to recharge a primary battery or short circuiting a battery. By the nature of their design they are a sealed vessel and due to the hazardous nature of their chemical contents, this can be particularly dangerous. In the case of larger lead-acid batteries, overcharging can lead to the evolution of hydrogen gas through the electrolysis of water increasing the risk of explosion. Additionally if a battery is exposed to extremes of heat or fire, again due to their sealed nature, a serious explosion can occur.

Fuel cells on the other hand only contain a small amount of fuel when in use whereas the bulk is stored in a separate vessel or tank. While this in itself may be cause for concern, for example in the case of hydrogen in a PEMFC (Proton Exchange Membrane or Polymer Electrolyte Membrane Fuel Cell), it is in fact relatively safe. As a primary use for PEMFCs is in the automotive industry where fire safety is a serious concern, it is worth quickly comparing the use of hydrogen fuel to that of current day petroleum in this regard (Figure 1.01). Hydrogen gas is approximately fifteen times less dense than air, and if released disperses remarkably quickly making it more difficult to ignite than one might initially imagine. If ignited it burns extremely quickly and cleanly and will do so well above, for example, the passenger compartment of a vehicle. As well as this clear advantage

over liquid petroleum which pools below a vehicle and will effectively incinerate it, hydrogen burns at a far quicker rate than petroleum thus making hydrogen less of a fire threat both before and after ignition. Hydrogen burns cleanly, producing nothing other than water vapour as a by-product, again in contrast to petroleum which produces amongst many other toxic emissions, NO_x, CO, CO_2 and particulate matter which are an extreme hazard in an accidental fire as they can quickly overcome anyone unfortunate enough to inhale these gases. Hydrogen itself is also non-toxic, again in contrast to petroleum which is extremely toxic in its liquid form. The fuel cell itself is not sealed, and if exposed to fire or impact will simply fail rather than explode as in the case of a battery.[5]

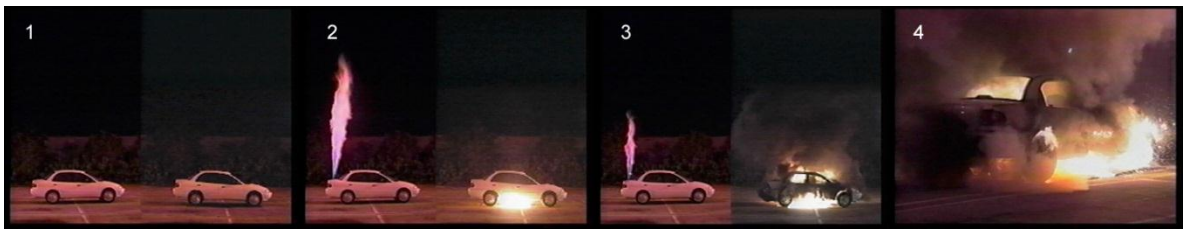

Figure 1.01. Series of frames from a 3 minute video of a fire test between a hydrogen powered vehicle (left) and a traditional petroleum powered vehicle (right). In both cases the fuel line was severed and then the fuel ignited. Frame 2 shows both vehicles 3 seconds after ignition, frame 3 is 60 seconds after ignition and frame 4 shows the petroleum powered vehicle 140 seconds after ignition by which time the hydrogen powered vehicle was no longer alight.[5]

As well as the increased risk of explosion associated with batteries over fuel cells, another point worth considering is the possibility of leakage. Hydrogen is non-toxic and disperses extremely rapidly, thus in the case of a leakage or spill is not particularly dangerous unless in large amounts or near a source of ignition where it becomes a fire hazard, though as we have already discussed, a generally less serious one than petroleum. A battery on the other hand typically contains materials that are corrosive, toxic or both. In the case of leakage through accident or misuse this can pose a more serious problem. In many zinc-based batteries,

the battery casing is in fact made of zinc, forming both the battery casing and an electrode. In this case if the battery is run all the way down or is recharged after being run down too far, the contents of the battery are liable to leak from their zinc casing. This can easily occur over long periods of inactivity as the battery slowly self-discharges which is why manufacturers advise removal of batteries from equipment when not being used for extended periods of time. In carbon based batteries or “dry” cells (often referred to as “heavy duty”), self-discharge leads to the slow evolution of hydrogen gas within the battery causing a pressure build up and eventual failure of the battery seals, again leading to leakage of the battery contents. The same process can also lead to swelling of the battery which depending upon its situation within a piece of equipment can lead to the cell becoming stuck and rendering the equipment unusable. When leakage does occur from any battery, aside from the obvious health and safety concerns associated with these generally toxic and corrosive chemicals contained therein, there is often also the risk of permanent damage to the equipment in which they are installed.

The widespread use of batteries also gives rise to several environmental concerns, most importantly the toxic metal pollution that can arise from their improper disposal. In contrast with, for example, a Direct Methanol Fuel Cell (DMFC), suited for use with small appliances such as laptop computers and mobile phones, the fuel cell is a permanent fixture in the equipment, and all that is disposed of is empty plastic cartridges once their methanol fuel has been exhausted. One assumes that as the technology develops, the ability to refill these cartridges may well become an option.

As with batteries there are several different types of fuel cell which vary according to the type of fuel or electrolyte being used, and therefore have varying specific operating conditions with a range of power outputs suitable for a multitude of applications. The most common types are the PEMFC, the Direct Methanol Fuel Cell (DMFC), the Alkaline Fuel Cell (AFC), the Phosphoric Acid Fuel Cell (PAFC), the Molten Carbonate Fuel Cell (MCFC) and the Solid Oxide Fuel Cell (SOFC). The use of DMFCs for example is generally targeted at portable applications such as laptop computers and mobile telephones as, while the fuel efficiency of these

fuel cells is significantly lower than most other types, methanol has a high energy density enabling a DMFC to produce a low power output for extended periods of time with the use of small volumes of fuel. Methanol is reasonably stable under all of the conditions in which these types of device could reasonably be expected to operate, and typical operating temperatures of a DMFC are within the range of 50-120°C. In contrast the use of SOFCs are generally suited to much larger scale applications ranging from auxiliary power units in large vehicles to power supplies for entire buildings. Typical operating temperatures are 500-1000°C, requiring an initial start-up sequence to heat the fuel cell, but these higher operating temperatures negate the use of expensive platinum catalysts required in many other low temperature fuel cells. SOFCs are high output fuel cells which can achieve fuel efficiencies of up to 60%, have a comparatively long operational lifetime as well as being relatively low cost and produce few emissions. Research and development is on-going with all of these fuel cell types, though only the PEMFC will be discussed in detail here as it is this type of fuel cell that is the focus of this project.[3,4]

1.1.2 Proton Exchange Membrane Fuel Cells (PEMFCs)

1.1.2.1 Introduction to Proton Exchange Membrane Fuel Cells

There are several main advantages in the use of fuel cells, the most obvious of which are their efficiency as well as their cleanliness, in part due to the lack of any form of combustion within a fuel cell or in the case of hydrogen fuel cells, the lack of toxic or corrosive fuels. In a PEMFC the only by-products of fuel cell operation are heat and water. The heat can be utilised with the use of a cogeneration system, or used for a secondary purpose such as central heating in a PEMFC powered vehicle. Some of the water can also be recycled within the fuel cell for use in the water management system which ensures that the polymer membranes

within the cell are sufficiently hydrated without being flooded. Far higher fuel efficiencies can be achieved than in standard conventional power generation methods due to the complete absence of mechanical work involved in the operation of a fuel cell (between 30-65% depending on fuel cell type and operating conditions compared to an approximate maximum of 20% for a standard internal combustion engine). Hydrogen fuel for use in PEMFCs can be generated by the electrolysis of water which while requiring electricity to produce, this electricity can be obtained from any source including all renewable forms of power generation. Hydrogen fuel can also be produced by a variety of other methods including steam reforming from fossil fuels, partial oxidation and plasma reforming. These other forms of hydrogen generation are of particular interest, as in theory they can be performed on a small scale in a PEMFC powered vehicle with the use of an on-board reactor. This would potentially allow a hydrogen powered vehicle to run on fossil fuels, which while negating some of the environmental benefits of PEMFC use in personal transport, would initially aid the viability of such a vehicle during the period of time it would take to set up a national hydrogen fuel infrastructure.

PEMFCs are comprised of several basic components including the unit cell (Figure 1.02), unit cell stack (Figure 1.03), and the Balance of Plant (BoP). The unit cell is the fundamental building block of a fuel cell, and is the region where the actual electrochemical reaction occurs, consisting of a cathode and an anode separated by an electrolyte (in the case of a PEMFC, a proton conducting, electrically insulating polymer membrane). The unit cell itself is small and has a low power output (typically less than a volt), but multiple unit cells are combined in electrically connected stacks that can be tailored to an overall desired output.

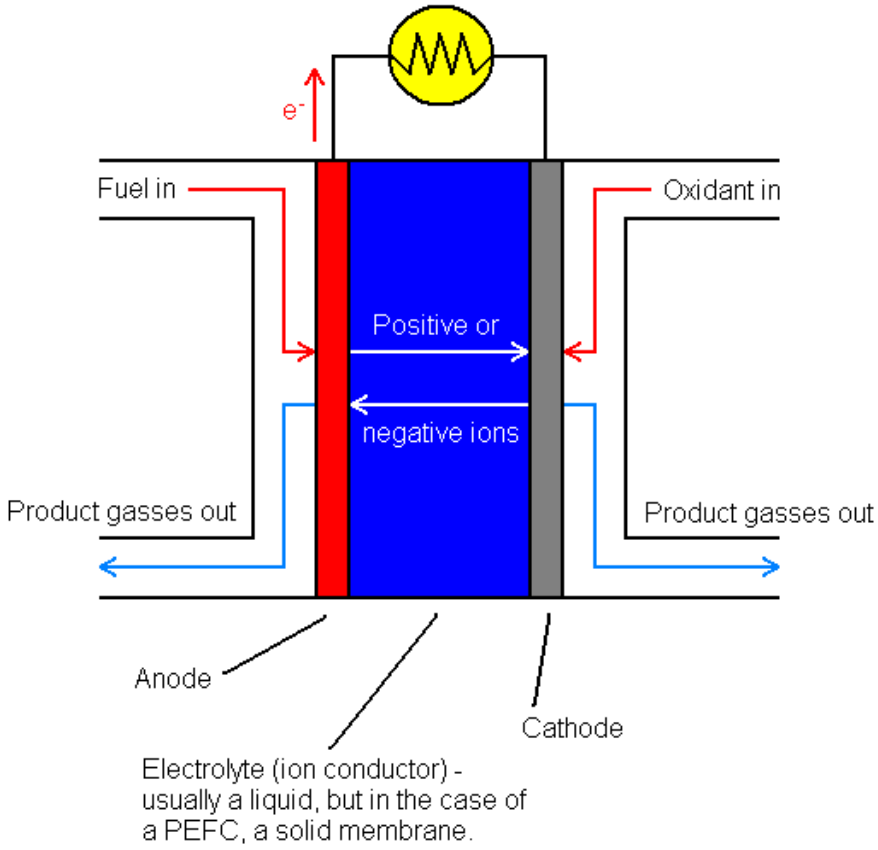

Figure 1.02. Schematic diagram of a typical unit cell in a fuel cell.

The unit cell stack is the part of the fuel cell where electricity is actually generated, and the balance of plant (BoP) is the part that carries out all of the other functions that are necessary for fuel cell operation. These functions vary depending on the type of fuel cell in question, but typical examples include fuel preparation where fuels other than pure hydrogen are being used, maintaining a consistent fuel supply, maintaining constant air supply to the cathode (oxidant), thermal management to ensure unit cell stack remains within its optimum operational temperature range, water management as will be discussed later, and electrical conditioning to provide a constant stable electrical output.

A PEMFC utilises the electrochemical reaction between hydrogen and oxygen to

generate electricity, requires pure hydrogen fuel and typically uses ambient air as a source of oxygen. Hydrogen is the most abundant gas in the universe, is colourless, odourless and tasteless, and though the lightest element, has the highest energy content per unit weight of all fuels. It is also producible from a variety of sources, including fossil fuels such as natural gas, methane and coal, by means of steam reformation, as well as several renewable sources including the wind, solar, geothermal and hydroelectric powered electrolysis of water.

As already mentioned, the only by-products of PEMFC operation are heat and water, both of which are potentially useful within the fuel cell or to the system it is supplying with power. Because the electrolyte in a PEMFC is a solid membrane as opposed to a liquid, the manufacturing process is less complex than for some other fuel cell types, which can involve the handling of liquid electrolytes, often corrosive acids or bases. The unit cell stack in a PEMFC typically operates at a temperature of 60-80˚C which is far lower than other fuel cell types (e.g. SOFC cell stack operational temperature is 500-1000˚C) which often require lengthy initial start-up times. As already discussed, fire tests on petroleum and hydrogen powered cars have shown that if the fuel tank was to catch fire, hydrogen is actually no more dangerous a fuel than petroleum. All of these factors combined make PEMFC technology a viable fuel cell technology for use in automotive transport.

The unit cell in a PEMFC consists of the anode where hydrogen is split into protons and electrons by a platinum catalyst, the cathode where oxygen reacts with the protons and the electrons to form water, and the polymer membrane which forms a solid barrier between the two thus separating the fuel (hydrogen) and oxidant (air). Carbon electrodes are typically used, both with a platinum catalyst which is poisoned by carbon monoxide, thus requiring the use of extremely pure hydrogen (directly or via filters / fuel converter in the BoP). The polymer membrane is usually a fluorinated sulfonic acid polymer (Nafion) or similar, the properties of which are crucial to the overall working and efficiency of the fuel cell. It must be a good conductor of protons such that they may cross the membrane easily and recombine with oxygen and their electrons to form water. It must also be an electrical insulator in order to insulate the anode from the cathode, so that the

electrons liberated from the hydrogen fuel by the platinum catalyst are forced to travel around an external circuit that connects the two electrodes. In addition to this, the polymer membrane must also act as a physical barrier between the fuel and the oxidant in order to prevent them from reacting directly with each other and chemically short circuiting the cell.

On either side of the unit cell (anode | polymer membrane | cathode) is a “porous backing layer” or “Gas Diffusion Layer” (GDL). It is these layers that form the electrical interconnects between unit cells to form the unit cell stack (Figure 1.03), but they also perform several other important tasks. As the name suggests they act as a gas diffuser by means of a network of small grooves termed “channels” that give an even and consistent spread of gas (fuel or oxidant i.e. hydrogen or air depending on the electrode in question) over the surface of the electrode. They also offer mechanical support to the unit cell stack, and allow an exit pathway for water to be removed from the electrodes.

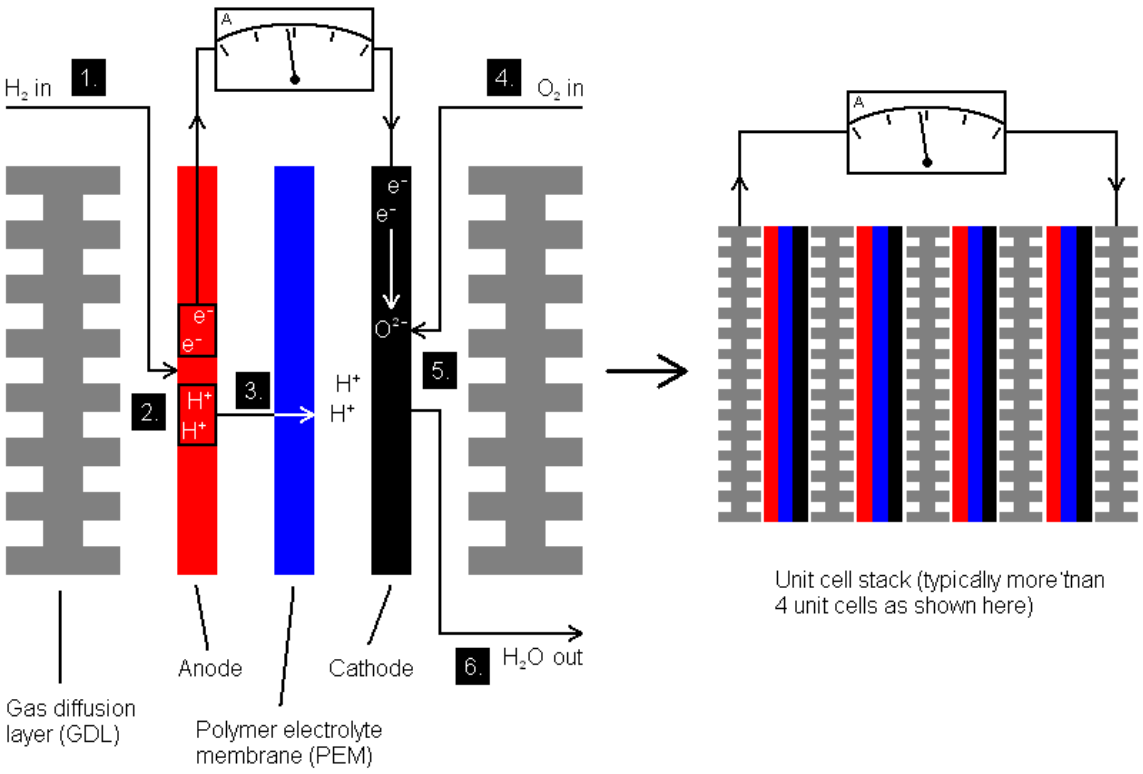

Figure 1.03. Diagram of a unit cell (left) and cell stack (right) in a PEMFC. 1. Pure hydrogen is fed to the anode directly (or through filters / fuel converter etc) via the channels in the GDL ensuring an even distribution over the anode. 2. At the anode the hydrogen is split into its constituent protons and electrons by the platinum catalyst. 3. The polymer electrolyte membrane conducts the protons through to the cathode side of the unit cell but blocks the passage of electrons which are forced to travel around an external circuit thus electrical current is generated. 4. On the other side of the unit cell, air (containing oxygen) is fed to the anode, again via channels in the GDL. 5. The oxygen molecules then combine with the electrons and protons to form water as a by-product. 6. The water is channelled away from the electrode to avoid flooding of the unit cell.

Water management is a key problem in the design and operation of PEMFCs, as the polymer membrane must be kept hydrated without being allowed to flood. As previously stated, water is the only chemical by-product of the electrochemical reaction taking place in the unit cell, and thus when the fuel cell is running water is being produced within the unit cell stack continuously. Therefore water must be removed from the unit cell stack at the same rate as it is produced within the stack

to ensure the correct level of hydration.

The requirements for hydration of the polymer membrane are twofold. First, the polymer membrane must be hydrated to a certain extent as its proton conducting ability relies heavily upon bound and free water associated with ionic groups within the polymer structure. If it was allowed to dry, the membrane would no longer conduct protons from the anode to the cathode, and the unit cell would cease to generate electricity. Secondly, if the membrane is allowed to dry out completely it will eventually crack, allowing the hydrogen fuel to react directly with the oxygen thus creating a gas short circuit. This short circuit would not only cause the unit cell to cease generating electricity, but the direct reaction of fuel and oxidant would generate large amounts of heat which would cause irreparable damage to the fuel cell.

However, the amount of water must be maintained at a constant level, otherwise if it is not efficiently removed the anodes and cathodes within the unit cell stack will become physically flooded, and reactant gases will not be able to reach them leading to a serious decrease in efficiency. So it can be seen that water management within the cell stack is crucial not only to the efficient running of the cell, but also to avoid cracking of the polymer membrane and subsequent irreversible damage to the fuel cell.[3,4]

1.1.2.2 The Gas Diffusion Layer (GDL)

As previously discussed, the Gas Diffusion Layer performs several vital roles within the unit cell stack, thus requiring several important properties. The GDL has a series of reactant channels etched into it, which are designed to allow an even distribution of reactant gas over the anode and cathode. The areas between these channels are known as “lands” and are in contact with approximately 50% of the surface area of each electrode (the other 50% comprising of contact with channels). These lands provide the electrical connectivity between adjacent unit

cells within the cell stack. As well as this basic function, the GDL must possess several other important properties. It must have good reactant gas permeability, allowing reactant gas access to the catalyst and electrodes, including in-plane permeability, again to allow an even distribution of reactant gas over each electrode. The GDL must also possess good water permeability, allowing the water produced as a by-product of fuel cell operation to be removed in order to avoid flooding. They must possess good through-plane and in-plane electrical conductivity between electrodes they separate and also the bipolar plates at either end of the cell stack. In addition to this they must provide good thermal conductivity to allow for the efficient removal of heat from the unit cell stack to the bipolar plates where coolant channels are located. Finally the GDL must have good mechanical strength, both to support the unit cell stack in case of reactant gas pressure differences occurring within the unit cell, and equally importantly to maintain the shape of the reactant gas channels. The interfacial conductivities between GDL and electrode, or GDL and bipolar plate, are strong functions of compression, and so the channels in the GDL must be able to resist collapse under this compression, which would prevent reactant gasses from reaching the electrodes resulting in a substantial loss of efficiency.

One of the main areas of research in the field of PEMFCs is in the design, optimisation and manufacture of the GDL, and it is this component that our research is intended for. A typical GDL in a PEMFC is made from a base sheet of carbon fibre, used for its high porosity and good electrical conductivity. This carbon fibre sheet is then typically coated by dipping in a polymer solution containing polytetrafluoroehtylene (PTFE), fluorinated ethylene propylene (FEP) or some other hydrophobic polymer to further increase hydrophobicity. Our research is aimed at the manufacture of low molecular weight, low surface energy, end-functionalised polymer additives which can be used in exceptionally small amounts (~0.1-5% by mass relative to the unfunctionalised base or matrix polymer) to tailor the surface hydrophobicity of the resulting polymer coated carbon fibre sheet. It was envisaged that this additive could either be used in place of existing fluoropolymers which are expensive and challenging to disperse easily in the

matrix, or to allow the use of much reduced quantities of fluoropolymer. An additional potential benefit of the designed additives is that they may act as macromolecular surfactants to aid the dispersion of the fluoropolymers. The end-functionalised additive is added to the polymer solution used for dipping and, as will be discussed in more detail in the following section, due to its low surface energy, undergoes spontaneous surface adsorption giving rise to a more hydrophobic surface after the dipping and drying processes are complete. By varying the quantity of the additive or the type of end-group, the resulting hydrophobicity of the GDL can then be tailored to a desired specification. The ability to do this is of specific interest as being able to tailor the hydrophobicity of the GDL, which is adjacent to all sites where flooding can occur within a unit cell stack (catalyst, anode and cathode), could aid greatly in the process of water management and help to prevent flooding at these sites, thus increasing the efficiency and reliability of the fuel cell.[3,6]

1.2 Low molecular weight polymers as surface modifying additives

The behaviour of end-functionalised polymers incorporating fluoroalkyl chains at surfaces and interfaces has been studied by several research groups in recent years.[7-20] The aim of our research, as previously stated, is to synthesise a low molecular weight, end-functionalised polymer additive in order to modify the surface properties (specifically hydrophobicity) of its corresponding bulk polymer. This is achieved by virtue of a low surface energy, fluorinated end-group which, when blended with the un-functionalised bulk polymer (either in solution or significantly above its T_g), gives rise to rapid spontaneous surface adsorption of the functionalised additive, resulting in a polymer with a low energy, fluorine-rich surface. This highly efficient method of surface functionalisation of a bulk polymer by spontaneous surface segregation of a low molecular weight polymer additive bearing 2-4 fluoroalkyl chains on a pendant end-group has been demonstrated previously.[21-26] Work has also been done in this area utilising singly end-functionalised low molecular weight polymers, however it has been shown that the use of a mono-functional end-group is less beneficial,[27] and as such our work is concerned with end-groups bearing two or three fluoroalkyl chains.

This general approach has the benefit of requiring only a very small amount of additive, relative to the bulk (~0.1-5% by mass in the case of our work), in order to achieve the desired change in surface property, but also does not compromise the desirable properties of the bulk polymer - mechanical strength, conductivity etc. Additionally, this approach does not require any special treatment of the surface, or indeed any additional process step, as the surface is modified simply by adding a small amount of additive into the polymer solution used in the dipping process. As well as this clear benefit, this method also has several advantages over other methods of surface modification such as plasma treatment,[28-31] wet chemical modification[32-34] and the application of polymeric surface coatings.[35,36] Beyond the synthesis of the low molecular weight additive, there is no additional waste hazardous or otherwise, it is relatively safe and also comparatively cheap if the

right materials are used in low concentrations. The low molecular weight polymer additive can also easily be incorporated into the polymer processing step in the manufacture of whatever is being made (such as a Gas Diffusion Layer in a PEMFC), safely, on any scale and to within precise specifications (simply by accurately adding the appropriate amount) giving rise to a surface with very specific properties.

The ability of such an additive to modify the surface of its corresponding bulk polymer is due to the low surface energy of its pendant end-group. When added to the bulk polymer in solution, the low surface energy of the end-group gives rise to rapid, spontaneous surface adsorption of the additive, resulting in a polymer with a fluorinated surface. The extent to which this process occurs depends upon an equilibrium between free and aggregate additive molecules within the polymer bulk, which can be considered as analogous to the equilibrium existing in the case of surfactants in solution.

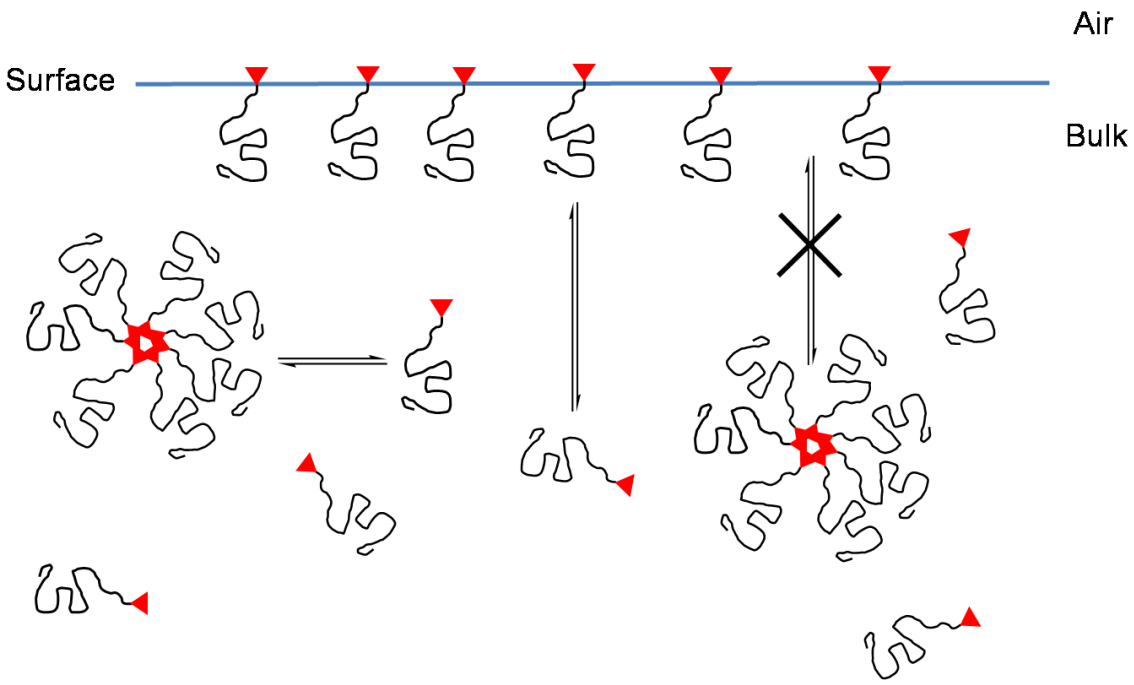

Figure 1.04. Schematic[37] depicting the behaviour of a low molecular weight polymer additive, with a pendant low surface energy end-group (red triangle), in the polymer bulk when in solution or significantly above the polymer T_g. An equilibrium exists between free additive chains and aggregate structures but it is only the free chains that are able to surface segregate.

The end-functionalised polymer additive consists of a low molecular weight polymer chain (the same as, or compatible with, the bulk polymer) and a heavily fluorinated end-group comprising a number of C_8F_{17} fluoroalkyl chains. These fluoroalkyl chains interact unfavourably with the bulk polymer and have a low surface energy, providing the thermodynamic drive for surface segregation when the bulk polymer is in solution or above its glass transition temperature. As in the case of surfactants in solution where an increase in concentration of surfactants leads to the eventual formation of micelles at the CMC (Critical Micellisation Concentration), an increase in the concentration in our end-functionalised polymer additive gives rise to the formation of aggregates at the CAC (Critical Aggregation Concentration). Once this critical concentration has been reached, the addition of more additive results only in the formation of additional aggregate structures within

the polymer bulk, and does not increase the surface concentration of fluorine any further. While this equilibrium between molecularly dissolved free additive chains and aggregate structures is dynamic, the aggregate structures will diffuse through the bulk at a much slower rate than the free chains. Additionally the very nature of the aggregate structures will have an encapsulating effect on the low surface energy end-groups, reducing their unfavourable interactions with the bulk polymer. These factors combined effectively mean that only the free chains will be capable of surface segregation.

As with the analogous situation of surfactants in solution, there is also an equilibrium existing between molecularly dissolved free additive chains within the bulk and those at the surface. The factors affecting this equilibrium are threefold, the first of which is the structure of the end-group, dictating the amount of fluorine present, or more specifically in the case of this work, the number of C_8F_{17} chains. Secondly, the molecular weight of the additive chain as it will dictate its rate of diffusion through the bulk polymer. Finally the packing density of additive chains at the surface which will directly affect the surface energy, and hence the thermodynamic gain from surface segregation of additional additive chains.[38] In this work the requirement to understand the relationship between additive molecular weight and resulting surface properties necessitated the use of a controlled polymerisation mechanism in order to produce well defined polymer additives.

1.3 Controlled Radical Polymerisations

1.3.1 Introduction to Controlled Radical Polymerisations

Traditional free radical polymerisation techniques give little or no control over the molecular weight distribution of the resulting polymer. This is due to the reactivity of the propagating free radical chain end and its ability to readily undergo several different side reactions including chain transfer to monomer, polymer or solvent, and termination by disproportionation or combination. Before the advent of controlled radical polymerisation (CRP) techniques, living anionic and cationic methods, in addition to transition metal-catalysed methods, were the only way of polymerising a material with good control over its molecular weight, a narrow molecular weight distribution (MWD) and controlled molecular architecture. Simply put, a "living" polymerisation is a chain growth polymerisation which proceeds in the absence of the kinetic steps of termination or chain transfer.[39,40] However these approaches are only useful for polymerising a narrow range of monomer types due to their intolerance of many functional groups. The extremely reactive propagating carbanion species react readily with many of the functionalities found in common vinyl monomers (e.g. the amide group present in *N*-vinyl pyrrolidone as intended to be used in this project). These techniques are also experimentally far from trivial due to the rigorous requirements for purity, necessitating the use of extremely pure starting materials and the complete absence of any oxygen or protic impurities such as water, thus requiring high vacuum techniques to be employed. It is for these reasons that these methods are unsuitable for the polymerisation of *N*-vinyl pyrrolidone and hence the work presented here.

Generally speaking, any free radical polymerisation will proceed by means of a radical species being created in an initiation step, which in turn reacts with a monomer (often via homolytic bond cleavage of a π-bond) thus forming a covalent bond between the two and forming a new radical (propagating) species on the monomer. It will then react with another monomer and the polymer will continue to

grow in this fashion. This process is sensitive to the presence of molecular oxygen as it is a di-radical species and will terminate active free radical chain ends, but is otherwise far more tolerant to impurities and the presence of many functional groups than are living ionic techniques. It is for this reason that so much research has gone into trying to incorporate the living features of controlled ionic polymerisations into free radical polymerisations, and Nitroxide Mediated Polymerisation (NMP) and Reversible Addition-Fragmentation Transfer Polymerisation (RAFT) are two important synthetic techniques that have been developed as a consequence of this research.

The development of controlled radical polymerisation (CRP) has spawned a range of "pseudo living" techniques that are useful for the production of well defined, narrowly polydisperse materials. Though there are several variations of this general theme including NMP[41,42], RAFT[43-46] and ATRP[47,48] (Atom Transfer Radical Polymerisation), they are all based on a singular mechanistic concept whereby the active free radical chain ends integral to the polymerisation process are in a state of equilibrium between an activated and a deactivated state. This is accomplished in different ways depending upon the technique being used, but the fundamental concept behind the "pseudo livingness" of these CRPs is that the instantaneous concentration of active free radical chain ends within the reaction medium is kept to a minimum, thus minimizing the possibility of termination by combination.

1.3.2 Nitroxide Mediated Polymerisation (NMP)

In NMP, a rapid dynamic equilibrium is established between the propagating free radical species and an end-capped dormant species, where the propagating radical has reversibly coupled to a relatively stable nitroxyl radical. Nitroxides are suitable for this not only because they can form thermally transient adducts, but also because they are free radical inhibitors and will not initiate polymerisation (which has been a problem in past research with some other mediating species).

Another advantage of nitroxides is that they can promote the dissociation of peroxide initiators, which means that in conjunction with such an initiator they can help to enable the simultaneous initiation of all of the polymer chains which in itself is a prerequisite for a living system.[41,42]

The first example of NMP was a bimolecular process involving benzoyl peroxide as an initiator and a stable nitroxyl radical, TEMPO, as a polymerisation mediator in an attempt to polymerize styrene. This process yielded polystyrene with a polydispersity index (PDI) of 1.2-1.3 when no previous free radical polymerisation had ever achieved a PDI of less than 1.5. This had to be carried out at 130°C as it is only at elevated temperatures that TEMPO can act as a polymerisation mediator as opposed to a free radical inhibitor.[41]

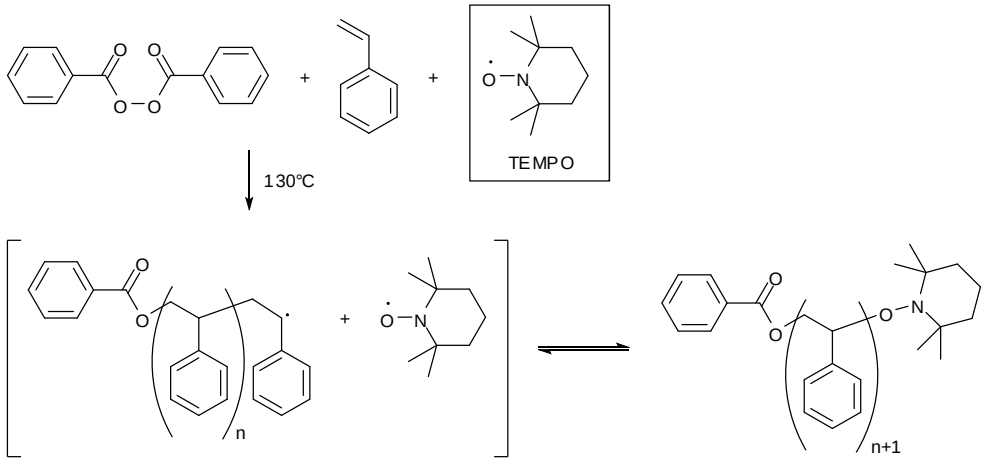

Figure 1.05. Bimolecular nitroxide mediated polymerisation of styrene.

One unfortunate drawback of the bimolecular process is that the concentration of the initiating species is unknown and thus good control over the molecular weight of the polymer produced is not always achievable. However, since the advent of TEMPO and the bimolecular process described above, Hawker's group were the first to develop several unimolecular initiators that offer far better control over molecular weight and polymer architecture.[49,50] The first of these initiators

consists of TEMPO bonded directly to a styrene unit, thus essentially at room temperature the TEMPO is acting as a free radical inhibitor and is trapping a styrene radical. Upon heating the styrene-TEMPO C-ON bond will cleave homolytically and will release the styrene radical which acts as an initiator, and the TEMPO nitroxyl radical itself will act as the polymerisation mediator.[42]

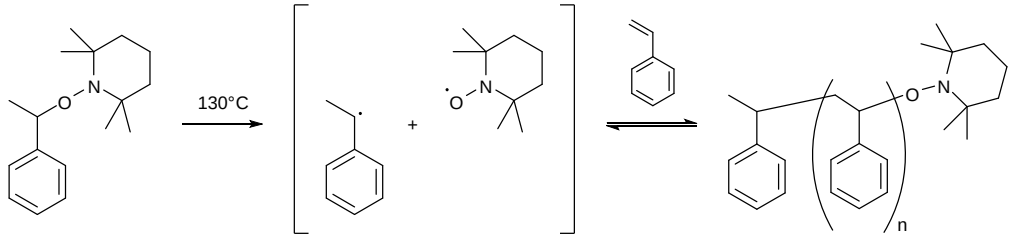

Figure 1.06. Unimolecular nitroxide mediated polymerisation of styrene.

Many of the current nitroxides used in NMP today are based on TEMPO, often with bulky substituents added to try and increase unfavourable steric interactions between the nitroxide and the radical. This is desirable so that the nitroxide will act as a polymerisation mediator (and not a radical inhibitor) at lower temperatures than 130°C. However the most successful nitroxides to date are in fact acyclic nitroxides which are structurally dissimilar to TEMPO and its derivatives.

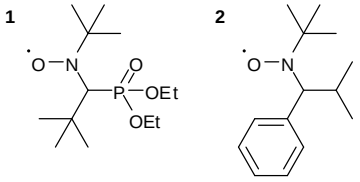

Figure 1.07. Two of the most successful nitroxides for use in NMP to date, able to polymerise a wide variety of monomer types and offering extremely accurate control over MW distribution (PDI as low as 1.05). 1.[51] 2.[52]

One of the key features of this new type of nitroxide is that there is a hydrogen atom bonded to one of the α-carbons which makes these nitroxides inherently less stable than the TEMPO based derivatives containing two quaternary α-carbons.

This makes them able to dissociate from the free radical chain end at a lower temperature i.e. they can act as polymerisation mediators for NMP at lower temperatures.[42]

The last aspect of NMP that needs considering is the kinetics, and the most important kinetic feature is known as the Persistent Radical Effect (PRE). This phenomenon is responsible in part for the control over molecular weight distribution that NMP exhibits and is relatively simple to explain. Consider a reaction where transient T• and persistent P• free radicals are produced simultaneously from a single precursor fragmenting (as in unimolecular NMP) as shown below in Figure 1.08.

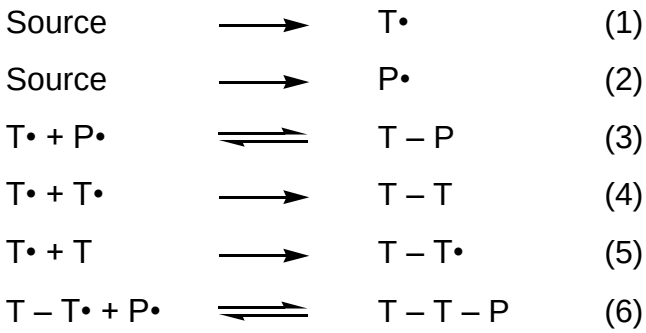

Figure 1.08. General reaction scheme for NMP where T• is the transient radical (initiator / monomer) and P• is the persistent radical (polymerisation mediator / nitroxyl radical).

In steps (1) and (2), the transient and persistent radicals are produced in a 1:1 molar ratio at exactly the same rate, and in step (3) they are recombining, though at the temperatures NMP is carried out at this step is reversible. However, when two transient radicals combine as in step (4) then this is irreversible and a low molecular weight oligomer results. Initially of course there are equal concentrations of T• and P•, but subsequently every T• – T• combination causes a build-up of excess of P• as by its very nature it cannot undergo a combination reaction with another P•, only with a T•. In step (5) we see propagation of the

radical polymer chain end (radical polymerisation), and in step (6) we see the reversible deactivation of the chain end by addition to P• (the crucial mediating step enabling control over molecular weight). In the initial stages of the reaction, step (4) will occur as the diffusing transient radicals are mobile and in reasonably high concentration. Yet as this occurs the resulting excess of P• will in itself be a limiting factor as an increased concentration in P• will result in more transient radical species being reversibly deactivated with the net result being a decreased concentration of transient (propagating) radical species. So as the concentration of P• increases, the concentration of all transient radical species decreases and control ensured by this low concentration. Also as the reaction proceeds and polymer is formed, the reaction medium will become more viscous thus the transient radical species will be less mobile.[53]

1.3.3 Reversible Addition-Fragmentation Transfer Polymerisation (RAFT)

The RAFT process[45,46,54] was originally discovered simultaneously by Rizzardo *et al.*[43] and Charmot *et al.*[44] in 1998, though Charmot's group's patent was only for a specific type of chain transfer agent known as "xanthates" and they named their invention "macromolecular design via the interchange of xanthates" or "MADIX". When xanthates are used to polymerise such monomers as styrenic and acrylate monomers, they typically have a low chain-transfer constant (i.e. low reactivity) and do not offer very good control over the molecular weight distribution of the resulting polymer. Rizzardo's group however, employed the use of a series of dithioesters (Figure 1.09) which when applied to the same monomer types had a much higher chain transfer constant (C_{tr}) thus were capable of producing polymers with a wide range of predictable molecular weights exhibiting narrow molecular weight distributions. They called this the "RAFT process".

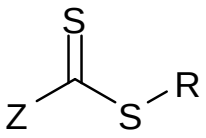

	Z	R
1	Ph	$C(CH_3)_2Ph$
2	Ph	$CH(CH_3)Ph$
3	Ph	CH_2Ph
4	Ph	$C(CH_3)_2CN$
5	Ph	$C(CH_3)(CN)CH_2CH_2CO_2Na$
6	CH_3	CH_2Ph

Figure 1.09. General structure of the dithioester reagents used by Rizzardo et al. and some examples from their initial publication.[43]

The main advantages of RAFT over other controlled radical polymerisation techniques such as ATRP and even NMP is that a far wider range of monomers can be polymerised, more functionalities are tolerated, as well as a broad range of solvents including water, a wide range of temperatures are appropriate (20-150°C), and it is suitable for use in several different types of process (bulk, suspension, emulsion etc.).[55]

The RAFT process is another example of a controlled free radical polymerisation. By carrying out a free radical polymerisation in the presence of a RAFT agent (Chain Transfer Agent – CTA) such as the dithioesters shown above in Figure 1.09, control is inferred in the same way as all other CRPs – by keeping low the concentration of propagating free radical species within the reaction medium, thereby reducing the probability of unwanted termination reactions. The mechanism involves the reversible addition of propagating radical species and the dithioester moiety, and in the same step the fragmentation of another radical species (initiator in the case of unreacted CTA, otherwise a second polymer chain)

from the CTA itself and vice versa. The living character of the ensuing polymerisations is due to the high transfer constants of the dithioester CTA relative to that of the monomer giving a rapid rate of exchange between the propagating and dormant species. The manner in which this is achieved is outlined in the reaction scheme shown in Figure 1.10. Two important points need to be considered when undertaking a RAFT polymerisation. The first is that the ratio of CTA to initiator should be high. This is to ensure the low instantaneous concentration of propagating radical species that is required for living polymerisation as previously discussed. As a rough guide, a molar ratio of 10:1 is usually sufficient. The second point is that the ratio of monomer to CTA will determine the molecular weight of the resulting polymer, thus it should be tailored for the specific molecular weight polymer that is desired.[55,56]

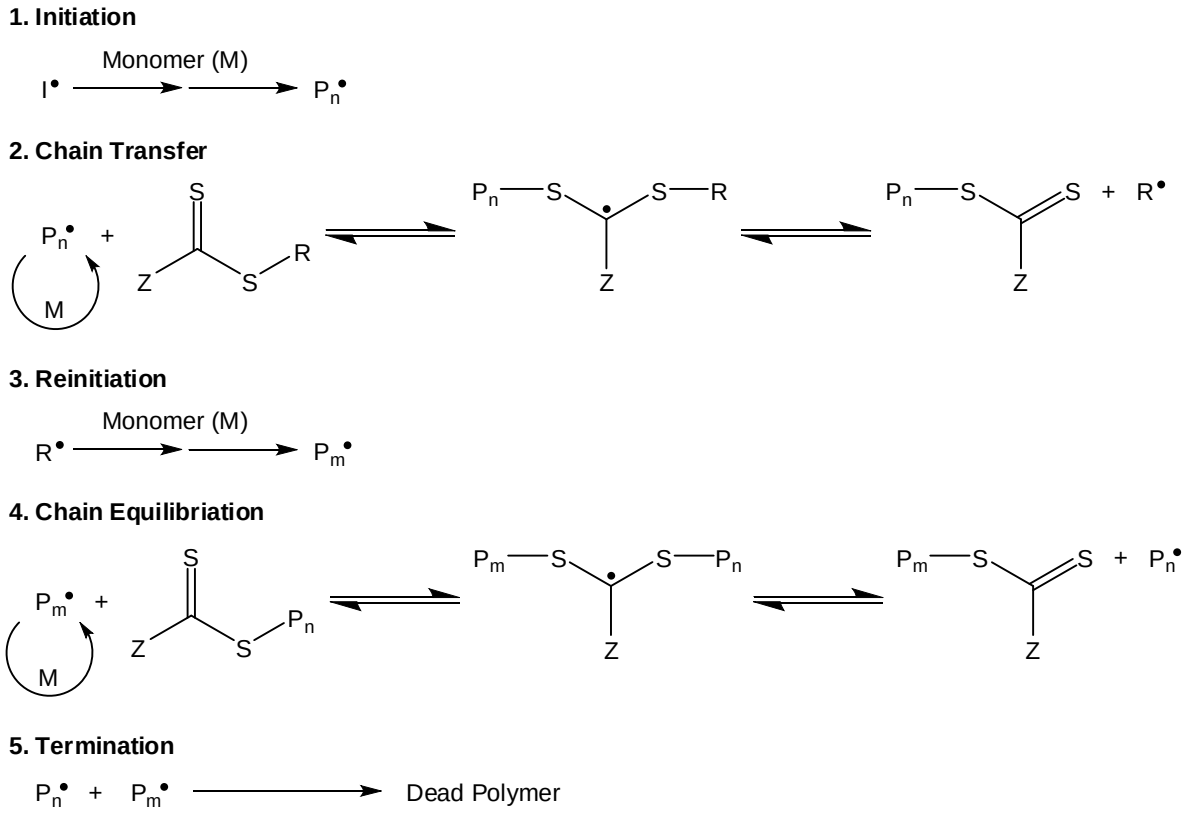

Figure 1.10. General mechanism for a RAFT polymerisation.[57]

The effectiveness of a given dithioester as a CTA is ultimately determined by its C_{tr} which is dependent upon the nature of the Z and R groups as well as that of the specific monomer being polymerised. Therefore a suitable CTA must be used for any particular monomer. In order for a dithioester to have a high C_{tr}, Z must be highly activating (towards the C=S bond) and R must be an extremely good free radical homolytic leaving group, as well as having the ability to reinitiate the monomer (Step 3 in Figure 1.10). The stability and steric bulk of the R• radical in part dictates R's leaving ability, and thus larger and more stable radicals make for better R groups, i.e. CH_3 would make a very poor R unit, whereas bulkier $C(CH_3)_2CN$ with an electron withdrawing nitrile group would make an effective one. The nature of the Z and R groups are crucial for an effective CTA and hence to obtain a polymer with a low MWD. Usually to achieve a PDI of less than 1.5, a system with a C_{tr} of greater than 2 is required, though polymers with a narrow MWD have been made with less active CTAs by the use of starved feed polymerisation whereby monomer is slowly and continuously fed into the reaction vessel throughout the course of the reaction to keep the overall concentration of monomer as low as possible.[58]

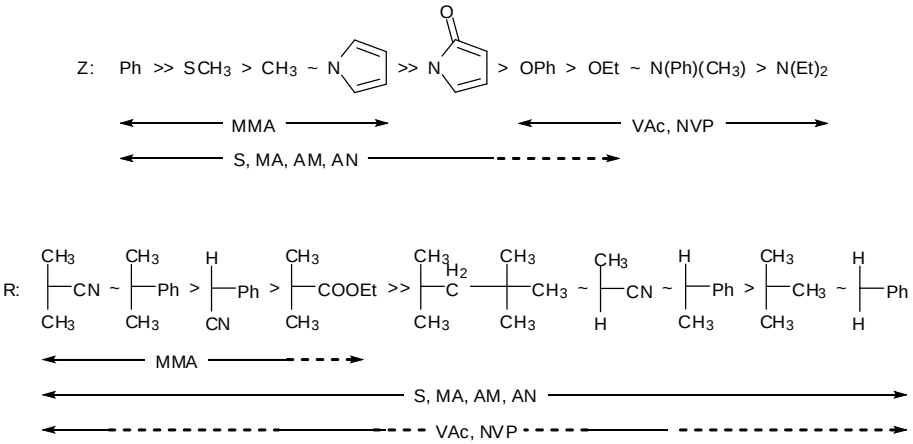

Figure 1.11. Guidelines for selection of RAFT CTAs for the polymerisation of various different monomers. For Z groups, addition rates decrease and fragmentation rates increase from left to right. For R groups, fragmentation rates decrease from left to right. Dashed lines indicate only partial control.[59]

As far as temperature is concerned, if a CTA has a C_{tr} of greater than 1 (as most do) then a decrease in temperature will lead to an increase in the activation energy of propagation, therefore the C_{tr} will increase. However, though this is useful for conducting polymerisations using CTAs with low C_{tr}s, too severe a reduction in temperature will slow the rate of polymerisation. In the case of CTAs with a C_{tr} of less than 1, an increase in temperature will increase the C_{tr}, but will also increase the amount of unwanted side reactions, so again the temperature can only be varied so much before control over M_n and MWD is adversely affected.

Although RAFT is undoubtedly one of the most useful controlled radical polymerisation techniques in use today, it does have some drawbacks. Typically rates of polymerisation are comparatively slow and though there is no metal waste as is the case in ATRP, most RAFT agents are toxic. In the case of xanthates and dithiocarbamates, their usual red colour often results in obtained polymers being pink, thought this is not an issue with trithiocarbonates.[60-62] Finally, until very recently there were no generic RAFT CTAs that were capable of polymerising a wide range of monomers, which can be a particular problem in the synthesis of

block copolymers. As the C_{tr} of any RAFT polymerisation is determined by the chemistry of both the CTA and the monomer, the CTA usually has to be carefully chosen (see Figure 1.11) in order to ensure control over the polymerisation of any specific monomer. However, in recent work, Moad et al. successfully demonstrated the use of a 'universal' or 'switchable' CTA, capable of controlling the polymerisation of monomers with a wide range of activities.[63-65] This is achieved by virtue of an acid 'switch' whereby the CTA can exist in a protonated or unprotonated form depending upon the local pH. This change affects the C_{tr} of the CTA and enables it to first polymerise a less activated monomer, and then upon a stimulus change (pH), a more activated monomer, or vice versa. However, this usual limitation of RAFT is not an issue in this work, as we are only concerned with the polymerisation of one monomer: *N*-vinyl pyrrolidone.

1.4 Controlled radical polymerisation of *N*-vinyl pyrrolidone (NVP)

1.4.1 Poly(N-vinyl pyrrolidone) (PVP)

PVP was first prepared via the free radical polymerisation of *N*-vinyl pyrrolidone by Fikentscher and Herrle in 1939.[66] Its first widespread application was in a salt water solution as a synthetic blood plasma volume expander during the Second World War. Since that time the use of PVP has been widely employed in medical science thanks to its high biological activity, zero toxicity, water solubility and ease of manufacture and subsequent processing.[67] PVP is an industrially important water soluble polymer that has many applications as a homo- or co-polymer ranging from use in drug delivery,[68,69] cosmetics,[70] stabilisation and clarification of beverages,[71] in adhesive sticks and water remoistenable adhesives,[72] as a phase transfer catalyst,[73] a selective chelating agent for the separation of metals,[74] a food thickener,[75] a blood plasma substitute,[76] or as previously discussed, a constituent part of the GDL in a PEMFC.[77,78] It is the latter application that is the focus of our research, and the aim of this research was to synthesise an end-functionalised PVP additive using either NMP or RAFT, and a fluorinated, multifunctional macro-initiator / CTA to provide the end-functionality. Our aim was to synthesise end-functionalised PVP additives with a molecular weight of up to 10,000 g mol^{-1} and a polydispersity index of less than 1.5 which should be sufficient for its use in the manufacture of a PEMFC GDL.

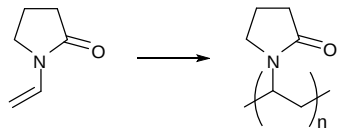

Figure 1.12. Chemical structures of N-vinyl pyrrolidone (NVP) and poly(N-vinyl pyrrolidone) (PVP). Due to the highly polar character of the amide group present in each repeating unit of PVP, and the non-polar character of the aliphatic backbone, PVP is soluble in both water and a range of organic solvents.[67]

Unfortunately, due to the amide group present in NVP, this monomer is incompatible for use with living cationic or living anionic polymerisation. Additionally this monomer is incompatible with ATRP due to its tendency to form complexes with transition metal catalysts. It was not until recently that PVP has been made in a controlled fashion using controlled radical polymerisation techniques such as RAFT[79,80] and NMP[80] which are far more tolerant towards impurities and functional groups. Before this, only traditional free radical polymerisation techniques have been employed which exhibit the same tolerances though offer little control over molecular weight distribution and only poorly defined PVP has been produced.

1.4.2 NMP and RAFT polymerisation of NVP

Hadjichristidis' group were simultaneously working on the RAFT and NMP of NVP[80] They experimented with several different CTAs for use in RAFT, and their best results were obtained using the CTA shown in Figure 1.13. They also investigated the impact of solvent and varied the [NVP] / [CTA] and [AIBN] / [CTA] ratios to find out what effect this would have on the polymerisation characteristics.

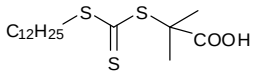

Figure 1.13. S-1-dodecyl-S'-(α,α'-dimethyl-α''-acetic acid)trithiocarbonate

The first important point this group made was that an increase in the [NVP] / [CTA] molar ratio led to decrease in percentage conversion of monomer, however it also led to a narrower polydispersity. They experimented with a difunctional CTA which gave the highest monomer conversion (65%) though invariably produced polymers with broad polydispersities indicating that termination reactions were occurring during polymerisation. When carrying out polymerisations in THF at 80°C using the CTA shown in Figure 1.13, with [AIBN] / [CTA] and [NVP] / [CTA] ratios of 0.83 and 1680 respectively, 55% conversion was achieved in 1 hour yielding a polymer with M_n = 90,000 g mol^{-1} and PDI = 1.5.

In the same paper, the relatively successful nitroxide mediated polymerisation of NVP was reported using both unimolecular and bimolecular initiation systems. 2,2,6,6-tetramethyl-1-(phenylethoxy)piperidine was used in the case of the unimolecular initiator and the well-known AIBN / TEMPO system was used in the case of bimolecular initiation. In both cases acetic anhydride was used as an accelerator for the polymerisation reaction, and *without this reagent polymerisation did not occur or only very low yields were obtained*. All polymerisations were carried out in bulk at 95°C which is lower than usual for NMP, but was necessary due to the thermal instability of the monomer. This is the reason attributed by the authors to the low monomer conversions achieved (10-45%) as they suggested that the slower rate may be leading to an increased number of termination reactions, though attempts at increasing temperature beyond 100°C resulted in even lower yields. All polymerisations were carried out in bulk due to the inability to find a suitable solvent for PVP which led to the eventual solidification of the reaction mixture and thus making high monomer conversions hard to achieve, the best being 45%.

Gnanou's group have successfully polymerised NVP using the RAFT process utilising *S*-malonyl *N*,*N*-diphenyldithiocarbamate (DPCM) as a CTA.[79] The DPCM was synthesised in house using a previously published procedure,[81] and all polymerisations were carried out at 80°C in 1,4-dioxane using AIBN as an initiator.

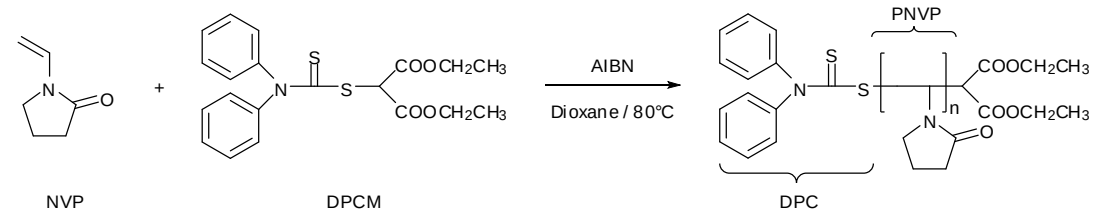

Figure 1.14. RAFT polymerisation of NVP using DPCM by Gnanou's group. Carried out in 1,4-dioxane using DPCM as CTA and AIBN as initiator.[79]

At first they experimented with the initiator / CTA ratio and found that a [AIBN] / [DPCM] ratio of 0.125 yielded the polymer with an optimum PDI of 1.3. Having set the [NVP] / [DPCM] ratio to 100 and the [AIBN] / [DPCM] ratio to 0.125, they then experimented with reaction time and found that there was a linear increase in molar mass with monomer conversion and time, and also that PDI increased with conversion, almost levelling off at approximately 1.5-1.6 at around 50% monomer conversion. Having established that the optimal ratio of [AIBN] / [DPCM] was 0.125, the ratio of [NVP] / [DPCM] was varied between 25 and 500, obtaining polymers with PDIs ranging from 1.2-1.5. The best result was obtained with a [NVP] / [DPCM] ratio of 200, resulting in a polymer of M_n = 20,000 g mol^{-1} and PDI = 1.2, with 85% conversion of monomer.

1.5 Dendritic macro initiators for NMP and RAFT

1.5.1 NMP

Fréchet *et al*. have successfully used dendrons containing a single styrene / TEMPO unit at their focal point to polymerise styrene and methyl methacrylate in a controlled fashion. The result was well defined [G-1]-[G-4] dendritic-linear diblock copolymers with significant molecular weights (good control over MWD up to c.a. 30,000 g mol^{-1}) and PDIs as low as 1.14. The dendritic macroinitiators were made by reaction of n^{th} (where n=1-4) generation poly(benzyl ether) bromide dendrons with a hydroxyl-benzyl-TEMPO derivative in the presence of sodium hydroxide as shown in Figure 1.15. The resulting macro initiator was then used to polymerise styrene in a controlled manner by heating at 123°C under argon.[82]

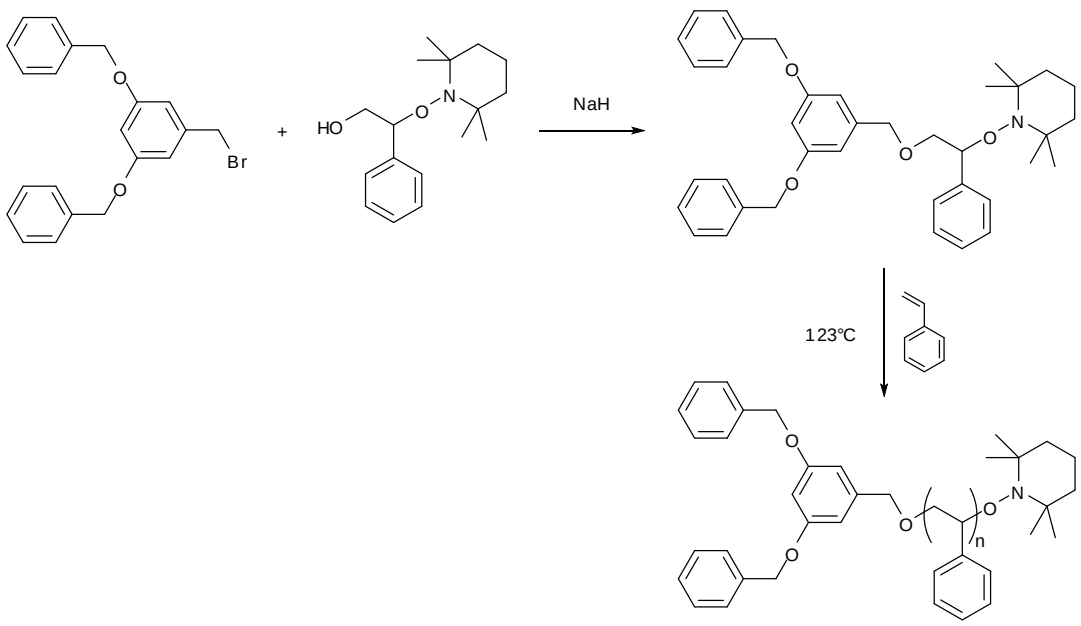

Figure 1.15. Reaction scheme used by Fréchet et al. showing the synthesis of a [G-1] dendritic macro initiator and its subsequent use in the NMP of styrene. In this case polymers with M_n=13500, 25000 and PDI=1.19, 1.27 respectively were successfully made, and further experiments were carried out with [G-0] and [G-2,3,4] initiators yielding similar results.

This work shows that it is indeed feasible to use dendritic macro initiators of varying generations in nitroxide mediated polymerisations. However, all of the problems discussed previously with regard to applying the technique of NMP to the polymerisation of NVP still apply, such as having to carry out the polymerisations at temperatures well below the optimum temperature due to the thermal instability of the monomer, and subsequent lack of control over MWD.

1.5.2 RAFT

Little work has been done on the use of dendritic macro initiators in RAFT polymerisation and most of it seems focussed around the synthesis of star polymers via a multifunctional dendritic macro initiator (i.e. the CTA functionalities

are situated on the terminal units at the periphery of the dendrimer).[83-85] In fact to the best of our knowledge (and the authors of the paper) only one paper has been published whereby a dendritic-linear diblock copolymer has been made via RAFT polymerisation and a monofunctional dendritic macro initiator (i.e. CTA functionality situated at the focal point of the dendron).[86] In this paper was reported the synthesis of a poly(benzyl ether)-poly(*N*-isopropylacrylamide) dendritic-linear diblock copolymer via RAFT polymerisation of *N*-isopropylacrylamide (NIPAM) using a dendritic CTA. The CTA was synthesised by addition of a second or third generation dendritic poly(benzyl ether) bromide (Frechét-type dendrons) to a solution mixture of phenylmagnesium bromide and carbon disulphide in THF. The dendritic poly(benzyl ether) bromides used have actually been used as initiators in their own right in ATRPs themselves, and though this would seem a more facile route to the dendritic-linear diblock copolymer, this CRP technique is not suitable for the polymerisation of NIPAM due to interactions between NIPAM and the Cu(I) complexes involved in ATRP. The same problem applies for our intended polymerisation of NVP which is why ATRP is not considered in this literature survey as a potential route to our desired polymer. The polymerisations were carried out using AIBN as an initiator along with the dendritic CTA and NIPAM in 1,4-dioxane at 80°C for 12 hours. Polymerisations exhibited pseudo-first-order kinetics i.e. there was linear plot of $ln([M]_0/[M]_t)$ vs. time, and the line almost passed through the origin suggesting that there was no induction period for this system. 80% conversion of monomer was exhibited after c.a. 12 hours and a degree of polymerisation (DP) of 220 with a PDI of less than 1.3 was achieved. Liu *et al.* successfully demonstrated that a dendritic-linear diblock copolymer can be synthesised using RAFT polymerisation and a dendritic chain transfer agent in a controlled fashion.[86]

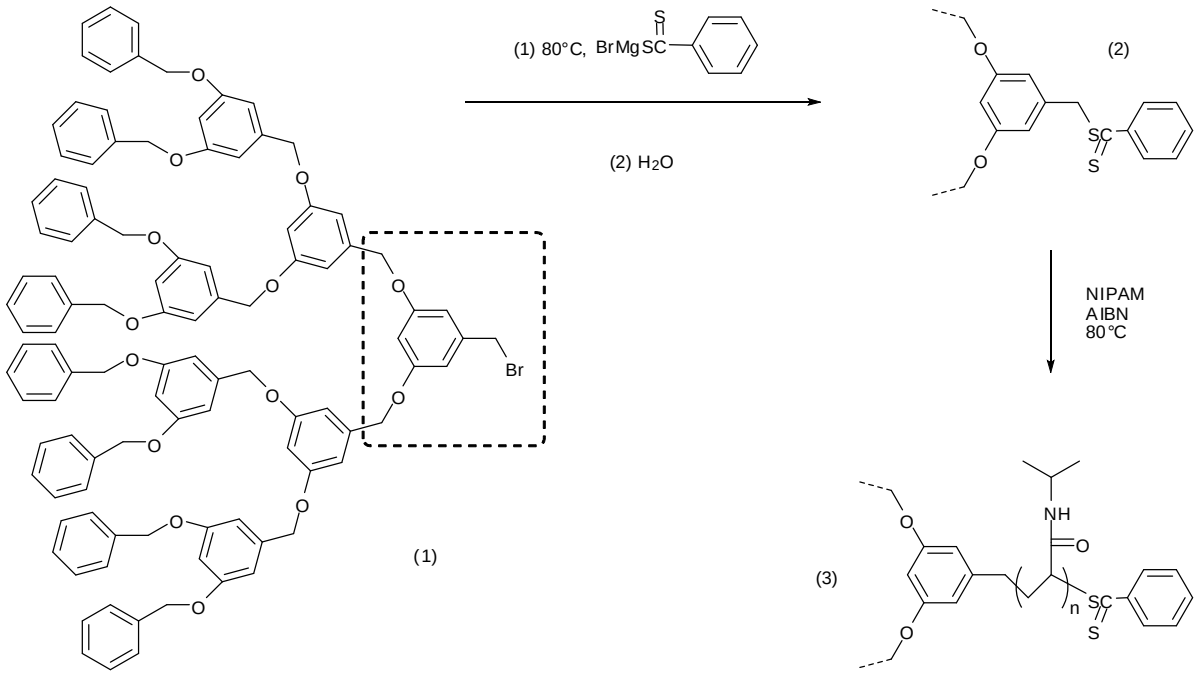

Figure 1.16. Reaction scheme for the synthesis of [G-3]-PNIPAM$_{220}$ (3) via the conversion of [G-3]-CH$_2$Br (1) into a dendritic CTA [G-3]-CH$_2$SSCPh (2) and subsequent reaction with NIPAM and AIBN in 1,4-dioxane at 80°C.

1.6 Fluorinated initiators for NMP and RAFT

An important issue in our intended synthesis is any potential incompatibility between fluorine and RAFT or NMP, as we wish to use a fluorinated dendritic macro initiator to polymerise NVP via one of these methods thus equipping the resulting PVP with a fluorinated dendritic end group in one step.

1.6.1 NMP

There seems to be no examples of the use of fluorinated initiators in NMP in the literature, though some examples have been reported of the use of NMP to produce well defined fluorinated polymers.[87,88]

1.6.2 RAFT

In the case of RAFT, it turns out that not only do there seem to be no incompatibilities with fluorinated initiators, but the incorporation of fluorine can actually be advantageous to the design of a CTA by virtue of its high electronegativity. Their electron withdrawing nature can be useful when they are incorporated into the R group as this makes R a better homolytic leaving group. The first example of a fluorinated CTA for use in RAFT is shown in Figure 1.17, and this is a good example of where modification with fluorine has been used to enhance the C_{tr} of an otherwise poor CTA.[89]

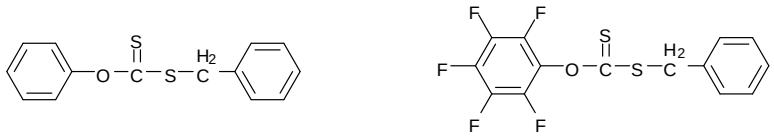

Figure 1.17. A xanthate used in the photo-iniferter process (only upon UV irradiation can it behave as a poor CTA in RAFT) and its fluorinated analogue which as a result of the electron withdrawing F's on the alkoxy moiety (R group) has a higher C_{tr} and is a useful RAFT agent.[89]

The same group undertook further work in this area and synthesised a series of ω-perfluorinated dithioesters (Figure 1.18) which were successfully used to make well defined end-functionalised polymers via the RAFT process. These particular examples are interesting because they were made by the reaction of the appropriate dithioester with phenylmagnesium bromide, carbon disulphide and benzyl bromide which is the near identical synthesis used to make the dendritic macro initiator discussed earlier (Figure 1.16). Thus this reaction scheme is not only suitable for making a dendritic macro initiator, but would also seem tolerant to the presence of fluorinated reactants.[90] It would therefore seem reasonable to assume that there would be no problems with using this synthesis to make a fluorinated dendritic macro initiator from a fluorinated poly(benzyl ether) bromide precursor. In fact, given this information it would seem that the reaction scheme in Figure 1.16 slightly modified to incorporate fluoroalkyl groups on the terminal units of the poly(benzyl ether) bromide and resulting dendritic CTA, and substituting NIPAM for NVP would seem a viable synthesis for an example of the type of end-functionalised PVP that is the focus of this thesis.

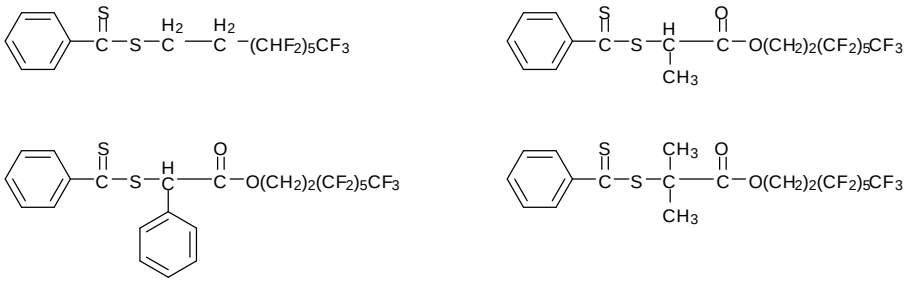

Figure 1.18. Four of the ω-perfluorinated dithioesters synthesised and successfully used as RAFT CTAs by Boutevin et al.[90]

In a paper published recently, a new kind of CTA was developed known as an "F-RAFT agent" where the Z group is actually a single fluorine atom.[91] The aim of this study was to develop a single CTA that was capable of controlling the polymerisation of monomers of widely varying reactivities (as opposed to having to tune the R and Z groups of the CTA to suit a specific monomer), and in order to do this it was "necessary to find RAFT agent substituents that promote fragmentation of unstable propagating radicals by destabilising the RAFT adduct radical rather than stabilising the RAFT agent".[91] The authors successfully synthesised Benzyl Fluoro Dithioformate (BFDF) (Figure 1.19) and used it as a CTA in the controlled RAFT polymerisation of polystyrene.

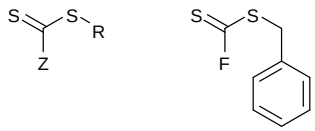

Figure 1.19. General structure of the dithioester CTAs used in RAFT, and Benzyl Fluoro Dithioformate (BFDF) where R=Bn and Z=F.[91]

Though in this case the fluorine is in itself the Z group, unlike in the [G-2] / [G-3] fluorinated dendritic macro initiators that we intend to use where the fluorine atoms

will be on the R group and will be fairly far removed from the dithioester moiety, it at least goes further to show that there is no intrinsic incompatibility with the presence of fluorine in a CTA and the RAFT process. There does not seem to be any information in the literature to suggest any intrinsic incompatibilities between fluorine and RAFT. Moreover, the identical synthetic route in making the fluorinated CTAs in Figure 1.18 to that used in the making of the dendritic CTA in Figure 1.16 means that it should be suitable for use in making the analogous fluorinated dendritic CTA that we require.

1.7 Conclusions pertaining to relevant polymerisation technique

It would appear from the recent work done on both NMP and RAFT with PVP that RAFT would be the more suitable mechanism for our intended research. There does not seem to be anything in the literature that would suggest a problem with the use of a fluorinated dendritic macro initiator in the NMP or RAFT polymerisation of NVP, though there is more information to advocate that it would work well with RAFT. In addition, RAFT can be carried out at an optimum temperature of 80°C whereas NMP would ideally be carried out at 120°C but in this instance the temperature has to be lowered to 95°C due to the thermal instability of the NVP monomer. With this limitation taken into account it would seem that for the purposes intended RAFT offers better control over molecular structure and narrower polydispersities, typically better percentages of conversion of monomer, far shorter reaction times and all at a lower temperature.

1.8 Proposed Chain Transfer Agents and polymer additives

1.8.1 Design of RAFT CTAs to impart end-functionality

Upon examination of the general mechanism for RAFT (Figure 1.10), it can be seen that in step 2 the R group of the CTA is homolytically cleaved, and in step 3 this radical species then reinitiates the polymerisation. It is in this way that the R group becomes the end group of the nascent polymer chain while the rest of the CTA (Z-CS=S dithioester moiety) undergoes rapid reversible chain transfer with the propagating chain ends. It is this rapid transfer that ensures a low instantaneous concentration of the propagating radical species thus ensuring effective control over the molecular weight of the resulting polymer. The net result of this process can be visualised simply as the insertion of the polymer chain into the CTA [ZCS(S)-R] bond where R becomes one end group and the dithioester moiety becomes the other (though remains easily cleavable) as shown in Figure 1.20. Therefore the R group of the CTA can be tailored to give the desired end-functionality on the resulting polymer within certain limitations. If necessary, the dithioester moiety residing at the other chain end is cleavable by means of thermolysis,[92] radical coupling[93] or radical reduction.[94-96] Alternatively chain end functionality can be introduced by converting the dithioester moiety into a thiol functional group either via aminolysis[97-99] or via reduction with sodium borohydride,[100,101] or the dithioester can be converted to a hydroxyl group, or an aldehyde via hydrolysis.[102]

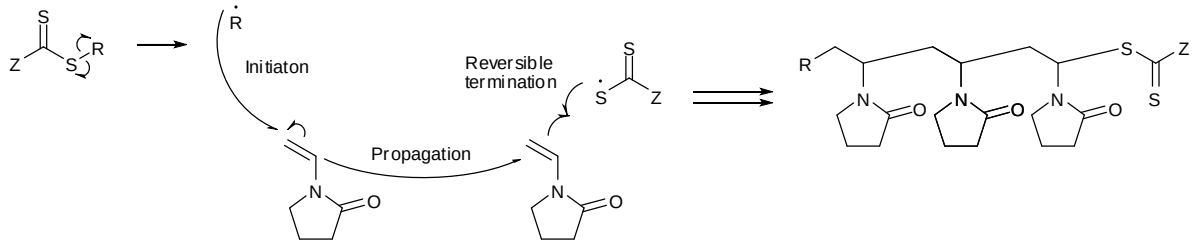

Figure 1.20. Net result of a RAFT polymerisation (for actual mechanism see Fig. 1.10) with the Z group-bearing dithioester moiety becoming one end group (subsequently cleavable), and the R group becoming the other end group.

The nature of both the Z and the R groups are vital to the CTAs activity. The Z group must be strongly activating towards the C=S bond and the R group must be a good free radical homolytic leaving group (i.e. must form a stable radical) whilst also being able to reinitiate the polymerisation. In our efforts to create a CTA to make well defined, end-fluorinated PVP, we are obviously going to have to alter the R group as ultimately it must be our desired end group. However, as DPCM has been shown to work well with NVP, we are basing our CTAs on DPCM and retaining the same Z group. In the synthesis of DPCM shown in Figure 1.21, the molecule is essentially constructed from the Z group over to the R group which is added in the final step via reaction with its chloride. Thus it is not hard to envisage a series of DPCM-type CTAs with different R groups being made via this original synthesis simply by using different chlorides in the final step. This is the basic principle of all of our intended syntheses.

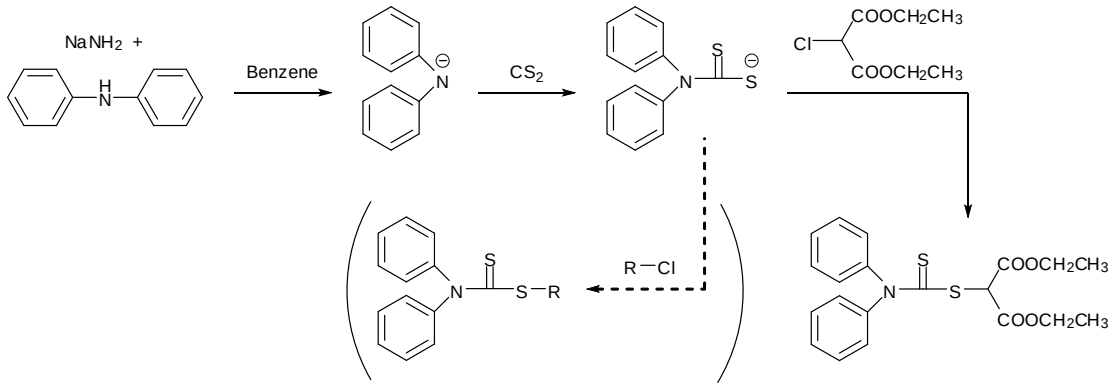

Figure 1.21. Reaction scheme for original DPCM synthesis. Bracketed step demonstrates how any R group can be grafted onto the molecule in the last step in the form of its chloride, R-Cl (or its bromide).

1.8.2 Via chlorination of readily available fluoro-alcohols

Our first proposed CTA synthesis was to start from readily and cheaply available fluoro-alcohols such as the DuPont "Zonyl" fluorotelomer intermediates (Figure 1.22).[103] It was hoped that these could be easily chlorinated with the use of thionyl chloride, and then the resulting chlorides used in the final step of the original synthesis of DPCM (Figure 1.21) in place of diethyl chloromalonate to give two fluorinated CTAs with the same Z group as DPCM. It is these fluorinated groups (R groups) that will fragment from the CTA and initiate polymerisation of NVP thus becoming the functional end group of the resulting polymer. The larger citric acid derivative, zonyl TBC, is sterically bulky and the resulting tertiary free radical would be stabilised by the electron withdrawing ester groups. Therefore we would expect it to be a good leaving group and form a stable radical, two of the main requirements for an effective R group. The smaller zonyl BA would probably be a much poorer R group due to its small size and the instability of the primary free radical that it would have to form during the RAFT process.

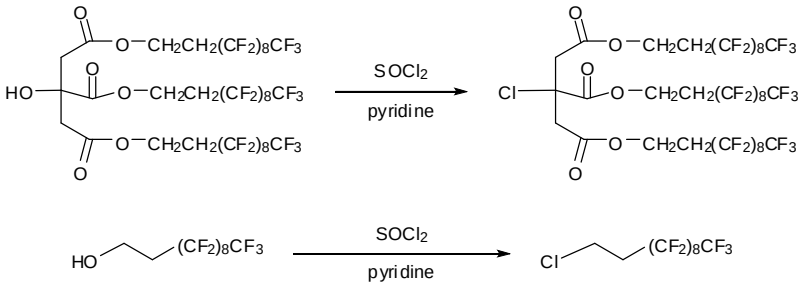

Figure 1.22. Chlorination reactions of zonyl TBC and zonyl BA fluorotelomer intermediates respectively. These chlorides would then be incorporated into the final step of the DPCM synthesis shown in Figure 1.21.

1.8.3 Via synthesis of fluorinated analogue of diethyl chloromalonate

The second proposed strategy involved the synthesis of a fluorinated analogue of diethyl chloromalonate as used in the final step of the DPCM synthesis. This would then be incorporated into the last step of the DPCM synthesis to give fluorinated DPCM as shown in Figure 1.23. The addition of these fluoroalkyl chains, significantly removed from the carbon atom on which the radical would be generated during the RAFT process, should have little effect on the activity of the CTA which is already known to be effective in the RAFT polymerisation of NVP.

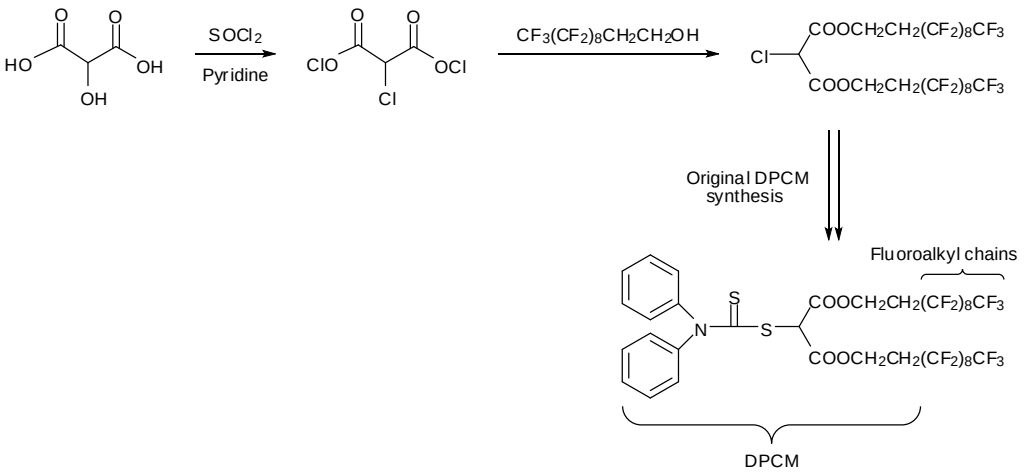

Figure 1.23. Alternative synthesis for a fluorinated CTA whereby a fluorinated analogue of diethyl chloromalonate is made from scratch and then used in the final step of the original DPCM synthesis as before.

1.8.4 Via synthesis of fluorinated Frechét-type dendritic bromide

Our third proposed synthesis is that of a fluorinated dendritic CTA, composed of the original DPCM fragment with a fluorinated Fréchet-type (poly(aryl ether)) dendritic R group.[104] This R group is again sterically bulky and the aromatic ring at the focal point of the dendritic R group will stabilise the radical species formed during the fragmentation step of the RAFT process. Therefore it should again be a good leaving group and form a stable free radical making it a suitable R group for a RAFT CTA.

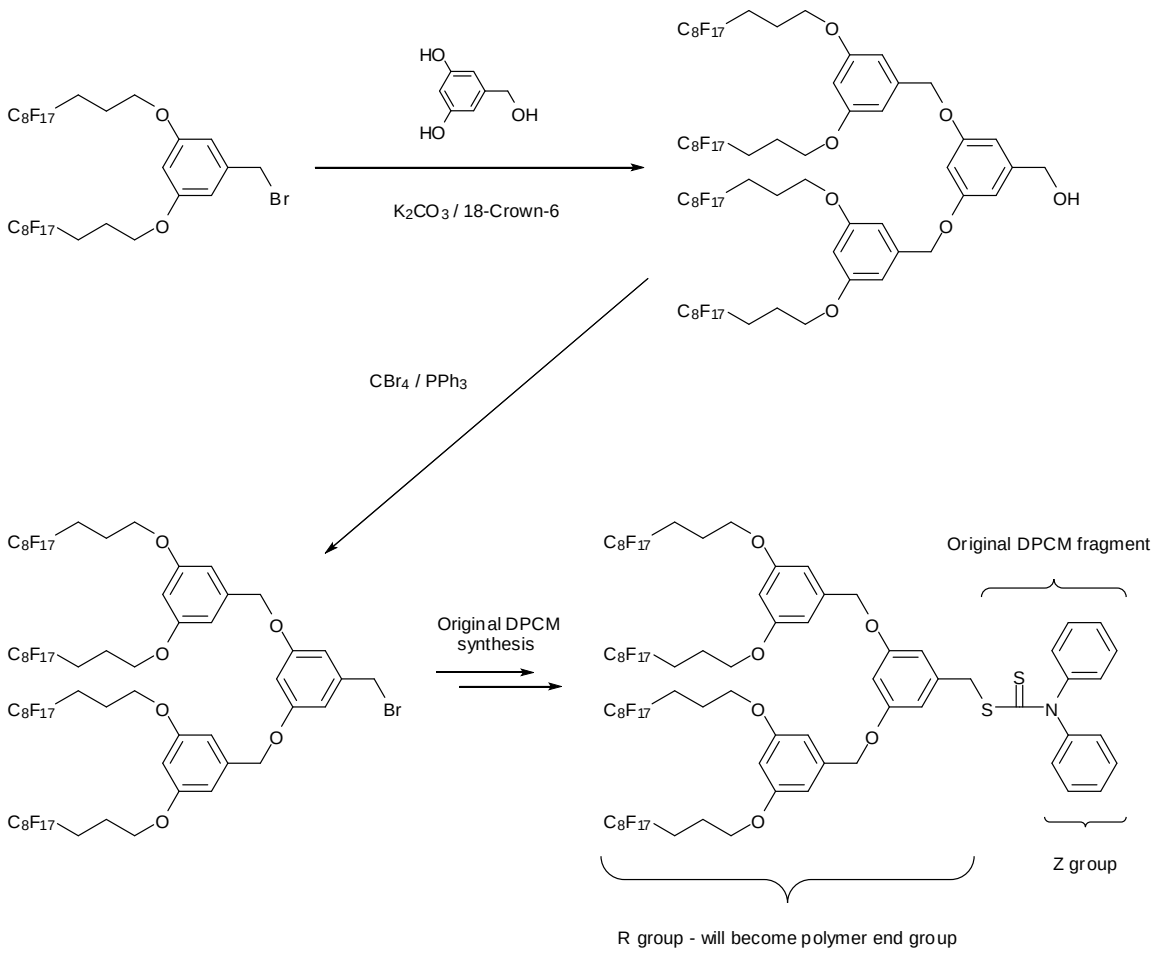

Figure 1.24. Suggested reaction scheme for the synthesis of an end-fluorinated dendritic CTA, starting with DPFPB-Br (Figure 1.25).

1.8.5 Via synthesis of dendritic perfluorooctyl propanol based additives

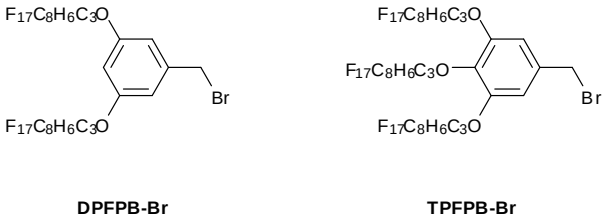

Figure 1.25. 3,5(di-3-(perfluorooctyl)propyloxy)benzyl bromide (DPFPB-Br) and 3,4,5(tri-3-(perfluorooctyl)propyloxy)benzyl bromide (TPFPB-Br).

Our fourth and ultimately successful strategy, which was taken to completion, involves the synthesis of 3,5(di-3-(perfluorooctyl)propyloxy)benzyl bromide (DPFPB-Br) and 3,4,5(tri-3-(perfluorooctyl)propyloxy)benzyl bromide (TPFPB-Br)[105] shown above (Figure 1.25), and their subsequent incorporation into the original DPCM synthesis to give two novel CTAs, one di-functional and one tri-functional. These proposed R groups had the advantage of possessing an aromatic ring adjacent to the site of free radical generation during the RAFT process, and hence again were expected to form a stable radical, in addition to their reasonable steric bulk. It was for these reasons that they were chosen as suitable R groups.

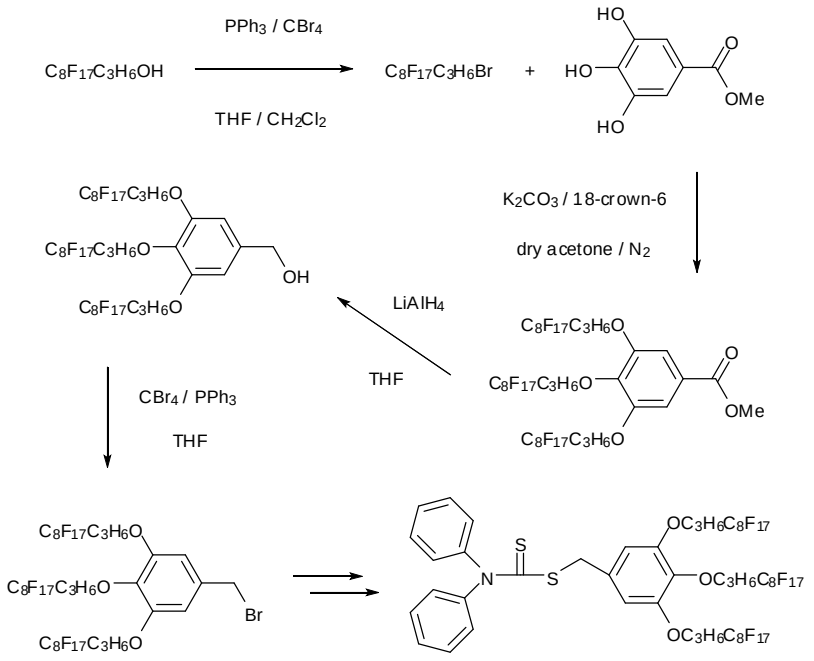

Figure 1.26. Synthesis of 3,4,5(tri-3-(perfluorooctyl)propyloxy)benzyl bromide (TPFPB-Br). Last step is the original DPCM synthesis using this TPFPB-Br in place of diethyl chloromalonate to give TPFPB-DPCM, our tri-functional CTA.

1.9 Aims and Objectives

1. To synthesise and characterise a series of novel RAFT CTAs, compatible with the NVP monomer, and bearing various R group functionalities incorporating between two and four C_8F_{17} fluoroalkyl chains
2. To synthesise and characterise a series of novel well defined, low molecular weight, end-functionalised PVP additives via RAFT polymerisation using the aforementioned CTAs
3. To spin coat a series of polymer thin films comprising of an unfunctionalised bulk PVP matrix and a measured quantity of end-functionalised PVP additive, varying the following attributes:
    - Weight percentage of end-functionalised PVP additive
    - Molecular weight of end-functionalised PVP additive
    - Number of C_8F_{17} fluoroalkyl chains in additive end group
    - Molecular weight of unfunctionalised bulk PVP matrix
4. To ascertain the extent / efficiency of surface segregation of the aforementioned end-functionalised PVP additives, and the resulting effect on the surface hydrophobicity / oleophobicity of the unfunctionalised bulk PVP matrix, taking in to account the above measured attributes, by means of contact angle measurements and Rutherford Backscattering Ion Beam Analysis
5. To investigate thoroughly the effects of the above four attributes on the surface properties of the resulting PVP thin films
6. To test the effects of incorporating these novel end-functionalised PVP additives into simulated Gas Diffusion Layers and subjecting them to “water uptake tests” under standard Polymer Electrolyte Membrane Fuel Cell operating conditions

1.10 References

[1] 'Battery', *Encyclopaedia Britannica Online Academic Edition*, <http://www.britannica.com/EBchecked/topic/56126/battery> (18th Jan 2011)

[2] Huggins, R. A.; *Advanced Batteries: Materials Science Aspects*, Springer, **2009**

[3] EG&G Technical Services, Inc.; *Fuel Cell Handbook*, 7th Edition, **2004**

[4] Srinivasan, S.; *Fuel Cells: From Fundamentals to Applications*, Springer, **2006**

[5] Swain, M. R.; *Fuel Leak Simulation*, unpublished material

[6] Fleming, J.; Lehnert, W.; Mathias, M.; Roth, J.; *Handbook of Fuel Cells: Fundamentals, Technology & Applications*, Volume 3, Chapter 46

[7] Kiff, F. T.; Richards, R. W.; Thompson, R. L.; *Langmuir*, **2004**, *20*, 4465

[8] van de Grampel, R. D.; Ming, W.; Gildenpfennig, A.; van Gennip, W. J. H.; Laven, J.; Niemantsverdriet, J. W.; Brongersma, H. H.; de With, G.; van der Linde, R.; *Langmuir*, **2004**, *20*, 6344

[9] van de Grampel, R. D.; Ming, W.; Gildenpfennig, A.; Laven, J.; Brongersma, H. H.; de With, G.; van der Linde, R.; *Langmuir*, **2004**, *20*, 145

[10] Koberstein, J. T.; *J. Polym. Sci., Part B: Polym. Phys.*, **2004**, *42*, 2942

[11] O'Rourke Muisener, P. A. V.; Jalbert, C. A.; Yuan, C.; Baetzold, J.; Mason, R.; Wong, D.; Kim, Y. J.; Koberstein, J. T.; *Macromolecules*, **2003**, *36*, 2956

[12] O'Rourke Muisener, P. A. V.; Koberstein, J. T.; Kumar, S.; *Macromolecules*, **2003**, *36*, 771

[13] Hutchings, L. R.; Richards, R. W.; Thompson, R. L.; Bucknall, D. G.; Clough, A. S.; *Eur. Phys. J. E.*, **2001**, *5*, 451

[14] Hopkinson, I.; Kiff, F. T.; Richards, R. W.; Bucknall, D. G.; Clough, A. S.; *Polymer*, **1997**, *38*, 87

[15] Schaub, T. F.; Kellogg, G. J.; Mayes, A. M.; *Macromolecules*, **1996**, *29*, 3982

[16] Clarke, C. J.; Jones, R. A. L.; Clough, A. S.; *Polymer*, **1996**, *37*, 3813

[17] Clarke, C. J.; *Polymer*, **1996**, *37*, 4747

[18] Elman, J. F.; Johs, B. D.; Long, T. E.; Koberstein, J. T.; *Macromolecules*, **1994**, *27*, 5341

[19] Jones, R. A. L.; Norton, L. J.; Shull, K. R.; Kramer, E. J.; Felcher, G. P.; Karim, A.; Fetters, L. J.; *Macromolecules*, **1992**, *25*, 2359

[20] Shull, K. R.; *J. Chem. Phys.*, **1991**, *94*, 5723

[21] Hutchings, L. R.; Narrainen, A. P.; Eggleston, S. M.; Clarke, N.; Thompson, R. L.; *Polymer*, **2006**, *47*, 8116

[22] Narrainen, A. P.; Hutchings, L. R.; Ansari, I. A.; Clarke, N.; Thompson, R. L.; *Soft Matter*, **2006**, *2*, 126

[23] Narrainen, A. P.; Hutchings, L. R.; Ansari, I.; Thompson, R. L.; Clarke, N.; *Macromolecules*, **2007**, *40*, 1969

[24] Thompson, R. L.; Narrainen, A. P.; Eggleston, S. M.; Ansari, I. A.; Hutchings, L. R.; Clarke, N.; *J. Appl. Polym. Sci.*, **2007**, *105*, 623

[25] Hutchings, L. R.; Narrainen, A. P.; Thompson, R. L.; Clarke, N.; Ansari, L.; *Polym. Int.*, **2008**, *57*, 163

[26] Hardman, S. J.; Norazilawati, M. S.; Riggs, H. J.; Thompson, R. L.; Rigby, J.; Bergius, W. N. A.; Hutchings, L. R.; *Macromolecules*, **2011**, *44*, 6461

[27] Hutchings, L. R.; Richards, R. W.; Thompson, R. L.; Bucknall, D. G.; *Eur. Phys. J. E.*, **2002**, *8*, 121

[28] Ward, L. J.; Badyal, J. P. S.; Goodwin, A. J.; Merlin, P. J.; *Polymer*, **2005**, *46*, 3986

[29] Cheng, T. S.; Lin, H. T.; Chuang, M. J.; *Mater. Lett.*, **2004**, *58*, 650

[30] Selli, E.; Mazzone, G.; Oliva, C.; Martini, F.; Riccardi, C.; Barni, R.; Macandalli, B.; Massafra, M. R.; *J. Mater. Chem.*, **2001**, *11*, 1985

[31] Sigurdsson, S.; Shishoo, R.; *J. Appl. Polym. Sci.*, **1997**, *66*, 1591

[32] Kawase, T.; Sawada, H.; *J. Adhes. Sci. Technol.*, **2002**, *16*, 1121

[33] Kawase, T.; Yamane, M.; Fugi, T.; Minigawa, M.; *J. Adhes. Sci. Technol.*, **1997**, *11*, 1381

[34] Biltresse, S.; Deschamps, D.; Boxus, T.; Marchand-Brynaert, J.; *J. Polym. Sci., Part A: Polym. Chem.*, **2000**, *38*, 3510

[35] Schmidt, D. L.; Coburn, C. E.; DeKoren, B. M.; Potter, G. E.; Meyers, G. F.; Fischer, D. A.; *Nature*, **1994**, *368*, 39

[36] Saïdi, F.; Guittard, F.; Guimon, C.; Géribaldi, S.; *Macromol. Chem. Phys.*, **2005**, *206*, 1098

[37] Hutchings, L. R.; Norazilawati, M. S.; Thompson, R. L.; *Polym. Chem.*, **2011**, *2*, 851

[38] Ansari, I. A.; Clarke, N.; Hutchings, L. R.; Narrainen, A. P.; Terry, A. E.; Thompson, R. L.; Webster, J. R. P.; *Langmuir*, **2007**, *23*, 4405

[39] Szwarc, M.; Levey, M.; Milkovich, R.; *J. Am. Chem. Soc.*, **1956**, *78*, 2656

[40] Szwarc, M.; *Nature*, **1956**, *178*, 1168

[41] Georges, M. K.; Hamer, G. K.; Kazmaier, P. M.; Veregin, R. P. N.; *Macromolecules*, **1993**, *26*, 2987

[42] Bosman, A. W.; Harth, E.; Hawker, C. J.; *Chem. Rev.*, **2001**, *101*, 3661

[43] Chiefari, J.; Chong, Y. K.; Ercole, F.; Krstina, J.; Jeffery, J.; Le, T. P. T.; Mayadunne, R. T. A.; Meijs, G. F.; Moad, C. L.; Moad, G.; Rizzardo, E.; Thang, S. H.; *Macromolecules*, **1998**, *31*, 5559

[44] Charmot, D.; Corpart, P.; Michelet, D.; Zard, S.; Biadatti, T.; *Chem. Abstr.*, **1999**, *130*, 82018

[45] Moad, G.; Rizzardo, E.; Thang, S. H.; *Aust. J. Chem.*, **2005**, *58*, 379

[46] Zard, S. Z.; *Aust. J. Chem.*, **2006**, *59*, 663

[47] Wang, J. S.; Matyjaszewski, K.; *J. Am. Chem. Soc.*, **1995**, *117*, 5614

[48] Matyjaszewski, K.; Xia, J.; *Chem. Rev.*, **2001**, *101*, 2921

[49] Hawker, C. J.; *J. Am. Chem. Soc.*; **1994**, *116*, 11185

[50] Barclay, G. G.; Dao, J.; Devonport, W.; Hawker, C. J.; Orellana, A.; *Macromolecules*, **1996**, *29*, 5245

[51] Benoit, D.; Finet, J. P.; Gnanou, Y.; Grimaldi, S.; Robin, S.; Tordo, P.; *J. Am. Chem. Soc.*, **2000**, *122*, 5929

[52] Benoit, D.; Braslau, R.; Chaplinski, V.; Hawker, C. J.; *J. Am. Chem. Soc.*, **1999**, *121*, 3904

[53] Fischer, H.; *Chem. Rev.*, **2001**, *101*, 3581

[54] Barner-Kowollik, C.; *Handbook of RAFT Polymerization*, Wiley-VCH, **2008**

[55] Monteiro, M. J.; *J. Polym. Sci., Part A: Polym. Chem.*, **2005**, *43*, 3189

[56] Adamy, M. M.; Destarac, M.; Leeuwen, B. J.; Monteiro, M. J.; van Herk, A. M.; *Macromolecules*, **2005**, *38*, 1538

[57] Chong, Y. K.; Le, T. P. T.; Moad, G.; Rizzardo, E.; Thang, S. H.; *Macromolecules*, **1999**, *32*, 2071

[58] Monteiro, M. J.; Smulders, W.; *Macromolecules*, **2004**, *37*, 4474

[59] Chen, M.; Chong, B.; Moad, G.; Rizzardo, E.; Skidmore, M.; Thang, S. H.; *Macromol. Symp.*, **2007**, *248*, 104

[60] Chiefari, J.; Krstina, J.; Moad, G.; Mayadunne, R. T. A.; Postma, E.; Rizzardo, E.; Thang, S. H.; *Macromolecules*, **2000**, *33*, 243

[61] Chen, Z.; Gao, J.; Gao, T.; Ran, R.; Wan, T.; *Polym. Int.*, **2008**, *57*, 28

[62] Huang, Y.; Ma, Y.; Maschmeyer, T.; Moraes, J.; Mori, C.; Ohno, K.; Perrier, S.; Tsujii, Y.; *Macromolecules*, **2011**, *44*, 8944

[63] Benaglia, M.; Chiefari, J.; Chong, Y. K.; Moad, G.; Rizzardo, E.; Thang, S. H.; *J. Am. Chem. Soc.*, **2009**, *131*, 6914

[64] Benaglia, M.; Chen, M.; Chong, Y. K.; Moad, G.; Rizzardo, E.; Thang, S. H.; *Macromolecules*, **2009**, *42*, 9384

[65] Guerrero-Sanchez, C.; Keddie, D. J.; Moad, G.; Rizzardo, E.; Thang, S. H.; *Macromolecules*, **2011**, *44*, 6738

[66] Fikentscher, H.; Herrle, K.; *Modern Plastics*, **1945**, *23*, 157

[67] Kirsh, Y. E.; *Water Soluble Poly-N-Vinylamides: Synthesis and Physiochemical Properties*, Wiley, **1998**

[68] Rüs, T.; Bauer-Brandl, A.; Wagner, T.; Kranz, H.; *Eur. J. Pharm. Biopharm.*, **2007**, *65*, 78

[69] Lai, M. C.; Hageman, M. J.; Schowen, R. L.; Borchardt, R.T.; Topp, E. M.; *J. Pharm. Sci.*, **1999**, *88*, 1073

[70] Vogel, F. G. M.; *Soap Cosmetics Chemical Specialities*, **1989**, *65*, 42

[71] McMurrough, I.; *Cerevesia*, **1998**, *23*, 27

[72] *PVP Product Information Page*, <http://ispadhesives.com/products/polymers.htm> (24 April 2011)

[73] Kondo, S.; Ozeki, M.; Nakashima, N.; Suzuki, K.; Tsuda, K.; *Angew. Makromol. Chem.*, **1988**, *163*, 139

[74] del C. Pizarro, G.; Marambio, O. G.; Jeria, M. O.; Huerta, M.; Rivas, B. L.; *J. Appl. Polym. Sci.*, **2006**, *100*, 178

[75] Schwarz, W.; *PVP: Critical Review of the Kinetics and Toxicology of Polyvinylpyrrolidone (Povidone)*, CRC Press, **1990**

[76] Samaras, S. C.; Dietz, N.; *American Journal of Physiology*, **1951**, *167*, 823

[77] Smitha, B.; Sridhar, S.; Khan, A. A.; *J. Power Sources*, **2006**, *159*, 846

[78] Qiao, J.; Hamaya, T.; Okada, T.; *Polymer*, **2005**, *46*, 10809

[79] Bindu, R. L.; Borsali, R.; Devasia, R.; Gnanou, Y.; Mougin, N.; *Macromol. Symp.*, **2005**, *229*, 8

[80] Bilalis, P.; Hadjichristidis, N.; Pitsikalis, M.; *J. Polym. Sci., Part A: Polym. Chem.*, **2006**, *44*, 659

[81] Charmot, D.; Destarac, M.; Frank, X.; Zard, S.; *Macromol. Rapid Commun.*, **2000**, *21*, 1035

[82] Dao, J.; Fréchet, J. M. J.; Hawker, C. J.; Leduc, M. R.; *J. Am. Chem. Soc.*, **1996**, *118*, 11111

[83] Barner-Kowollik, C.; Davis, T. P.; Hao, X.; Jesberger, M.; Malmström, E.; Nilsson, C.; Östmark, E.; Stenzel, M. H.; *J. Polym. Sci., Part A: Polym. Chem.*, **2004**, *42*, 5877

[84] Hong, C.-Y.; Liu, J.; Pan, C.-Y.; You, Y.-Z.; *J. Polym. Sci., Part A: Polym. Chem.*, **2005**, *43*, 6379

[85] Pan, C.-Y.; Zheng, Q.; *Macromolecules*, **2005**, *38*, 6841

[86] Ge, Z.; Liu, S.; Luo, S.; *J. Polym. Sci., Part A: Polym. Chem.*, **2006**, *44*, 1357

[87] Andre, P.; Boutevin, B.; Desimone, J. M.; Lacroix-Desmazes, P.; Ruzette, A.-V.; *J. Polym. Sci., Part A: Polym. Chem.*, **2004**, *42*, 3537

[88] Burton, D. J.; Wang, Y.; Xu, J.; *J. Org. Chem.*, **2006**, *71*, 7780

[89] Améduri, B.; Boutevin, B.; Lacroix-Desmazes, P.; *Collect. Czech. Chem. Commun.*, **2002**, *67*, 1383

[90] Améduri, B.; Boutevin, B.; Corpart, J.-M.; Lebreton, P.; *Macromol. Chem. Phys.*, **2002**, *203*, 522

[91] Barner-Kowollik, C.; Coote, M. L.; Davis, T. P.; Stenzel, M. H.; Theis, A.; *Aust. J. Chem.*, **2005**, *58*, 437

[92] Chong, B.; Moad, G.; Rizzardo, E.; Skidmore, M.; Thang, S. H.; *Aust. J. Chem.*, **2006**, *59*, 755

[93] Perrier, S.; Takolpuckdee, P.; Mars, C. A.; *Macromolecules*, **2005**, *38*, 2033

[94] Destarac, M.; Kalai, C.; Petit, L.; Wilczewska, A. Z.; Mignani, G.; Zard, S. Z.; *Polym. Prepr. (Am. Chem. Soc., Div. Polym. Chem.)*, **2005**, *46*, 372

[95] Liard, A.; Quiclet-Sire, B.; Zard, S. Z.; *Tetr. Lett.*, **1996**, *37*, 5877

[96] Chong, Y. K.; Moad, G.; Rizzardo, E.; Thang, S. H.; *Macromolecules*, **2007**, *40*, 4446

[97] Chan, M. F.; Garst, M. E.; *J. Chem. Soc., Chem. Commun.*, **1991**, *7*, 540

[98] Lima, V.; Jiang, X.; Brokken-Zijp, J.; Schoenmakers, P. J.; Klumperman, B.; van der Linde, R.; *J. Polym. Sci., Part A: Polym. Chem.*, **2005**, *43*, 959

[99] Deletre, M.; Levesque, G.; *Macromolecules*, **1990**, *23*, 4733

[100] Sumerlin, B. S.; Lowe, A. B.; Stroud, P. A.; Zhang, P.; Urban, M. W.; McCormick, C. L.; *Langmuir*, **2003**, *19*, 5559

[101] Zelikin, A. N.; Such, G. K.; Postma, A.; Caruso, F.; *Biomacromolecules*, **2007**, *8*, 2950

[102] Pound, G.; McKenzie, J. M.; Lange, R. F. M.; Klumperman, B.; *Chem. Commun.*, **2008**, 3193

[103] *DuPont™ Zonyl® Fluorochemical Intermediates (product line information document)*, DuPont, **2002**

[104] Hawker, C. J.; Fréchet, J. M. J.; *J. Am. Chem. Soc.*, **1990**, *112*, 7639

[105] Narrainen, A. P.; Hutchings, L. R.; Ansari, I. A.; Thompson, R. L.; Clarke, N.; *Macromolecules*, **2007**, *40*, 1969

Chapter 2
Preliminary Work: Results and Discussion

Reversible Addition-Fragmentation Transfer Polymerisation of styrene and *N*-vinyl pyrrolidone; synthesis of a novel Frechét-type dendritic Chain Transfer Agent; preliminary attempts at the synthesis of novel fluorinated Chain Transfer Agents

2.1 Reversible Addition-Fragmentation Transfer Polymerisation of Styrene

2.1.1 Introduction

Having decided that Reversible Addition-Fragmentation Transfer (RAFT) was the more suitable polymerisation method over Nitroxide Mediated Polymerisation (NMP) for the synthesis of the proposed end-functionalised *N*-vinyl pyrrolidone (NVP) additives, some initial RAFT polymerisations of styrene were performed in order to familiarise ourselves with the experimental process. Though RAFT is suitable for the controlled polymerisation of a wide range of monomers including NVP, the systems used (CTAs, solvents, temperatures etc.) vary greatly for different types of monomer. Due to the relative complexity and young age of the new system that had been developed for NVP, it was decided to start with something simpler and better documented, as the basic experimental techniques are similar. A small series of RAFT polymerisations of styrene were performed using cumyl dithiobenzoate (CDB) as a CTA,[1-3] as it met these criteria and there was already some experience within our research group in this area.

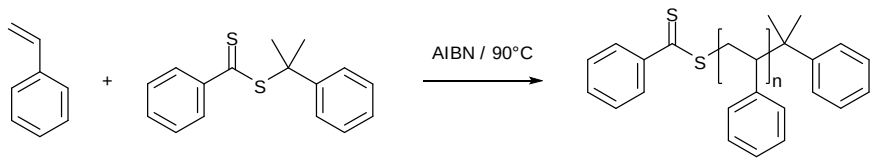

Figure 2.01. Reaction scheme for the RAFT polymerisation of styrene using cumyl dithiobenzoate (CDB) as a CTA.

The CTA, cumyl dithiobenzoate, was obtained from Dr S. Spain who had a previously synthesised supply readily available, though the experimental details of its synthesis have been included in the experimental chapter of this thesis for the sake of completeness.

2.1.2 RAFT polymerisations

While several polymerisations were carried out under varying conditions, ideal conditions found to yield successful results were performing the polymerisations in bulk (no solvent) at 90°C for 40 hours. Undertaking a RAFT polymerisation of styrene using CDB as CTA under these conditions, aiming for a molecular weight of 10,000 g mol^{-1}, polystyrene was produced with a M_n of 11,400 g mol^{-1} and a PDI of 1.29 as determined by triple detection Size Exclusion Chromatography (SEC), and a monomer conversion of 54%. The SEC data for this polymerisation is shown in Figure 2.02. By the end of the 40 hour period, the polymerisation mixture had solidified completely and it was necessary for it to be dissolved in a minimum amount of THF in order to facilitate the subsequent precipitation of the resultant polymer into a 20x volume excess of methanol prior to characterisation.

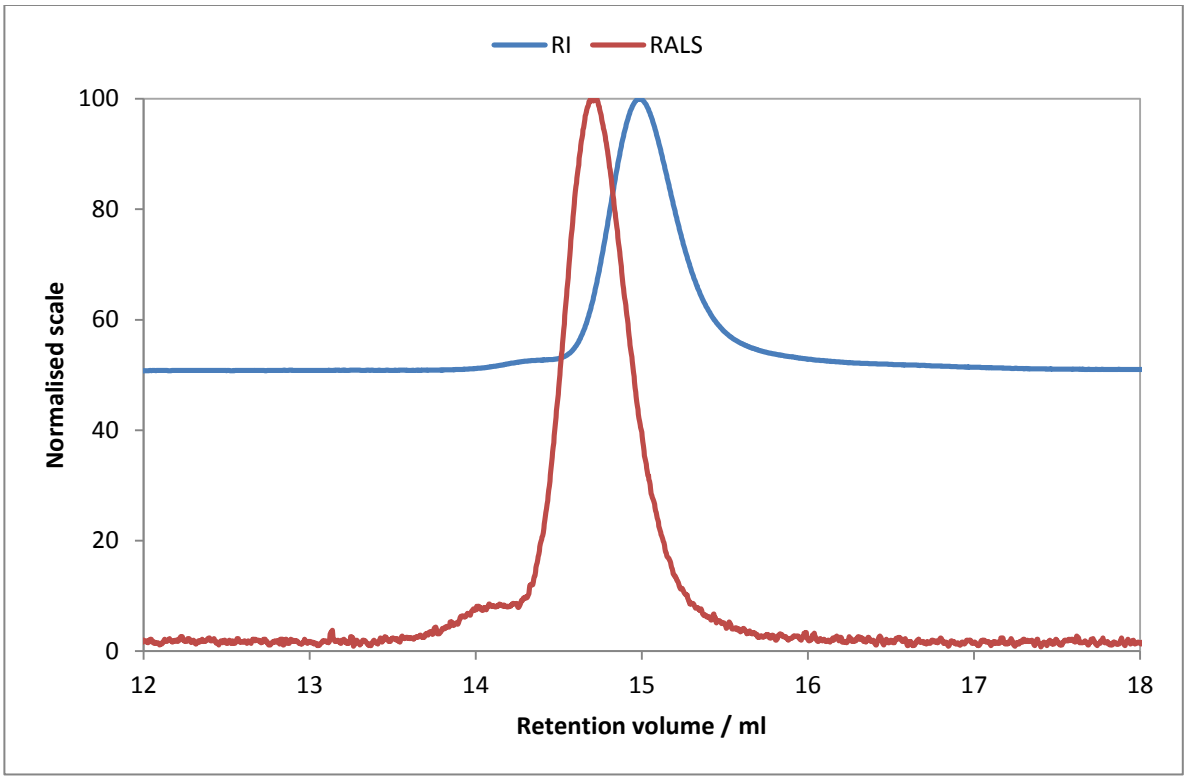

Figure 2.02. SEC data (Refractive Index and Right-Angle Light Scattering only) for the 10,000 g mol^{-1} RAFT polymerisation of styrene mediated by cumyl dithiobenzoate.

In an attempt to increase monomer conversion a polymerisation was conducted in solution as opposed to the bulk, using 1,4-dioxane as a solvent. Interestingly though this led to 100% monomer conversion and a degree of control was maintained over the molecular weight, it led to a complete loss of control over polydispersity yielding a polymer with a M_n of 8,300 g mol^{-1} and a PDI of 2.38. At this point it was decided to move on to RAFT polymerisation of the NVP monomer.

2.2 RAFT of NVP with *S*-malonyl *N,N*-diphenyldithiocarbamate (DPCM)

2.2.1 Introduction

Having familiarised ourselves with the RAFT process, it was then decided to try and replicate some of the work done by Gnanou *et al.*[4] with DPCM and NVP in order to gain some experience with the use of this monomer and also the synthesis of DPCM on which the syntheses of our proposed novel CTAs were to be based. Though NVP has been polymerised for many years by means of free radical polymerisations, it was only recently[4] that it has been successfully polymerised in a controlled fashion using the RAFT process (or any other form of controlled polymerisation). While the use of DPCM as a CTA was well documented in this paper, its synthesis was not described and at the time we were unable to find it described elsewhere in the literature. The synthesis described here was originally thought to be novel, though it later transpired that it was very similar to that used by Gnanou which was discovered later in a patent application.[5] Thus some of the CTA syntheses presented later in this thesis are slightly different to our original synthesis. The most important difference is whether the R-group focal point is a bromide or a chloride which determines the reactivity of the R-group during the CTA synthesis, resulting in a significant impact on the required reaction conditions. In addition the use of either sodium amide or sodium hydride is permissible as a deprotonating agent, sodium amide requiring storage and handling under an inert atmosphere and sodium hydride in mineral oil, though inert in air, requiring a time consuming washing process to remove the mineral oil. Other than these differences though, all of the CTA syntheses in this thesis are essentially based on the same underlying method.

2.2.2 CTA synthesis

The original DPCM synthesis shown in Figure 2.03 consists of a one pot process whereby the CTA is built up from the Z-group end (diphenylamino moiety) through to the R-group end (diethyl malonate moiety). This starts with the deprotonation of diphenylamine allowing subsequent nucleophilic attack by the resulting anion on carbon disulfide, and finally a nucleophilic substitution reaction (S_N2) with diethyl chloromalonate.

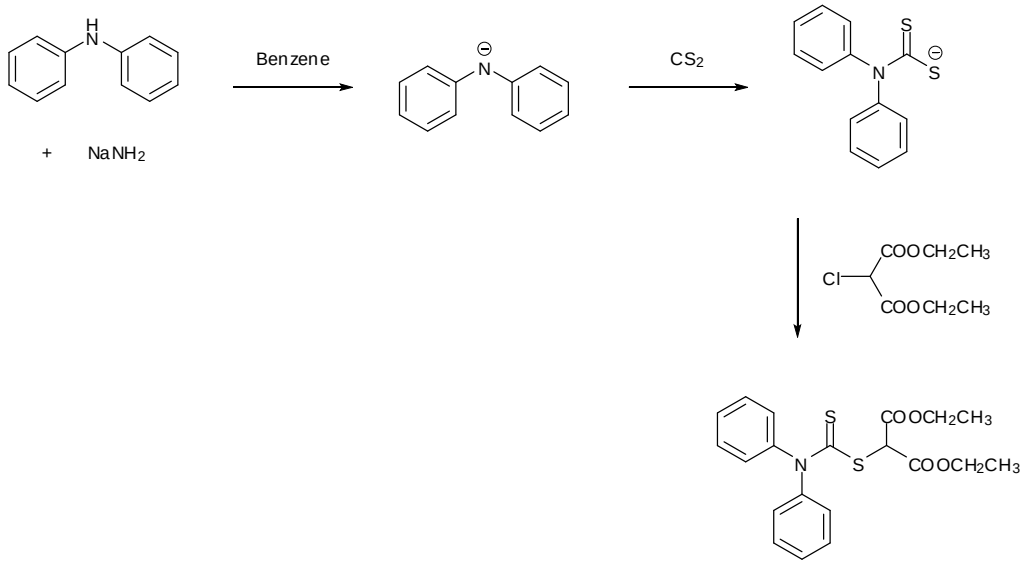

Figure 2.03. Reaction scheme for the synthesis of S-malonyl N,N-diphenyldithiocarbamate (DPCM), a CTA suitable for the RAFT polymerisation of N-vinyl pyrrolidone.

The synthesis was performed as described in the experimental chapter, and after washing the organic phase with water, separating, drying and filtering, the product was obtained as a light yellow solid in 82% yield. Whilst the procedure described in the aforementioned patent application[5] varied in minor details to that described here, the workup was essentially the same and at this point claimed the purity of the product was verified by ^{1}H NMR, however we found that further purification was

necessary by recrystallisation from toluene, the resulting final product being obtained as a light yellow solid in 21% yield.

2.2.3 RAFT polymerisations

RAFT polymerisations of NVP using DPCM as a CTA were performed as described in the experimental chapter, in 1,4-dioxane under a nitrogen atmosphere at 80°C for 36 hours, using AIBN as initiator. After filtration and drying under vacuum to a constant mass, the polymers were analysed by triple detection SEC.

Table 2.1. SEC data for 10,000 g mol^{-1} DPCM-mediated RAFT polymerisations of NVP.

Target M_n / g mol^{-1}	**M_n (SEC) / g mol^{-1}**	**PDI**	**% Monomer conversion**
10,000	9,500	1.25	82%
10,000	8,750	1.28	80%
10,000	10,200	1.27	82%

As can be seen from Table 2.1, the use of DPCM as a CTA in the RAFT polymerisation of NVP gave good control over both molecular weight and polydispersity, and its performance in this regard was directly comparable to that published in the literature.[4]

2.3 Attempt at a Zonyl fluorotelomer-based CTA

2.3.1 Introduction

Our first proposed fluorinated CTA synthesis was to start from readily and cheaply available fluoro-alcohols such as the Aldrich "Zonyl" fluorotelomer intermediates[6] as shown in Figure 2.04. The main advantage of these materials was their extremely low cost compared to that of the 3-perfluorooctyl propanol used as the basis for the later novel fluorinated CTAs presented in this thesis. In addition to the financial benefits of using these materials, it was also hoped that after one halogenation reaction they would be ready for incorporation into the DPCM synthesis in order to make the first of the proposed novel fluorinated CTAs. In theory the Zonyl-based CTAs would be considerably less labour intensive to make than the 3-perfluorooctyl propanol-based CTAs discussed in the next chapter.

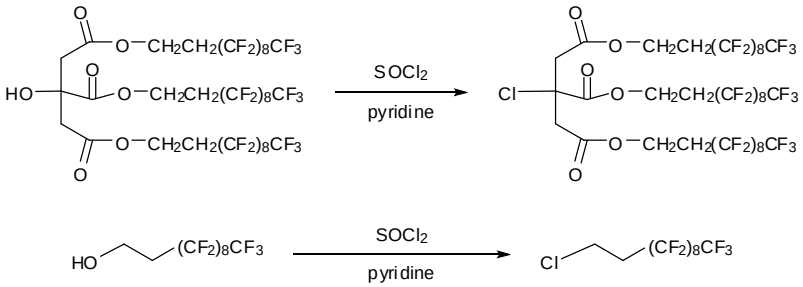

Figure 2.04. Chlorination reactions of Zonyl TBC and Zonyl BA fluorotelomer intermediates respectively. These R-group chlorides would then be incorporated into the final step of the original DPCM synthesis.

It was hoped that these could be easily chlorinated with the use of thionyl chloride, and then the resulting chlorides used in the final step of the original synthesis of DPCM in place of diethyl chloromalonate to give two fluorinated DPCM analogues.

2.3.2 Halogenation of Zonyl fluorotelomer intermediates

The first step in the synthesis of these DPCM derived fluorinated CTAs was to chlorinate the alcohol groups of the commercially available Zonyl TBC and BA fluorotelomer intermediates. Initial experiments were carried out on a small scale (1-2g), using thionyl chloride to chlorinate each of the alcohols.

Either Zonyl BA or TBC was placed under a dry nitrogen atmosphere before being dissolved in dry acetone, to which was added dry benzene and an 8x excess of anhydrous pyridine. As can be seen from the reaction mechanism shown in Figure 2.05, pyridine is required in order to deprotonate the reaction intermediate and maintain a basic environment ensuring a high concentration of chloride ions. In the absence of pyridine, thionyl chloride would simply react with the Zonyl intermediate resulting in the chlorosulfite.

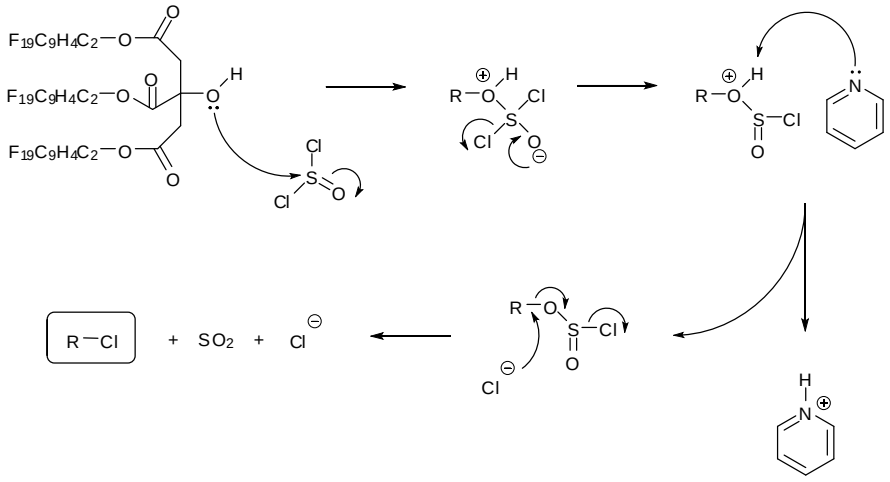

Figure 2.05. Reaction mechanism for the desired halogenation of the Zonyl TBC fluorotelomer intermediate using thionyl chloride and pyridine. The first step is a nucleophilic addition reaction and following rearrangement of the reaction intermediate the Zonyl compound is halogenated via an S_N2 nucleophilic substitution mechanism.

2.3.3 Results

Unfortunately several problems were encountered with these reactions, mainly to do with the limited solubility of the reactants in most common solvents. The Zonyl materials were only soluble in acetone and while it was thought it might be possible to chlorinate these materials in a mixture of acetone and benzene, this would not have been the case for the following CTA synthesis. The crude product was only obtainable in relatively poor yield, and even after being subjected to column chromatography was still a mixture of materials which proved inseparable and further purification was not possible. As such it was not possible to characterise these materials properly. It is strongly suspected that a side reaction may have occurred between the thionyl chloride and one of the solvents used in this reaction: acetone. Acetone is a ketone and what was not considered until after performing these two reactions is the possibility of a side reaction with acetone's enol tautomer. While the enol form was unlikely to be present in any great quantity under basic conditions (as not only is it orders of magnitude less stable than the keto form, but its formation is also acid catalysed), it may well have been enough to react with thionyl chloride over a 24 hour period in sufficient quantities to cause a problem.

The next step of the synthesis would have been to couple the chloride to DPCM to make the proposed Z_{TBC}-DPCM and Z_{BA}-DPCM CTAs, however it is necessary for this reaction to be performed in benzene (owing to the fact that benzene is the only solvent that all of the reactants are soluble in) and neither of the fluorotelomer intermediates was at all soluble in benzene. Due to the difficulties encountered with these very cheap fluorinated materials, it was decided to abandon this avenue of research and move on to the next step of making a dendritic CTA for use with NVP.

2.4 NVP RAFT with a first generation Frechét-type dendritic CTA (G1-DPCM)

2.4.1 CTA synthesis

Before moving on to synthesising the proposed novel fluorinated CTAs, both a labour intensive and expensive process, it was decided to attempt to make a simpler novel CTA for use with NVP. The diphenyldithiocarbamate of 3,5-dibenzyloxybenzyl chloride (G1-DPCM, Figure 2.06) was chosen as a suitable novel CTA for proof of concept: an otherwise unfunctionalised first generation, Frechét-type aryl-ether[7] dendritic CTA. This served both the purpose of demonstrating that it was possible to make a DPCM analogue with a different R-group, and also that an aromatic R-group (thus producing a benzyl radical during the RAFT process) would in fact still facilitate the controlled RAFT polymerisation of NVP. This is of note as G1-DPCM shares this trait with the planned fluorinated DPCM analogues discussed in the next chapter (DPFPB-DPCM and TPFPB-DPCM), and so would give a good indication of how well these fluorinated CTAs could be expected to perform in the RAFT polymerisation of NVP.

As discussed in Chapter 1, significant changes in the chemical structure of the R-group give rise to a CTA with a different chain transfer constant (C_{tr}) resulting in varying performance as a CTA with a specific monomer. The proposed G1-DPCM was an ideal proof of concept as not only did the dendritic R-group have a very similar structure to the proposed fluorinated CTA R-groups in terms of the part of the molecule that is involved in the re-initiation step of RAFT polymerisation, but also the manner in which the molecule is constructed is very similar as well. The synthesis of the G-1 dendritic R-group shown in Figure 2.06 comprises of an Appel reaction[8,9] and a Williamson ether coupling,[10] both of which are discussed in more detail in Chapter 3.

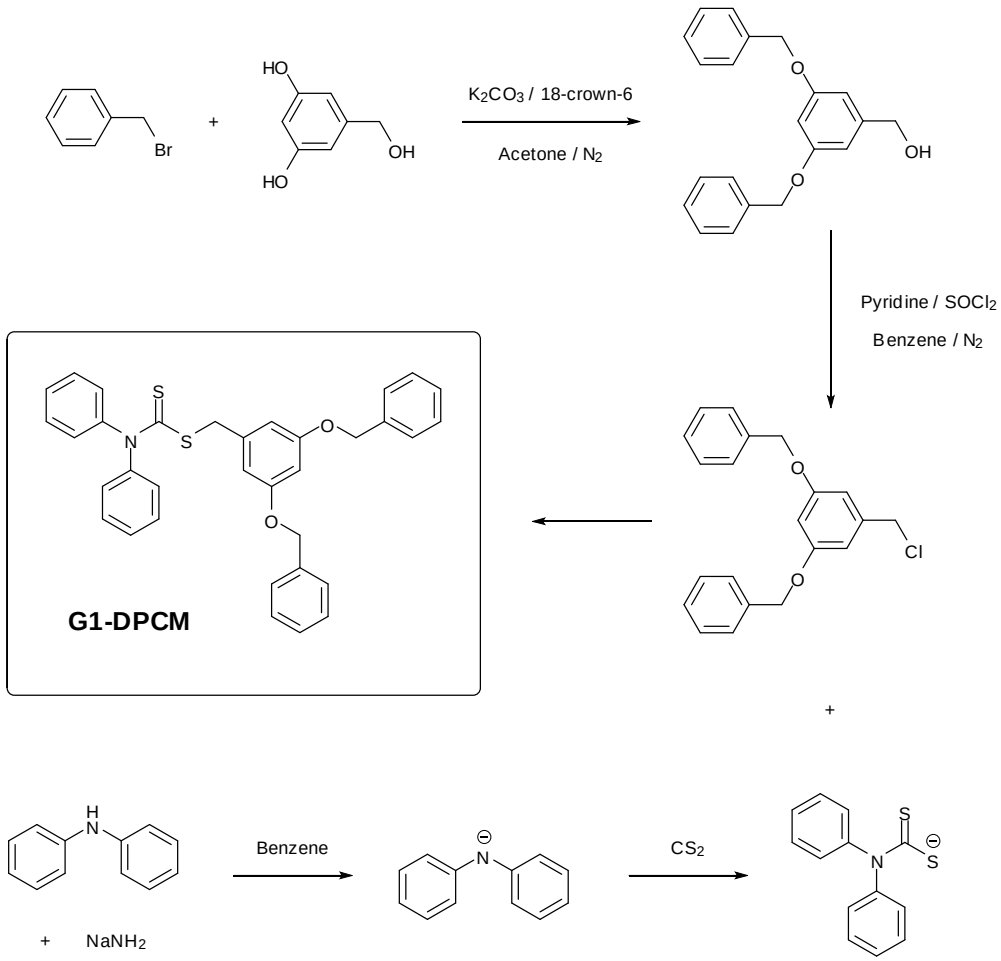

Figure 2.06. Reaction scheme for the synthesis of S-3,5-dibenzyloxybenzyl N,N-diphenyldithiocarbamate (G1-DPCM), a novel dendritic chain transfer agent for use in the RAFT polymerisation of N-vinyl pyrrolidone.

As can be seen in Figure 2.06 the synthesis is begun with the Williamson ether coupling of benzyl bromide to 3,5-dihydroxybenzyl alcohol, performed using dry potassium carbonate and 18-crown-6 crown ether as a catalyst in dry acetone under a dry nitrogen atmosphere. The procedure detailed in the experimental chapter was followed, affording the product (3,5-dibenzyloxybenzyl alcohol) as a white crystalline powder in 61% yield. The NMR spectra for each intermediate compound in this synthesis are shown in Figure 2.07, the second spectrum being for this compound and the first being for benzyl bromide. In the first spectrum for

benzyl bromide, the singlet attributable to the bromine-adjacent CH_2 and the multiplet corresponding to the five aromatic protons are clearly visible. Upon completing the coupling step described so far, we would expect a shift in the CH_2 peak owing to its new chemical environment, and the introduction of three new peaks attributable to the two different types of aromatic proton and the CH_2-OH peak now present in 3,5-dibenzyloxybenzyl alcohol, all of which can be seen in the NMR for this compound.

Having performed the initial coupling of benzyl bromide to 3,5-dihydroxybenzyl alcohol to give a Frechét-type G1 dendron with an alcohol group at its focal point, this alcohol then needed to be converted into a halide before continuing with the final CTA synthesis. This was accomplished by means of a chlorination reaction using thionyl chloride and pyridine in dry benzene under an atmosphere of dry nitrogen gas, as detailed in the experimental chapter, affording the product as a white powder in 62% yield. As can be seen in the NMR spectra shown in Figure 2.07, the spectrum for 3,5-dibenzyloxybenzyl chloride is almost identical to that of its precursor, though as one would expect the CH_2OH / CH_2Cl peak has shifted position owing to its new chemical environment.

This halogenation reaction has produced a G1 Frechét-type dendron with a chloride at its focal point making it a suitable R-group for incorporation into the original DPCM synthesis[11] in order to make a G1 Frechét-type dendronised CTA: G1-DPCM. In this final step the CTA is built up in a one pot synthesis with the use of diphenylamine, sodium amide as a deprotonating agent, carbon disulfide and the dendritic R-group, 3,5-dibenzyloxybenzyl chloride. The product was a yellow solid obtained in 55% yield. As can be seen from the ^{1}H NMR spectrum shown in Figure 2.07, there is a shift in the position of the formerly CH_2Cl peak (latterly CH_2S) owing to its new chemical environment, and we also see a doubling in intensity of the aromatic multiplet at ~7.4-7.5 ppm due to the introduction of 10 additional aromatic protons on the diphenylamino group. All expected and measured integral values that have been discussed for the NMRs shown in Figure 2.07 can be seen in Table 2.2.

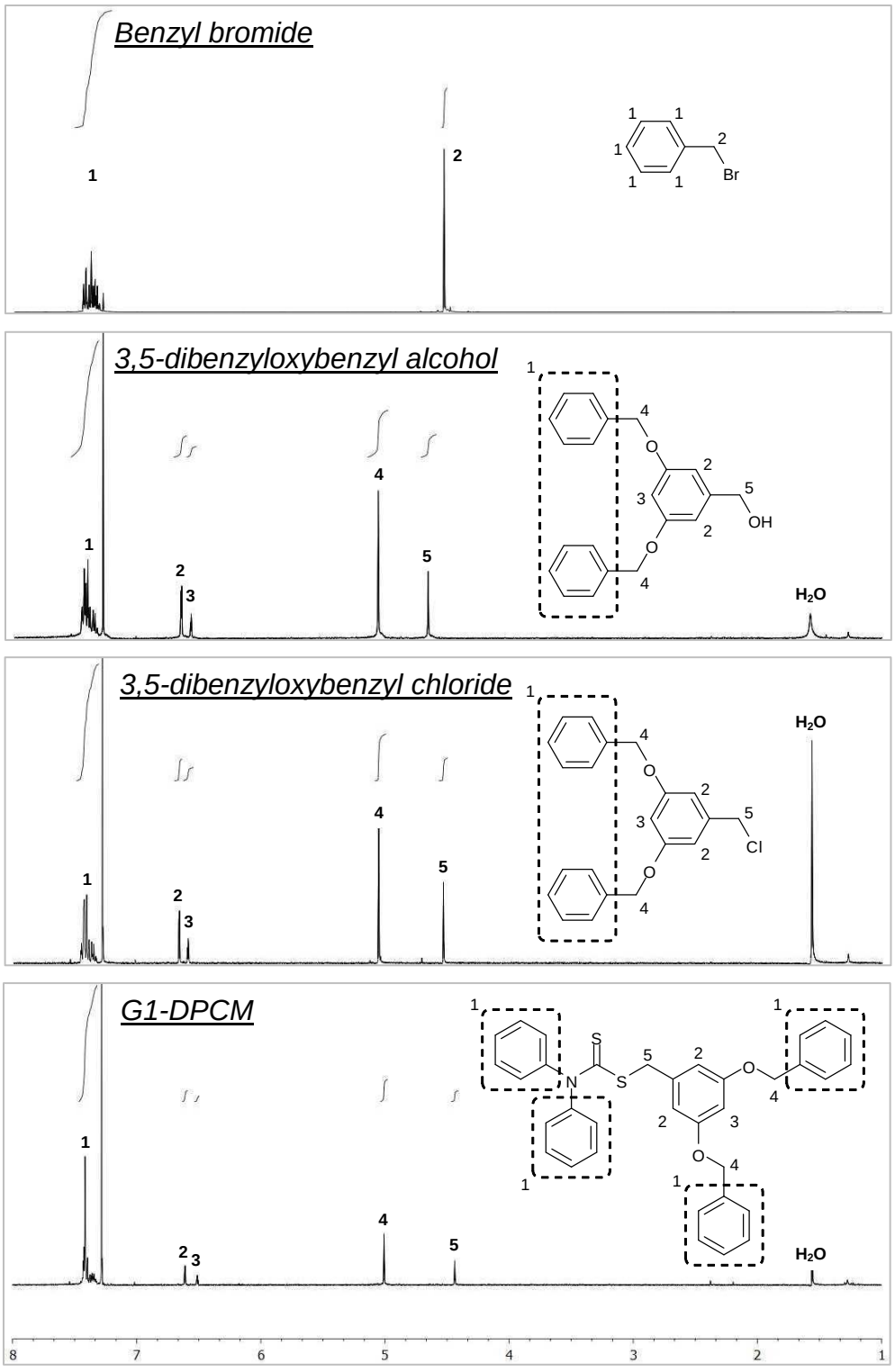

Figure 2.07. Series of NMR spectra showing the starting material (benzyl bromide), each reaction intermediate and the final product for the synthesis of the G1-DPCM dendritic CTA.

Table 2.2. Integral data for the ^{1}H NMR spectra shown in Figure 2.07 showing expected and measured integral values for each peak.

Compound	**Peak** #*	**Proton**	**Expected integral**	**Measured integral**
Benzyl bromide	1	Ar*H*	5	4.99
	2	CH_2Br	2	*2.00***
3,5-dibenzyloxybenzyl alcohol	1	2x*Ph*	10	10.59
	2	Ar*H*CH_2OH	2	2.04
	3	Ar*H*OCH_2Ph	1	*1.00***
	4	CH_2Ph	4	4.08
	5	CH_2OH	2	2.03
3,5-dibenzyloxybenzyl chloride	1	2x*Ph*	10	10.73
	2	Ar*H*CH_2Cl	2	2.01
	3	Ar*H*OCH_2Ph	1	*1.00***
	4	CH_2Ph	4	4.04
	5	CH_2Cl	2	2.01
G1-DPCM	1	4x*Ph*	20	20.02
	2	Ar*H*CH_2S	2	1.97
	3	Ar*H*OCH_2Ph	1	*1.00***
	4	CH_2Ph	4	3.99
	5	CH_2S	2	1.95

*Peak number in reference to assignments made in Figure 2.07.

**Normalised integral value set to relevant integer for this peak.

2.4.2 RAFT polymerisations

Having successfully made the first proposed novel CTA for use with *N*-vinyl pyrrolidone, two RAFT polymerisations were then performed aiming for molecular weights of 10,000 g mol^{-1} and 20,000 g mol^{-1}. The required amounts of CTA and initiator were calculated using the standard equation of RAFT polymerisation which is discussed in more detail in the experimental chapter of this thesis, and which is shown below as equation 2.1.

$$[RAFT]_0 = \frac{[M]_0 \cdot M_M \cdot x}{M_n - M_{RAFT}} \qquad 2.1$$

Where $[RAFT]_0$ is the initial concentration of CTA, $[M]_0$ is the initial concentration of monomer (worked out from density of NVP [1.045 g cm^{-3}]), M_M is the molecular mass of the monomer, **x** is a decimal between zero and one representing the assumed fractional conversion of monomer into polymer, M_n is the desired molecular weight of the polymer being produced, and M_{RAFT} is the molecular weight of the CTA.

Before discussing the results of these two polymerisations it is important to note that in calculating the appropriate amounts of CTA and initiator for the desired target molecular weights, a value of 0.8 was used for "**x**". This assumption that the polymerisations would proceed to 80% monomer conversion was simply based on our previous experience with the DPCM CTA used in earlier RAFT polymerisations of NVP and the original information in the literature pertaining to this CTA.[4]

Table 2.3. SEC data for the 10,000 g mol^{-1} and 20,000 g mol^{-1} G1-DPCM RAFT polymerisations of NVP.

Target M_n / g mol^{-1}	M_n (SEC) / g mol^{-1}	PDI	Revised Target M_n / g mol^{-1}
10,000	7,900	1.27	5,400 based on x = 0.41
20,000	14,000	1.36	14,150 based on x = 0.56

As can be seen from Table 2.3, the 10,000 g mol^{-1} polymerisation yielded a polymer with a M_n of 7900 g mol^{-1} and a PDI of 1.27 with 41% monomer conversion. The 20,000 g mol^{-1} polymerisation yielded a polymer with a M_n of 14,000 g mol^{-1} and a PDI of 1.36 with 56% monomer conversion. The first thing to note is that while in both cases the molecular weight is lower than expected, the CTA has clearly imparted a reasonable degree of control over the polydispersity of the resulting polymers (control polymerisations with AIBN initiator but no CTA yielded polymers with PDIs of typically greater than 2.0). While the achieved molecular weights are lower than their targets, when the lower monomer conversions are taken into account, the discrepancy actually becomes far less significant. When rearranging Equation 2.1 to make M_n the subject and substituting in the measured monomer conversions (x = 0.41 and 0.56 respectively), we are furnished with new expected molecular weights of 5,400 g mol^{-1} and 14,150 g mol^{-1} which are far closer to those measured by SEC.

While in the case of the higher molecular weight polymer, the new target molecular weight is in precise agreement with the experimentally determined molecular weight, there is still a slight discrepancy in the case of the lower molecular weight polymer. While this discrepancy is not hugely significant, it is worth noting that the monomer conversions for each polymerisation were calculated from the yield, which in turn was calculated from the mass of obtained polymer. While every care was taken to be as efficient as possible when working up the polymer, it would not

be unreasonable to assume at this lower molecular weight that the end-group may have an effect on the solubility of the polymer in diethyl ether, the non-solvent used to precipitate the polymer in the workup. If some of the polymer were lost through increased solubility in the diethyl ether then this would result in a lower calculated monomer conversion which when substituted into Equation 2.1 would give rise to a lower expected molecular weight. It is interesting to note that if we take the value of 56% monomer conversion from the higher molecular weight polymerisation and substitute x = 0.56 into the equation for the lower molecular weight polymerisation, we get an expected molecular weight of 7,150 g mol^{-1} which is much closer to the actual value as determined by SEC.

In undertaking the work presented in this chapter, several important objectives were achieved that were necessary to progress with the synthesis of novel fluorinated CTAs for the RAFT polymerisation of NVP, as discussed in Chapter 3. Firstly, we familiarised ourselves with the RAFT process by successfully performing several RAFT polymerisations of styrene using cumyl dithiobenzoate as CTA. We then synthesised DPCM, a CTA used for the RAFT polymerisation of NVP, and familiarised ourselves further with the RAFT process, specifically as applied to our monomer of interest. Several RAFT polymerisations of NVP were performed, yielding well-defined PVP of predetermined molecular weights. Finally, a novel synthesis was devised for a dendritic CTA, G1-DPCM, in order to make well-defined, end-functionalised PVP. This novel CTA performed adequately, giving good control over molecular weight and producing PVP with a high degree of end-functionalisation. Satisfied that a good understanding of RAFT had been obtained, and with a novel CTA successfully utilised in the RAFT polymerisation of NVP, focus was then turned to one of the primary objectives of this research: the synthesis of novel, fluorinated CTAs.

2.5 References

[1] Barner-Kowollik, C.; Quinn, J. F.; Morsley, D. R.; Davis, T. P.; *J. Polym. Sci., Part A: Polym. Chem.*, **2001**, *39*, 1353

[2] Plummer, R.; Goh, Y.-K.; Whittaker, A. K.; Monteiro, M. J.; *Macromolecules*, **2005**, *38*, 5352

[3] Arita, T.; Buback, M.; Vana, P.; *Macromolecules*, **2005**, *38*, 7935

[4] Bindu, R. L.; Borsali, R.; Devasia, R.; Gnanou, Y.; Mougin, N.; *Macromol. Symp.*, **2005**, *229*, 8

[5] United States Patent Application 20060088487 <http://www.freepatentsonline.com/y2006/0088487.html> (15th Jan 2008)

[6] *DuPont™ Zonyl® Fluorochemical Intermediates (product line information document)*, DuPont, **2002**

[7] Hawker, C. J.; Fréchet, J. M. J.; *J. Am. Chem. Soc.*, **1990**, *112*, 7639

[8] Downie, I. M.; Holmes, J. B.; Lee, J. B.; *Chem. Ind. (London)*, **1966**, 900

[9] Appel, R.; *Angew. Chem. Int. Ed. (English)*, **1975**, *14*, 801

[10] Williamson, A.; *Philos. Mag.*; **1850**, *37*, 350

[11] Charmot, D.; Destarac, M.; Frank, X.; Zard, S.; *Macromol. Rapid Commun.*, **2000**, *21*, 1035

Chapter 3
Results and Discussion

Novel fluorinated Chain Transfer Agent synthesis; Reversible Addition-Fragmentation Transfer polymerisation of *N*-vinyl pyrrolidone to give well defined, low molecular weight, end-functionalised poly *N*-vinyl pyrrolidone additives; thin film analysis by contact angle analysis, Ion Beam Analysis, Atomic Force Microscopy and Thermogravimetric Analysis

3.1 Synthesis

3.1.1 Functionalised R group synthesis

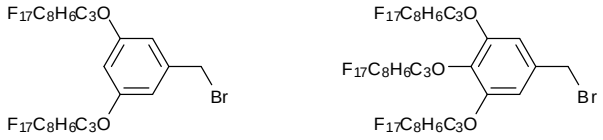

DPFPB-Br **TPFPB-Br**

Figure 3.01. Chemical structure of the di-functional R group (DPFPB-Br) and the tri-functional R group (TPFPB-Br).

Both the di-functional and tri-functional R groups are built up primarily by means of a series of Appel reactions[1,2] (in the case of this work, brominations of primary alcohols) and Williamson ether couplings,[3] starting with a commercially available, single chain fluoroalcohol (3-perfluorooctyl-1-propanol, PFP-OH) as shown in Figure 3.02. All reaction steps in this overall synthesis contain either moisture sensitive reagents or reaction intermediates and as such all were performed under anhydrous conditions with the use of pre-dried solvents and a dry nitrogen atmosphere, as detailed in Chapter 5.

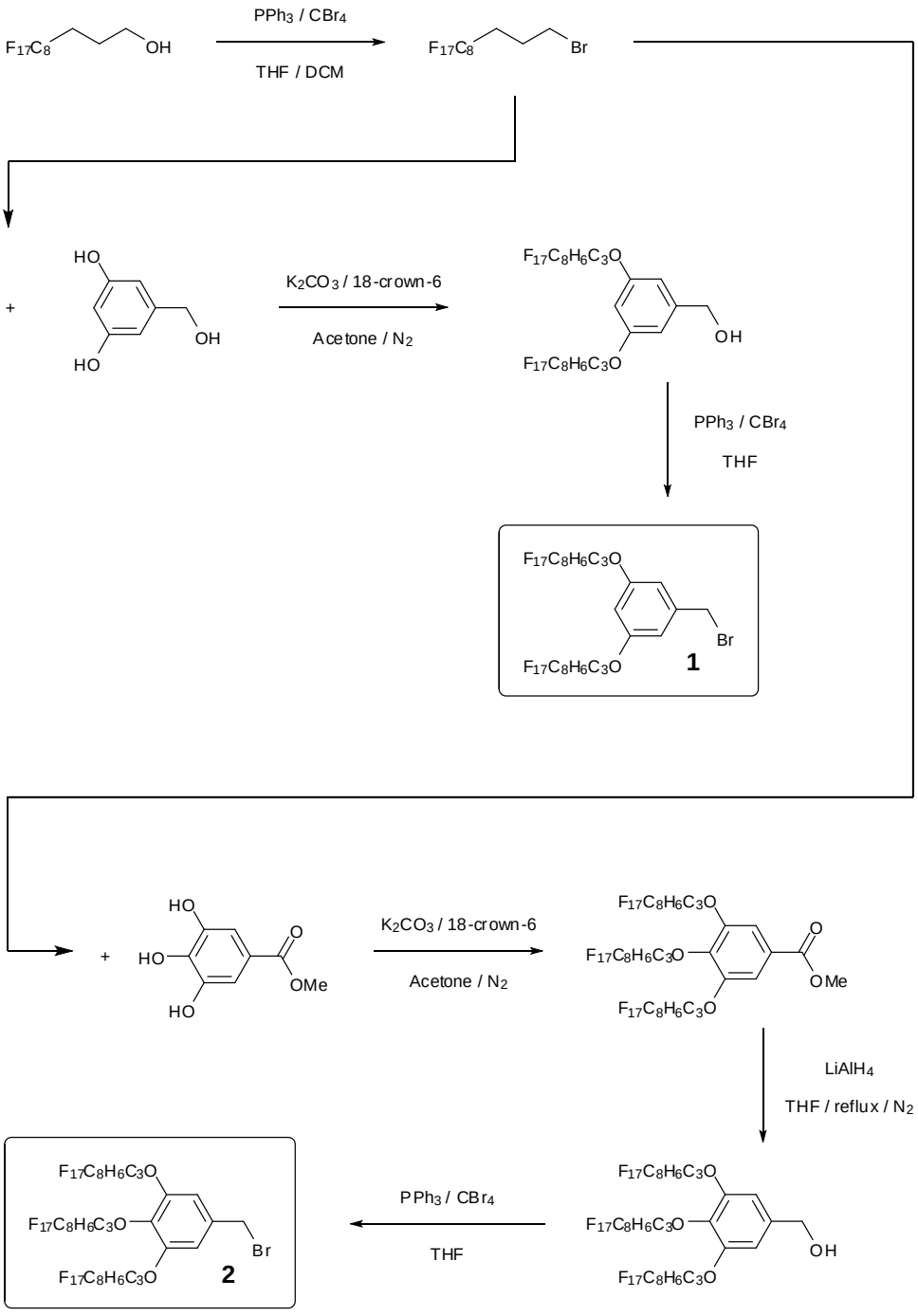

*Figure 3.02. Reaction scheme for the synthesis of the di-functional R group (DPFPB-Br, **1**) and the tri-functional R group (TPFPB-Br, **2**).*

The initial step in both syntheses is the bromination of PFP-OH by means of an Appel reaction to give 1-bromo-3-perfluorooctyl propane (PFP-Br). The term "Appel reaction" refers to the halogenation of an alcohol by means of a bi-molecular nucleophilic substitution (S_N2) as shown in Figure 3.03.[4] The product was obtained in 79-85% yield, and ^1H NMR spectra for PFP-OH and PFP-Br can be seen in Figure 3.05, showing a clear shift in the position of all three CH_2 peaks owing to the change in functionality.

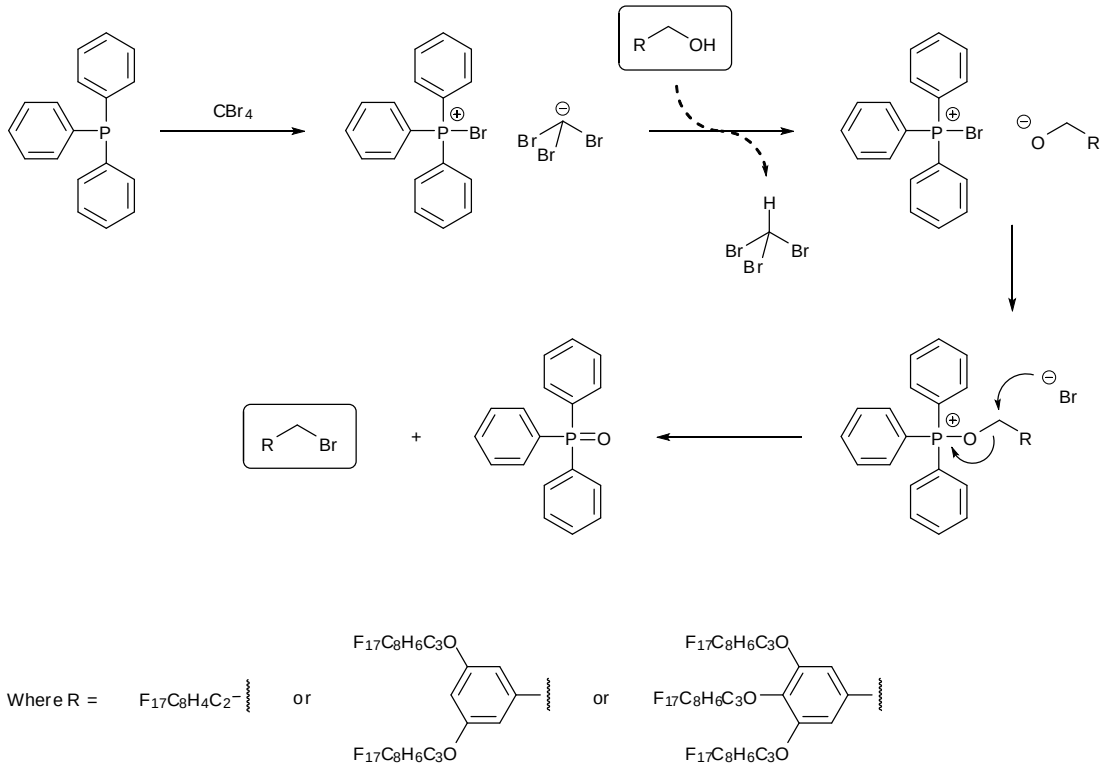

Figure 3.03. General reaction scheme for an "Appel reaction" whereby an alcohol is halogenated by means of a bi-molecular nucleophilic substitution (S_N2).[4]

Once brominated, PFP-Br can be coupled to the phenol groups of either 3,5-dihydroxybenzyl alcohol to give 3,5-(di-3-(perfluorooctyl)propyloxy)benzyl alcohol (DPFPB-OH), or methyl-3,4,5-trihydroxybenzoate (THB-COOMe) to give methyl-

3,4,5-(tri-3-(perfluorooctyl)propyloxy)benzoate (TPFPB-COOMe), depending upon which functionalised R group is being made. This is accomplished by means of a Williamson ether coupling reaction, an example of which is shown in Figure 3.04.[5] DPFPB-OH was obtained in 73-81% yield, and the ^{1}H NMR spectra for PFP-Br and DPFPB-OH are shown in Figure 3.05, where an obvious shift in the position of the $F_{17}C_8CH_2CH_2CH_2$- peak can be seen, as well as the introduction of two Ar*H* peaks, and a C*H*$_2$OH peak.

TPFPB-COOMe was obtained in 87-91% yield, and the ^{1}H NMR spectrum for PFP-Br and THB-COOMe are shown in Figure 3.06, where not only can be seen the introduction of an Ar*H* peak along with a –COO*Me* peak, but also the shifting in position of both the $F_{17}C_8CH_2CH_2CH_2$- and $F_{17}C_8CH_2CH_2CH_2CH_2$- peaks, in addition to their splitting in the ratio of 2:1 owing to their different *meta* and *para* positions on the aromatic ring.

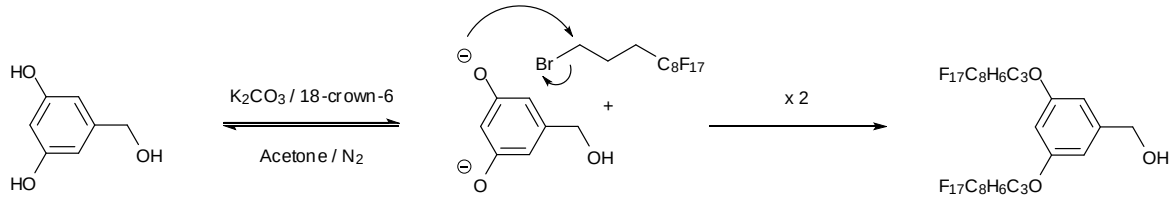

DPFPB-OH

Figure 3.04. Williamson ether coupling of PFP-Br to 3,5-dihydroxybenzyl alcohol to give DPFPB-OH.[5]

In the case of the di-functional synthesis, once this Williamson ether coupling has been performed to give DPFPB-OH, the benzyl alcohol is brominated by means of a second Appel reaction to give the final product, 3,5-(di-3-(perfluorooctyl)propyloxy)benzyl bromide (DPFPB-Br).[6] DPFPB-Br was obtained in 83-88% yield, and the ^{1}H NMR spectra for DPFPB-OH and DPFPB-Br are shown in Figure 3.05, where a clear shift in the position of the C*H*$_2$OH / C*H*$_2$Br

peak can easily be seen.

In the case of the tri-functional R group synthesis, the first coupling step gives TPFPB-COOMe and an extra step is required to first reduce the methyl ester functionality to an alcohol before it is brominated to give the final product. The methyl ester reduction is performed with the use of lithium aluminium hydride in order to give 3,4,5-(tri-3-(perfluorooctyl)propyloxy)benzyl alcohol (TPFPB-OH). TPFPB-OH was obtained in 86-88% yield, and the ^{1}H NMR spectra for TPFPB-COOMe and TPFPB-OH are shown in Figure 3.06, where a shift in the Ar*H* peak is seen, in addition to the disappearance of the –COO*Me* peak and appearance of a CH_2OH peak.

A last Appel reaction to brominate the benzyl alcohol gives the final product, 3,4,5-(tri-3-(perfluorooctyl)propyloxy)benzyl bromide (TPFPB-Br).[6] TPFPB-Br was obtained in 81-85% yield, and the ^{1}H NMR spectra for TPFPB-OH and TPFPB-Br are shown in Figure 3.06, where an obvious shift in the CH_2OH / CH_2Br peak can be seen.

In the case of both R group syntheses, it is important to note that the large fluorine content led to problems with solubility, and with each experiment being performed on a larger scale than previously reported,[6] the work-up of each product as well. In the separation with DCM and water that followed each reaction step, this was carried out using a four litre separating funnel, splitting the crude product into approximately 10-15g potions and partitioning it between 1.5L DCM and 1.5L water, all heated to at least 30°C. Care had to be taken due to the low boiling point of DCM, however without gentle warming, full dissolution of each crude product did not appear to be possible. It was found that keeping all of the water used for washing of the product (often up to 20L) and washing this with further DCM to extract any additional product still residing in the aqueous phase greatly enhanced overall yield. This was achieved by adding 1.5L of the water at a time with 1.5L DCM, which was reused unless any precipitate formed in which case the precipitate was redissolved with a small addition of extra solvent and gentle warming, and the solution was isolated and replaced with fresh DCM. This DCM

was then amalgamated, washed three times with clean distilled water, and then added to the rest from the first set of separations. This procedure necessitated the drying of large quantities of DCM over $MgSO_4$ before warm filtration (30°C) and removal of solvent by means of rotary evaporation to isolate the washed product in each reaction step, which contributed heavily to the lengthy production time of each material.

One final complication of note pertaining only to the lithium aluminium hydride reduction of TPFPB-COOMe to TPFPB-OH, was that fresh $LiAlH_4$ was required for each reaction. It was found that even after opening a fresh container under an inert atmosphere of dry nitrogen and resealing it, that subsequent use of the $LiAlH_4$ for this reduction yielded only partial or no success.

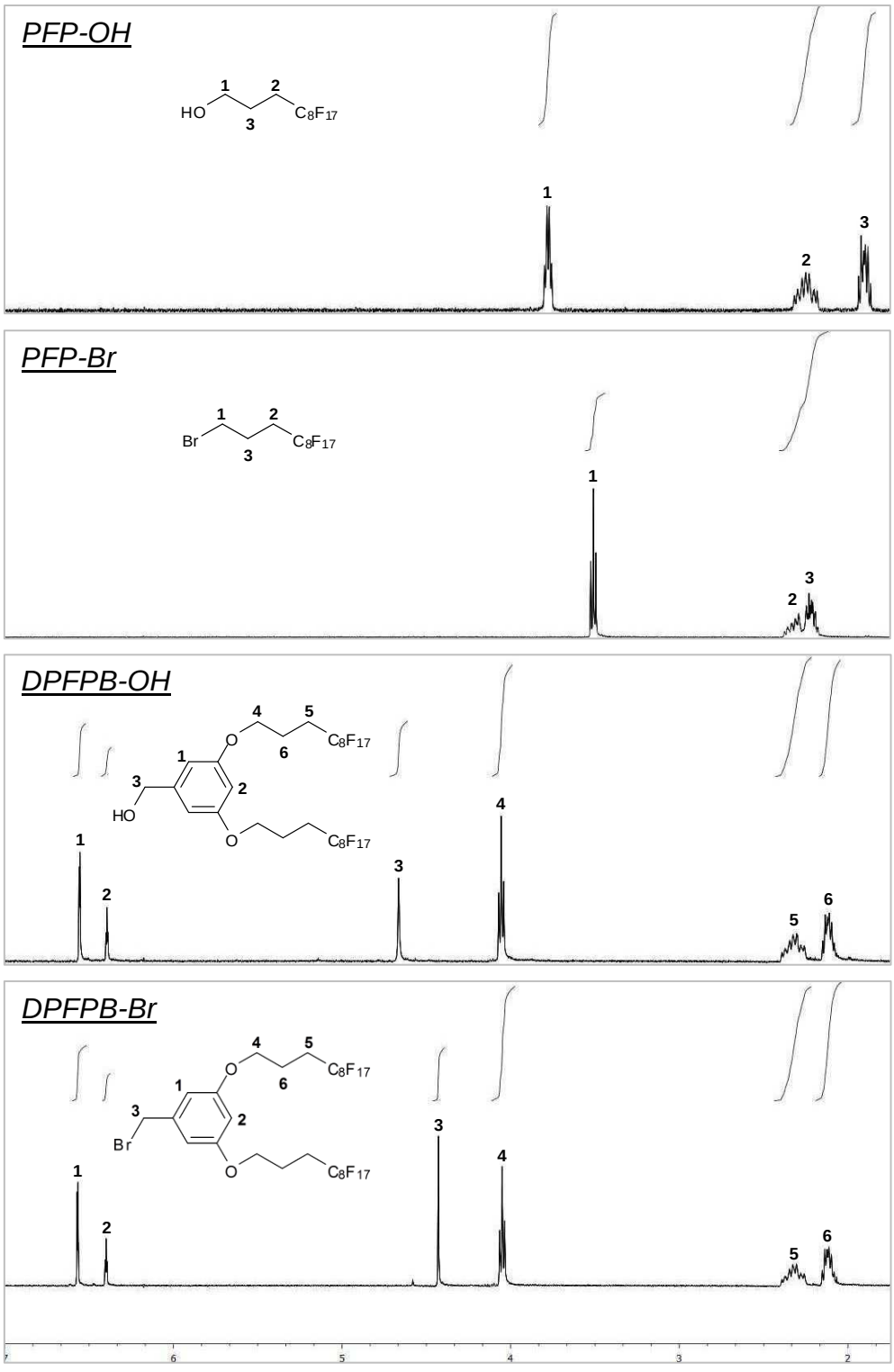

Figure 3.05. Series of NMR spectra showing the starting material (PFP-OH), each reaction intermediate and the final product for the synthesis of the DPFPB-Br R group.

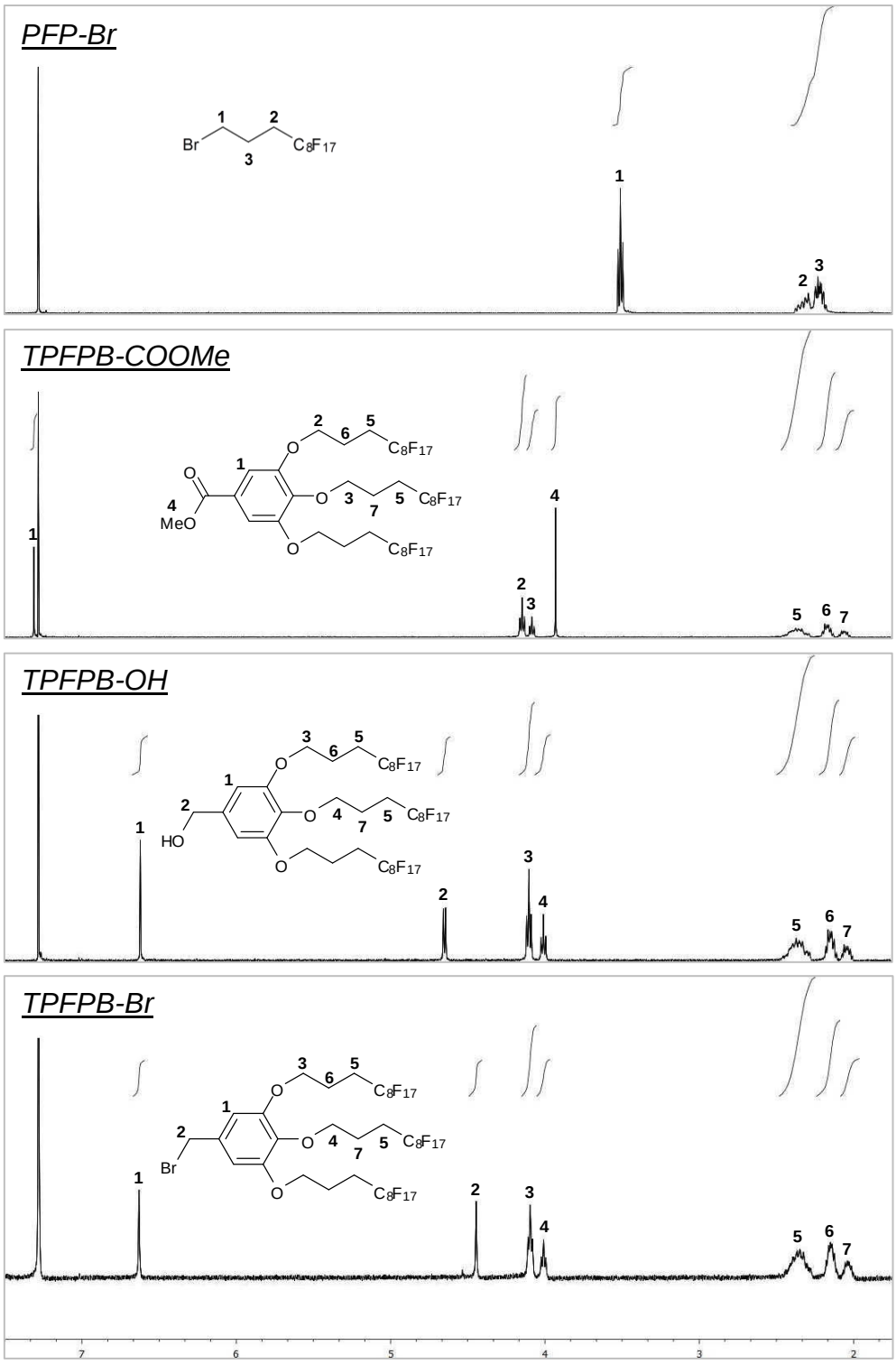

Figure 3.06. Series of NMR spectra showing each reaction intermediate and the final product for the synthesis of the TPFPB-Br R group (the first step involving the bromination of PFP-OH to give PFP-Br is the same as the di-functional synthesis shown in Figure 3.05).

3.1.2 Functionalised chain transfer agent (CTA) synthesis

With the synthesis of the two fluorinated “R groups” (with respect to the CTA, or “end-groups” with respect to the final polymer additive) completed, the next step was to use these R groups to synthesise a CTA for use in the planned subsequent RAFT polymerisations. As previously discussed in Chapter 1 (see pages 48-49), the CTA synthesis is based upon the original synthesis of *S*-malonyl *N,N*-diphenyldithiocarbamate (DPCM),[7] whereby the CTA is built up in a one pot synthesis, in which the R group (in the form of its bromide) is attached to the Z group bearing dithioester moiety in the final step as shown in Figure 3.07. Reaction with DPFPB-Br gives the di-functional CTA, *S*-3,5-(di-3-(perfluorooctyl)propyloxy)benzyl *N,N*-diphenyldithiocarbamate (DPFPB-DPCM), and reaction with TPFPB-Br gives the tri-functional CTA, *S*-3,4,5-(tri-3-(perfluorooctyl)propyloxy)benzyl *N,N*-diphenyldithiocarbamate (TPFPB-DPCM).

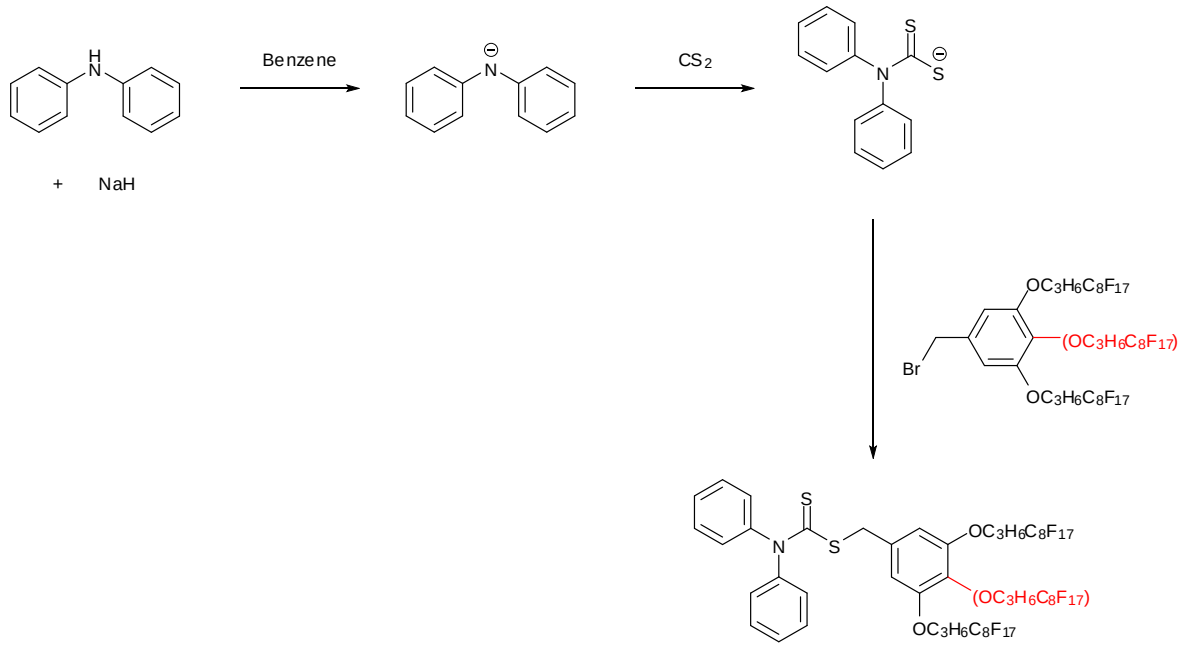

Figure 3.07. Reaction scheme showing the synthesis of both DPFPB-DPCM and TPFPB-DPCM functionalised CTAs.

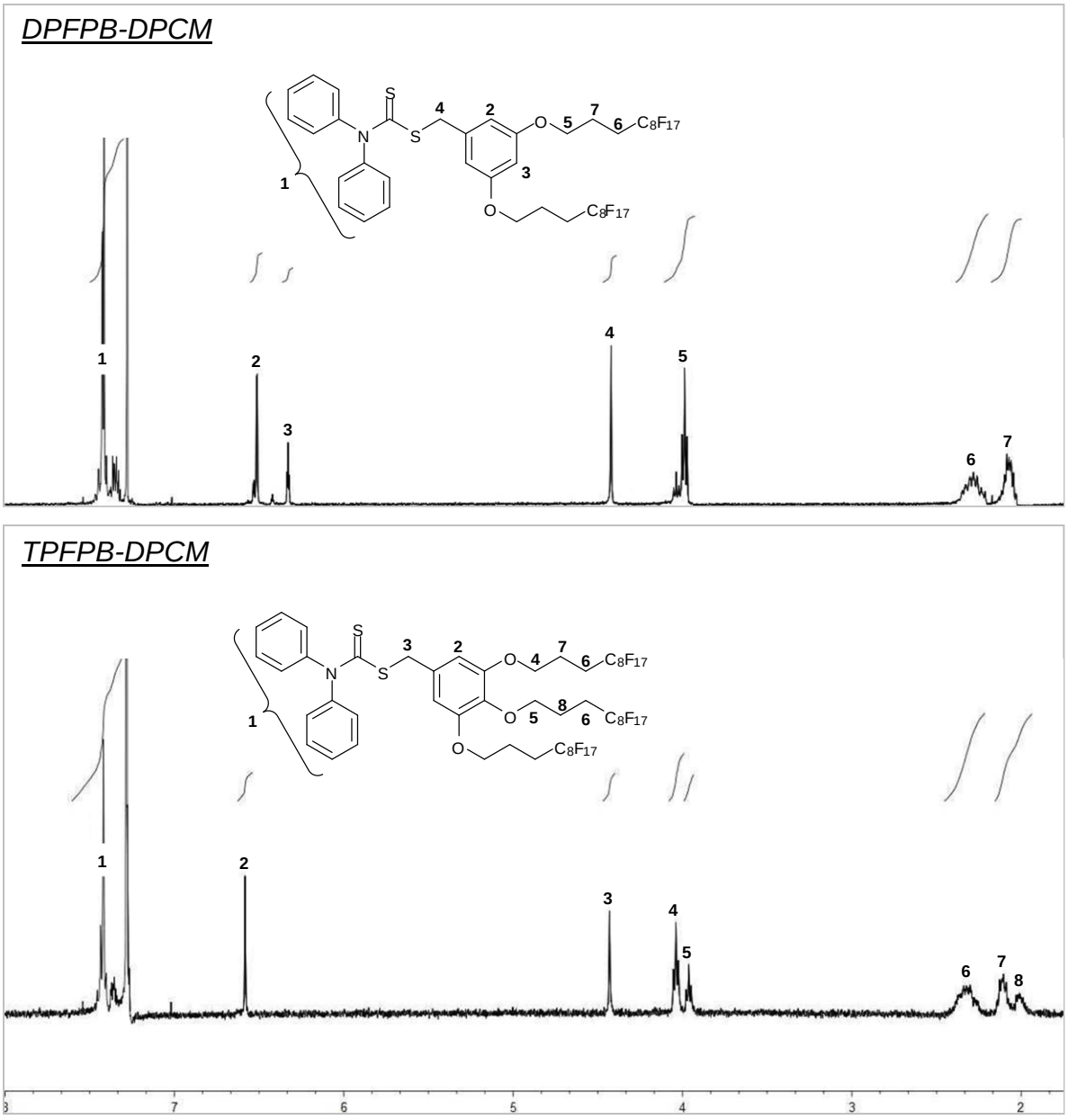

Figure 3.08. NMR spectra for both the di-functional and tri-functional CTAs.

3.1.3 Synthesis of low molecular weight end-functionalised polymer additive

Having made the di-functional and tri-functional CTAs, they were then used to perform RAFT polymerisations with *N*-vinyl pyrrolidone (NVP) in order to make low

molecular weight end-functionalised polymer additives. Before the results of these polymerisations are discussed; a word about notation. For the purposes of this work these additives are defined by the end-functionality (either di-functional or tri-functional according to the CTA used) and their number average molecular weight. Throughout the rest of this thesis they will be referred to in the format "#K# PVP", where the first digit(s) refers to the number average molecular weight (x1000 g mol^{-1}) of the additive as determined by SEC, and the second digit refers to the specific functionality ("2" for di-functional or "3" for tri-functional). For example, the additive referred to as "6K2 PVP" is a polyvinyl pyrrolidone polymer additive with a molecular weight of 6000 g mol^{-1}, end-capped with two C_8F_{17} fluoroalkyl groups.

In addition to the polymer additives that were made in this project, commercially available PVP was used as a PVP matrix in the preparation of thin films for surface analysis. Four different molecular weights of matrix PVP were used, denoted "K15 PVP", "K17 PVP", "K30 PVP" and "K90 PVP".

Table 3.1. Molecular weights for each PVP matrix as quoted by the manufacturer and as determined by SEC.

Type	M_n (manufacturer)	M_n (SEC)
K15 PVP	10,000	6,600
K17 PVP	12,600	32,650
K30 PVP	~40,000	64,400
K90 PVP	~360,000	366,000

All RAFT polymerisations were carried out as detailed in the Chapter 5. A typical polymerisation involved equal volumes of NVP and dioxane, appropriate amount of CTA and initiator based on the target molecular weight of the additive, under an oxygen-free nitrogen atmosphere at a temperature of 80°C. Molecular weights and

polydispersities were determined by means of triple detection SEC using DMF as eluent, and the degree of end functionalization was calculated by ^{1}H NMR spectroscopy, comparing peaks arising from a set of protons from the repeat unit of the polymer backbone against peaks corresponding to the aromatic protons of the fluorinated end-group.

In addition to SEC and ^{1}H NMR spectroscopy, ^{19}F NMR spectroscopy was routinely performed in order to verify the presence of the fluorinated end-group in the polymers. Early polymers were also subjected to dissolution in methanol and re-precipitation in diethyl ether (up to three times) and their ^{1}H NMR spectra repeated in order to verify the continued presence of the end-group signal. Re-precipitation was never required in terms of product purity, but it was performed in order to ensure that the polymer was in fact end-functionalised and not a mixture of unfunctionalised PVP and unreacted RAFT chain transfer agent. No re-precipitation of any end-functionalised polymer led to a change in end-group ^{1}H peak intensities, demonstrating that polymer and end-group were indeed covalently attached, as while diethyl ether is a non-solvent for PVP, it is an exceptional solvent for the fluorinated end-group.

Shown below in Figure 3.09 is a ^{1}H NMR spectrum for 6K2 PVP. In conjunction with the known molecular weight from SEC (and hence the degree of polymerisation), the degree of end-functionality of any specific additive can be calculated by comparing those NMR peaks attributable to the functional end-group with peaks attributable to protons situated within the repeat unit of the polymer backbone. When interpreting the ^{1}H NMR spectra of these additives, the only peaks attributable to the CTA residues on each end of the polymer additive (the diphenylamino-bearing dithioester moiety or the “Z group”, and the fluoroalkyl chain bearing end-functionality or the “R group”) that are visible are in all cases the aromatic protons contained within these residues. These are the only peaks with a chemical shift sufficiently different to and hence resolvable from those of the polymer backbone which are many times more intense in comparison.

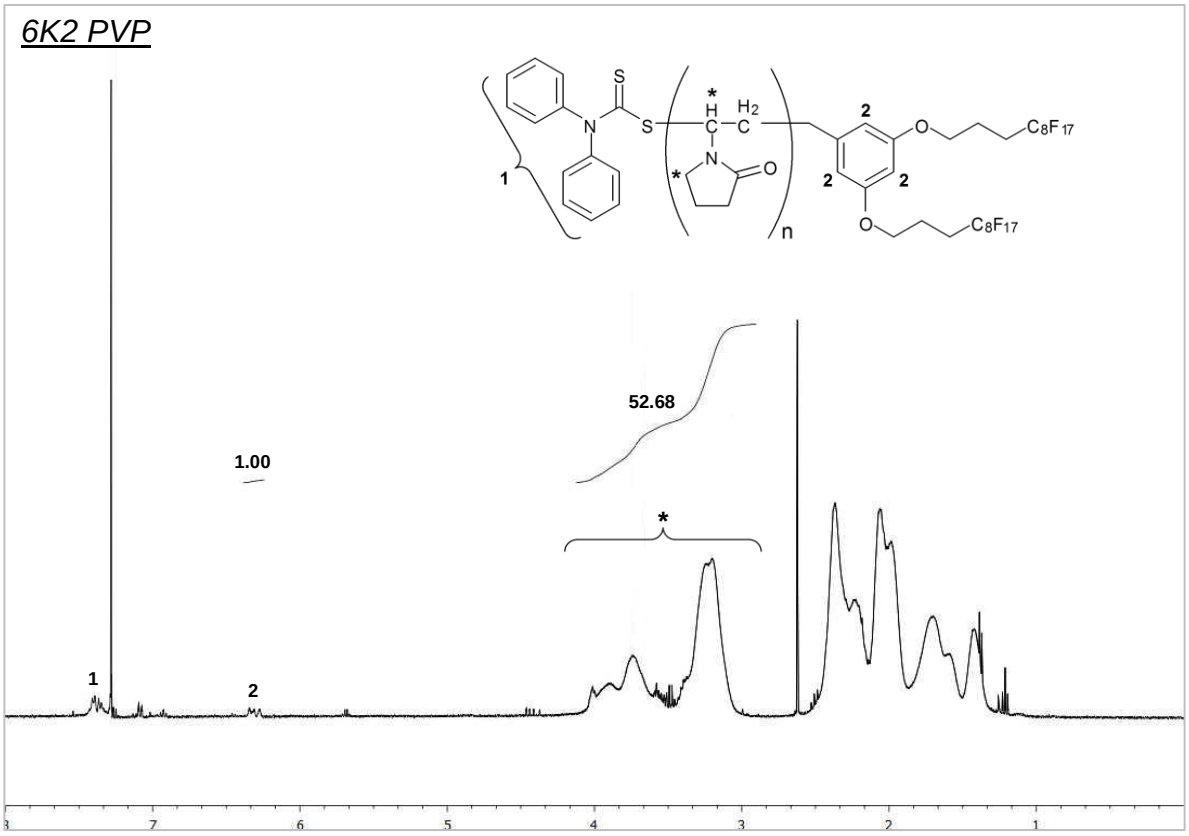

Figure 3.09. ^{1}H NMR spectra of the 6K2 PVP additive used in all of the di-functional additive contact angle measurements in the following section. Of particular note are the peaks ascribed to the ten Z group aromatic protons (1) and the three R group aromatic protons (2).

However, the peaks that have been chosen to calculate the degree of end functionality are those attributable to the aromatic protons in the fluoroalkyl R group (labelled “2” in the spectrum) as these are the only resolvable peaks from the end group that is of specific interest. They have been compared to the broad set of peaks (labelled “*”) attributable to the three protons bonded to the carbon atoms adjacent to the nitrogen atom in each monomer residue. This means that in the case of the di-functional additive, simply three protons from the functional end group are being compared to three protons per monomer residue. Following on from this, in the case of the tri-functional additive whose functional end group contains one less aromatic proton, two protons from the end group are being

compared to three protons per monomer reside.

In the specific case of the 6K2 PVP additive whose NMR spectrum is shown in Figure 3.09, the integral ratio between end group aromatic protons and the appropriate protons from the polymer backbone is 1:53 and the precise molecular weight of this additive from SEC is 5,400 g mol^{-1}.

The degree of polymerisation can be calculated from the known molecular weight, and from this the degree of end-functionalisation can be calculated by comparing the known degree of polymerisation to the degree of polymerisation inferred by NMR from the comparison between end group peaks and backbone peaks (assuming 100% end-functionalisation). From the difference between these two values can be calculated the percentage of chains bearing a functionalised end-group as per the following equations.

$$\mathbf{DP} = \frac{\mathbf{M_n} - \mathbf{M_{EG}}}{\mathbf{M_M}} \qquad \mathbf{3.1}$$

$$\mathbf{D_{func}} = \frac{\mathbf{1/IR}}{\mathbf{1/DP}} = \frac{\mathbf{DP}}{\mathbf{IR}} \qquad \mathbf{3.2}$$

Where **DP** is the degree of polymerisation, $\mathbf{M_n}$ is the number average molecular weight as determined by SEC, $\mathbf{M_{EG}}$ is the molar mass of the fluoroalkyl end-group, $\mathbf{M_M}$ is the molecular weight of the monomer (NVP = 111.14 g mol^{-1}), $\mathbf{D_{func}}$ is the degree of end-functionalisation, and **IR** is the NMR integral ratio between the three aromatic protons arising from the end group and the three protons per monomer residue within the polymer backbone. So for the 6K2 additive:

$$DP = \frac{5400 - 1043.4}{111.14} = 39.2 \qquad D_{func} = \frac{39.2}{53} \times 100 = \mathbf{74\%}$$

As discussed in the introduction chapter on RAFT polymerisations (see pages 24-28), a small amount of AIBN is required to initiate the polymerisation, and correspondingly a small amount of the resulting polymer chains will possess 2-cyanopropyl end groups derived from AIBN in contrast to the majority of chains which were initiated by the R group of the CTA, and therefore possessing the desired end-functionality imparted by the CTA itself. Therefore, when using a 1:8 molar ratio of AIBN to CTA, the maximum possible degree of end-functionality in a perfect RAFT polymerisation would be 87.5%. The calculated value of 74% is in reasonable agreement with what one would expect from a RAFT polymerisation using a molar ratio of 1:8 initiator to CTA as has been used in this work.

Table 3.2. SEC data for a selection of di- and tri-functional PVP additives as well as monomer conversion or yield and the degree of end-functionalisation as determined from ^{1}H NMR spectroscopy.

Type	Target M_n	M_n	PDI	% Yield	% Functionalisation
5K3	5,000	5,550	1.57	46%	82%
7K3	7,000	7,150	1.45	41%	65%
10K3	10,000	9,700	1.83	43%	54%
20K3	20,000	17,400	1.49	39%	45%
25K3	25,000	18,000	1.29	39%	39%
50K3	50,000	33,100	1.57	53%	0%
100K3	100,000	56,100	1.37	42%	0%
6K2a	6,000	5,400	1.19	37%	74%
6K2b	6,000	5,950	1.22	46%	79%
10K2	10,000	7,950	1.20	57%	67%
15K2	15,000	11,850	1.23	49%	71%
25K2	25,000	18,050	1.34	46%	32%
50K2	50,000	37,850	1.28	38%	0%

In Table 3.2 is shown a selection of polymer additives made using both the di- and tri-functional CTAs. It can clearly be seen that both CTAs are capable of producing end-functionalised polymers with good control over molecular weight and high degrees of end-functionalisation. Control over molecular weight is exceptionally good below 15,000 g mol^{-1}, however between 15,000 and 100,000 g mol^{-1} we do see a divergence between target and achieved molecular weights though it is consistent and predictable in nature.

From a glance at the polydispersity indices displayed in this table it can be seen that while both CTAs exhibit similar behaviour in terms of control over number average molecular weight and percentage monomer conversion, the di-functional CTA does perform noticeably better when considering control over polydispersity of the resulting polymers. It is possible that the cause of this is that in the case of the tri-functional CTA, the third fluoroalkyl group is in the *para* position on the aromatic ring of the R group. As such the electron donating ether group can directly affect both the likelihood of fragmentation and the stability of the radical formed in the reinitiation step of the RAFT process (see page 26). It is conceivable that this will alter the position of the addition-fragmentation equilibrium to the detriment of the polydispersity. While it is unarguable that the tri-functional CTA does not perform quite as well in this regard, the resulting low M_n polymers produced still maintain a high degree of end-functionalisation and are sufficiently well-defined to be used as effective surface modifying additives. As will be seen later in this chapter it is in fact the tri-functional polymers that perform the best in their role as surface modifying additives.

3.2 Contact angle measurements

3.2.1 Introduction

As previously discussed, the purpose of making these low molecular weight end-functionalised polymers is to use them in low concentrations as surface modifying additives in their corresponding unmodified bulk polymers. Taking contact angle measurements using a goniometer and the Sessile Drop Technique[8] is a convenient method for investigating the surface properties (in this case oleophobicity, which in turn is an indicator of fluorine concentration at the surface) of our range of polymer matrices incorporating either of the two classes of additives in varying concentrations. These contact angle measurements allow us to quickly investigate the surface properties of a range of polymer films enabling us to make direct comparisons between effects arising from the molecular weight of the polymer matrix, molecular weight of the functionalised additive, the number of fluoroalkyl groups on the additive and where appropriate, annealing temperatures and times.

All of the contact angle data in this section is presented as a function of either additive concentration or annealing time. While it would be more technically correct to present contact angle data as 'cosθ' as per Equation 3.3, it is presented in its raw form (θ / degrees), as many trends and comparisons seen in this work are easier to observe and discuss in this format. Plots of cosθ have been included in several figures for completeness.

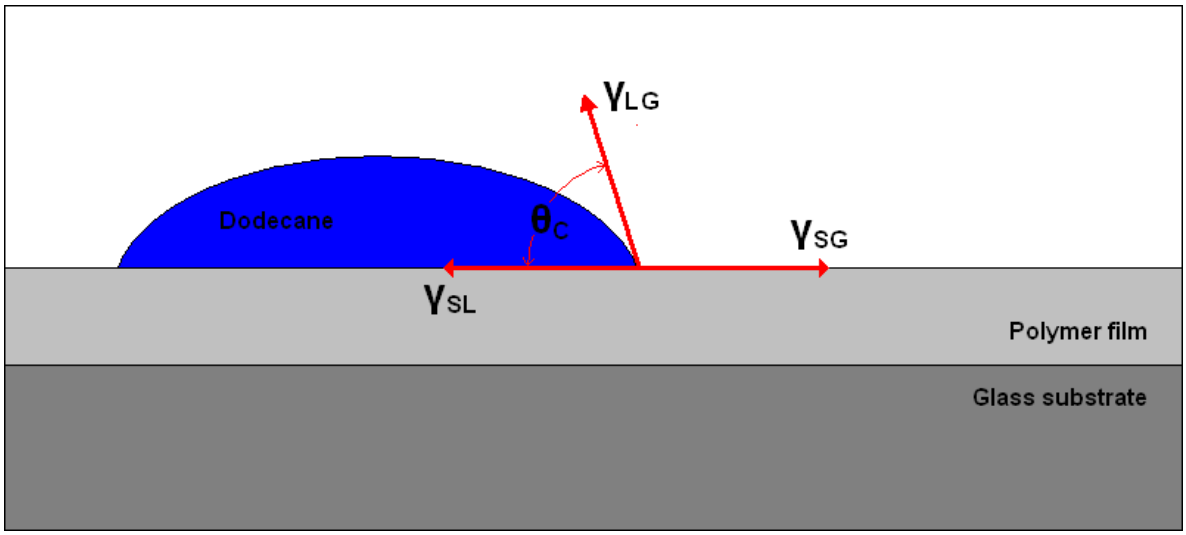

Figure 3.10. Diagram illustrating a drop of dodecane partially wetting a polymer surface and how this contact angle is influenced by surface energies at the solid-liquid (γ_{SL}), liquid-gas (γ_{LG}) and solid-gas (γ_{SG}) interfaces.[9]

The Sessile Drop Technique involves depositing a drop of contact fluid from a vertically held syringe onto the polymer surface. The contact angle is most simply described as the angle between the solid sample's surface and the tangent of the droplet's edge at the point where it makes contact with the solid surface as shown above (Figure 3.10). At equilibrium this situation is described theoretically by the Young Equation[10]:

$$\gamma_{SG} - \gamma_{SL} - \gamma_{LG}\cos\theta = 0 \qquad \textbf{3.3}$$

Where γ_{SG} is the solid-gas interfacial energy (or surface energy), γ_{SL} is the solid-liquid interfacial energy, and γ_{LG} is the liquid-gas interfacial energy as shown in Figure 3.10. It can be seen from this equation that as the energy at the solid-gas interface is decreased (as in this case by introducing low surface energy fluoroalkyl groups to the polymer surface), the contribution from the solid-liquid interface

becomes less significant and the droplet will contract in order to increase the contact angle and satisfy the above equilibrium equation.

Having deposited a drop of contact fluid from a vertically held syringe onto the polymer surface, the contact angle can then be measured using a contact angle goniometer. The sample is placed on a flat stage and the user can view the backlit side profile of the droplet and surface though an objective lens with a horizontally positioned microscope. Within the objective lens are two rotatable circular scales depicting angles from 0 through to 360 degrees which can be independently aligned to the surface and the tangent that the droplet's edge makes with the surface allowing the user to determine the contact angle. The sample stage which is adjustable to ensure that it is completely level, can be moved left and right by means of a screw allowing measurements to be taken from each side of the drop, and also providing the surface is big enough, multiple drops.

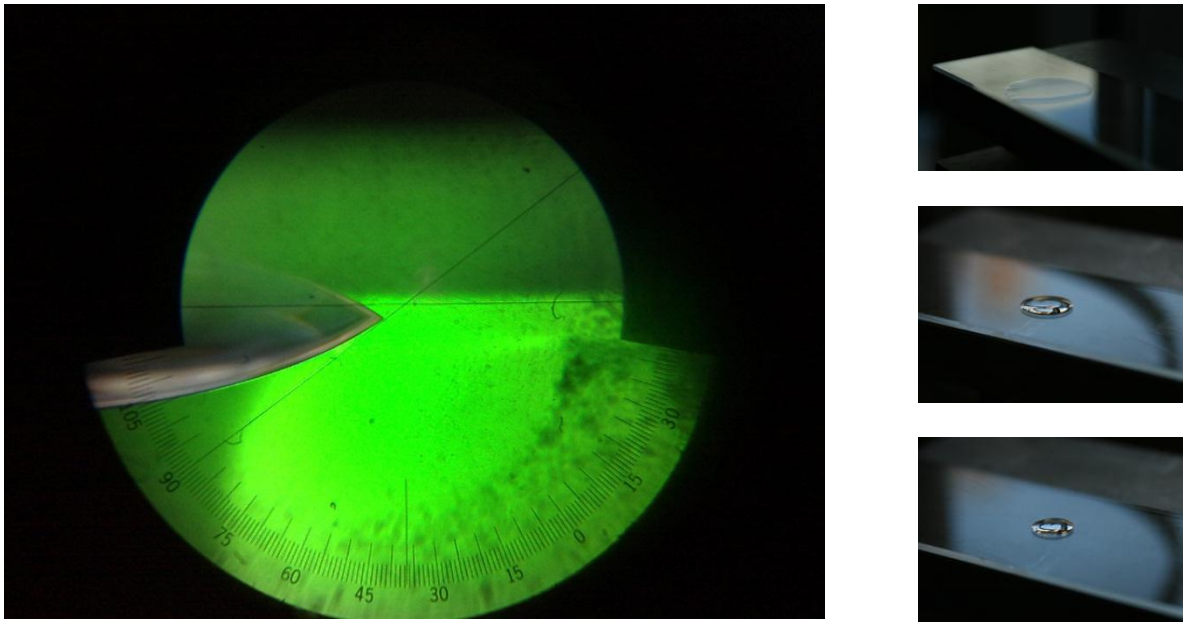

Figure 3.11. Photograph of the view through the objective lens of the goniometer (left) and three photographs of drops of dodecane on surfaces of K15 PVP containing various weight percentages of 6K2 PVP (0% top right, 1.5% middle right, 2.5% bottom right).

Contact angle measurements are commonly used to calculate surface energies and various other surface interactions mathematically, however in this work it was simply used to draw comparisons between the contact angles of the unmodified matrices and those containing varying concentrations of our two additives. These contact angles when plotted against percentage additive provide a good graphical representation of the effect that the additives have on the oleophobicity of the polymer surface and hence also allude to the surface concentration of fluorine and therefore the extent of surface segregation. Contact angles can be affected by surface roughness,[11] and Atomic Force Microscopy (AFM) was used to investigate surface roughness, as well as Ion Beam Analysis (IBA) to investigate near-surface elemental composition in order to establish that contact angle changes were a result of surface chemistry and not surface roughness.

In this work, all polymer films used for contact angle measurements were prepared as follows. Solutions of PVP (5 wt. %) were prepared in methanol (Analytical Grade, Fisher Scientific) containing a blend of one of four different molecular weight unmodified bulk PVP matrices (denoted K15, K17, K30 and K90 PVP – see Table 3.1 for MW details) containing up to 15 wt. % end-functionalised additive (DPFPB-PVP or TPFPB-PVP). These solutions were then used to spin coat polymer films onto glass microscope slides. All films were spun at 3000 rpm for 1 minute to give films with a thickness of approximately 250 nm. The conditions required to achieve a film thickness of approximately 250 nm were optimised previously by spin coating the same PVP / MeOH solutions of varying solution concentrations onto silicon wafers at varying speeds, and then measuring the resulting film thicknesses using a Sentech SE400 Ellipsometer (up to 200 nm film thickness) and a Sentech FTP500 White Light Interferometer (above 150 nm film thickness). Once films had been spun onto the glass slides they were dried in a vacuum oven to constant mass. Contact angle measurements were obtained using dodecane (≥99%, Sigma-Aldrich) as the contact fluid on a Ramé-Hart NRL contact angle goniometer (model number 100-00-230), taking the average result of six measurements taken from both sides of three separate drops of dodecane deposited on the surface from a vertically held syringe. In the case of any obvious

outliers sometimes caused by small pieces of debris or imperfections on the surface of the films, a fourth drop was deposited on the surface and the outlying results ignored. For each set of readings the levelness of the sample stage was verified using a spirit level and adjusted if necessary.

3.2.2 Films "as-spun"

The contact angle data presented here allows us to characterise independently the effects of additive type, additive molecular weight, matrix molecular weight, annealing time and annealing temperature on the surface properties of the polymer films. In this section we will look at data obtained from "as-spun" films (those that have not been subjected to annealing). The first set of data is for 6000 g mol^{-1} DPFPB-PVP or di-functional additive (6K2 PVP) in each of the four different PVP matrices; K15, K17, K30 and K90. The objective of these data is to explore the potential impact of the molecular weight of the matrix polymer on surface segregation.

Due to the large number of data points and their close proximity to one another in each set of data, the use of error bars has been forgone in favour of a single error bar on the top left or top right corner of each plot. This single error bar represents the average of the standard deviations arising from each set of six contact angle measurements of which each data point is an average. In other words this error bar is an average of all of the error bars in the associated plot.

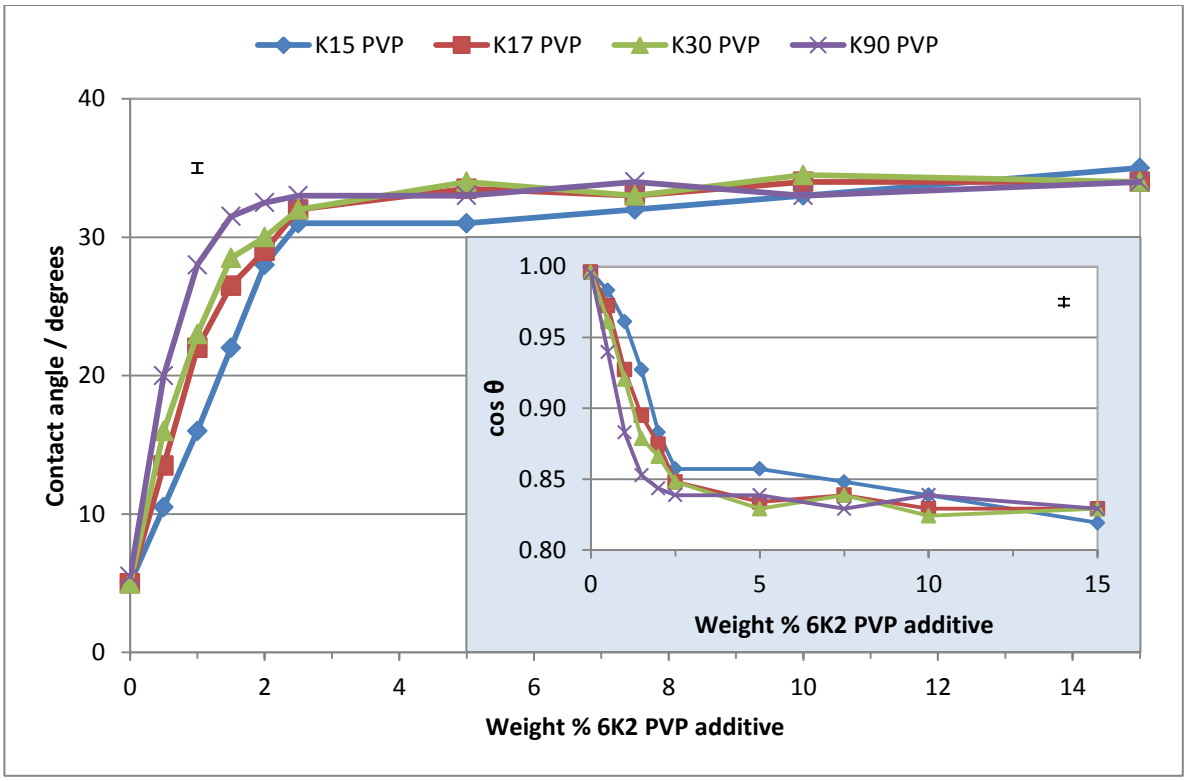

Figure 3.12. Plot of weight % 6K2 additive against contact angle in films prepared from each of the four different molecular weight PVP matrices. Smaller plot shows 'cosθ' data, illustrating the corresponding reduction in surface energy as a function of additive concentration.

As one would expect, the contact angles of the four bulk PVP matrices in the absence of any additive were all essentially the same. The contact angles of all four unmodified polymer surfaces were measured at 5° or 6° showing that these surfaces have a relatively high surface energy and therefore allow substantial wetting by the dodecane. However it can be seen that the addition of as little as 0.5 weight % additive has a significant and measurable effect on the contact angle, in the case of the K90 PVP matrix, the addition of 0.5 weight % of 6K2 additive results in a 15° increase in contact angle. Matrix molecular weight appears to have a significant impact upon contact angle at lower concentrations of additive, but this will be discussed in greater detail later.

In the case of all four matrices, the contact angle increases steadily with each

increasing concentration of additive until contact angles plateau at around 34° whereupon the addition of further additive seem to have little or no further effect. Initially one might be forgiven for interpreting this feature in the data as arising from a surface saturation effect, whereby the size of the pendant polymer chain on each fluoroalkyl group determines how many additive chains can physically fit at the polymer / air interface. However the situation is in fact somewhat more complicated than this, as previous work has shown.[12] The additive, which comprises of both a polymer chain identical in composition to and therefore compatible with the bulk polymer matrix, and a fluoroalkyl end-group that does not interact particularly favourably with the bulk polymer, can be said to behave in a fashion analogous to a surfactant in solution.[13-15] Just as in the case of a surfactant, where increasing its concentration in solution eventually leads to the formation of micelles at the critical micelle concentration (CMC),[16-18] increasing the concentration of polymer additive eventually leads to the formation of additive aggregates within the polymer bulk, at a critical aggregation concentration (CAC). The plateau region seen in this data corresponds to onset of the formation of aggregates and therefore the CAC of additive, whereupon the additive begins to spontaneously form aggregates within the polymer bulk in preference to further surface segregation. Unlike the free additive chains, there is no thermodynamic drive for surface segregation of additive aggregates as the low surface energy fluoroalkyl end groups are buried within the aggregate structure. In addition to this the aggregates are much larger than the free additive chains and therefore their rate of diffusion through the bulk polymer will be significantly lower.

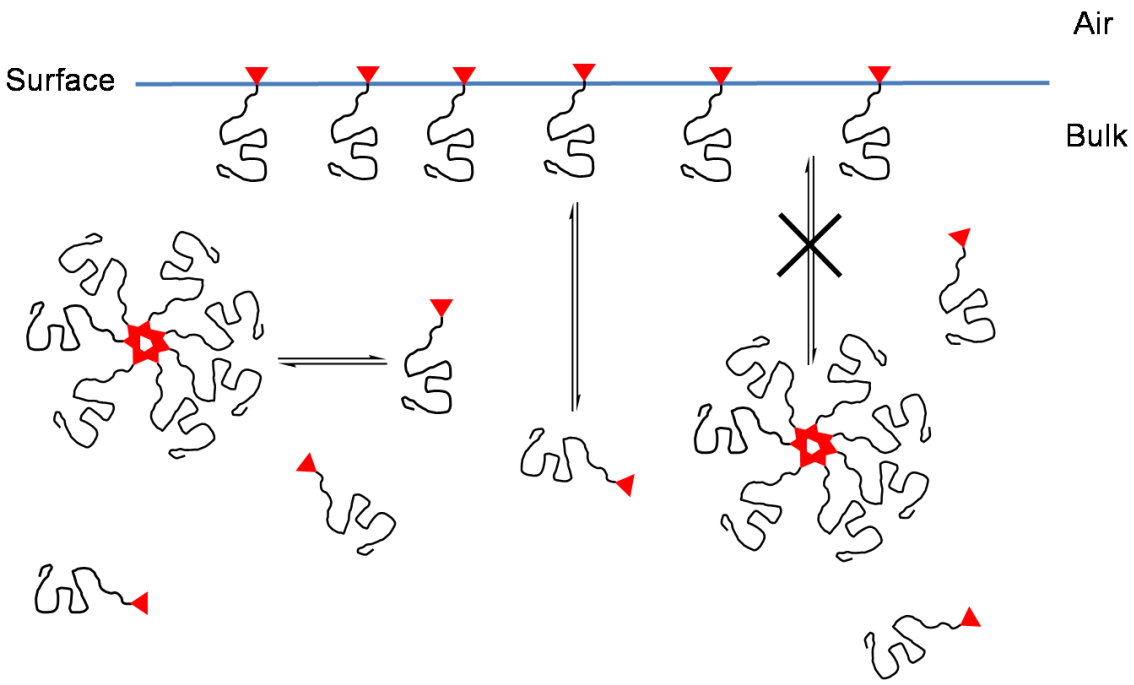

Figure 3.13. Schematic[15] depicting the behaviour of either fluorinated additive in the polymer bulk during the spin coating process. An equilibrium exists between free additive chains and aggregate structures but it is only the free chains that are able to surface segregate.

This behaviour has been demonstrated by Thompson et al.[12] The authors synthesised a series of deuteriopolystyrene (dPS) additives bearing very similar end-functionalities to those presented in this work, containing between two and four C_8F_{17} end-groups. Films containing varying concentrations of these additives in a polystyrene (hPS) matrix were then spin coated and contact angle measurements performed on the resulting polymer films, yielding similar trends to those seen here due to the same spontaneous surface segregation driven by the low surface energy of the fluoroalkyl end groups. By virtue of the deuterated nature of the dPS additive chains in a deuterium-free hPS matrix, small-angle neutron scattering (SANS) experiments were carried out to investigate the nature of the distribution of additive chains within the polymer matrix. Random phase approximation (RPA) was used to model the SANS data using a Flory-Huggins interaction parameter (χ) of 0 (χ describing the interactions between monomers of a

different species, therefore for monomers of the same type which for all intents and purposes *d*-styrene and *h*-styrene are, $\chi = 0$). For comparable polymer blends with a small Flory-Huggins interaction parameter, RPA simulations agree almost quantitatively with experimental SANS data.[19]

At low concentrations of additive, the SANS data was consistent with free additive chains, exhibiting no signs of aggregation, distributed evenly throughout the polymer matrix. This SANS data is consistent with what one would expect to see in the absence of any interactions between the fluoroalkyl end groups and the hPS matrix, in other words, in a polymer blend of unfunctionalised dPS and hPS. The RPA simulations at these low additive concentrations were also in good agreement with the experimental SANS data, further strengthening this hypothesis.

However at higher additive concentrations (above what has now been termed the CAC), the SANS data exhibited larger scattering cross-sections, indicating that the small-angle neutron scattering was now due to objects that were significantly larger than the dimensions of a free additive chain. In addition to this there was no longer good agreement between the experimental SANS data and the RPA simulations indicating that in reality the interaction parameter was no longer ~ 0, that is to say the experimental situation was no longer similar to a simple blend of dPS and hPS as before.

While it is most likely from these results that what is occurring is the formation of aggregates analogous to the formation of micelles in a surfactant solution as shown in Figure 3.13, it is not possible to prove this from the data presented in the paper up to this point. However the authors then went on to model the situation where aggregates were forming by substituting into the RPA simulations the parameters of a dPS star polymer. Using this approach, good agreement was obtained between the experimental and simulated data suggesting that aggregates existed within the bulk with dimensions of a star polymer with 6-7 arms.

Further to the use of RPA modelling, transmission electron microscopy (TEM) was used to investigate the structure of polymer blends incorporating a tetra-functional additive possessing an end-group with four C_8F_{17} fluoroalkyl chains. In those

blends whose contact angle measurements fell within the plateau region where the additive concentration was above the CAC, discrete objects were observed in the transmission electron micrograph that would appear to be aggregate structures. These structures were not observed in blends with additive concentrations below the CAC.

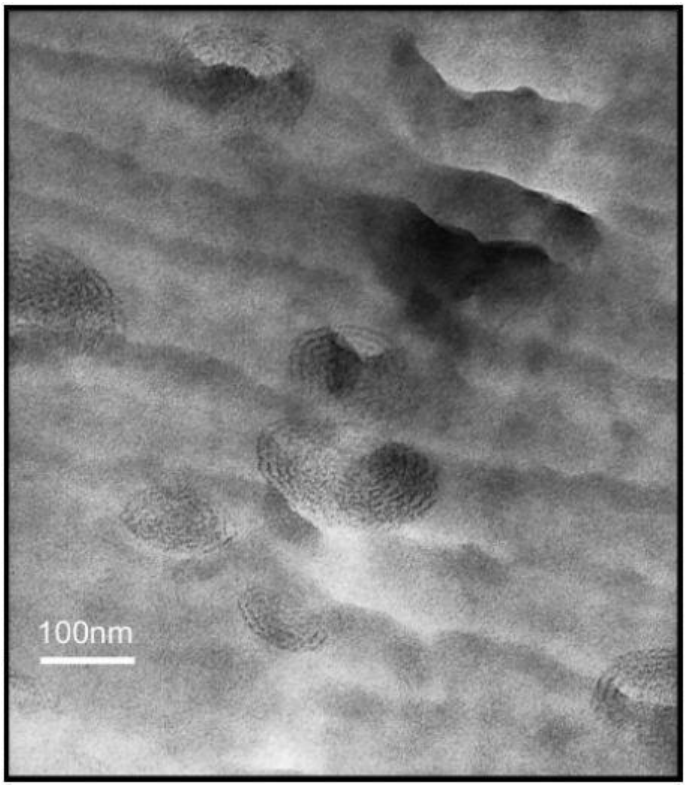

Figure 3.14. TEM image[12] of a blend of dPS additive (8 weight %) bearing an end-group containing four C_8F_{17} fluoroalkyl groups in an hPS matrix. Several discrete objects can be seen which would appear to be aggregate structures.

In addition to the evidence presented thus far for aggregation over surface saturation as the explanation for the plateau region seen in our contact angle data, further work has been performed in this area by investigating the effects of annealing similar polymer blends. It has been successfully demonstrated that

annealing above the T_g can have a significant beneficial effect on the surface segregation of these types of additive, which strongly supports the theory of a CAC over that of surface saturation.[6]

Returning now to the discussion of our own work and the data shown in Figure 3.12, we first see a sharp rise in observed contact angles with an increase in additive concentration below the CAC due to the spontaneous surface segregation of the additive and subsequent fluorine enrichment at the surface. The initial spontaneous surface segregation of the additive is thermodynamically driven by the lowering in overall free energy due to the resulting lowering of the surface energy in addition to the removal of the oleophobic fluoroalkyl groups from the polymer bulk. These enthalpic benefits combined overcome the entropic loss due to the ordering of the additive at the surface. Thus below the CAC an equilibrium exists between free additive molecules within the bulk, and those that are surface segregated, and as the overall concentration of additive is increased, the surface concentration of additive also increases.

However as the overall concentration of the additive increases and the CAC is reached, it becomes more thermodynamically favourable for the free additive chains to form aggregate structures within the bulk than for further surface segregation to occur. There now exists the same equilibrium between free additive chains within the bulk and those that are surface segregated, but in addition to this there is a second equilibrium between free additive chains in the bulk, and aggregate structures also in the bulk (see Figure 3.13). This second equilibrium can be thought of as having a buffering effect, so that if the additive concentration is increased further, more aggregate structures will form and the concentration of free additive chains within the bulk with remain unchanged, hence no additional surface segregation occurs.[16-18,20,21] So as the concentration of additive is increased beyond the CAC, the resulting surface concentration of additive in the spin coated polymer film will remain the same, the excess additive simply remaining in the bulk polymer in the form of aggregates, and this is the origin of the plateau region seen in the data (Figure 3.12).

As in this data set the molecular weight and type of the additive is constant, the plateau region exists at the same contact angle for all four molecular weight matrices as the molecular weight of the matrix plays little or no part in determination of the maximum possible surface concentration. However, there is a notable change in the gradient of each curve below the CAC, with surface concentrations of additive increasing faster with increased matrix molecular weight. It is possible that this is due to an increased rate of diffusion of the additive in higher molecular weight matrices (the matrix PVP molecules possessing a larger hydrodynamic volume relative to the additive), or it is also possible that it is a chain end effect (discounting the fluoroalkyl functional groups) which will be discussed later in this chapter.

3.2.2.1 Effect of matrix molecular weight on contact angle measurements

Maybe the most significant feature of this data set (Figure 3.12) is the effect of matrix molecular weight on surface segregation (and therefore surface properties) at low concentrations of additive. It can clearly be seen that despite all four plateau regions being reached at approximately 2.5 weight % additive and a contact angle of approximately 34°, at concentrations below 2.5 weight % (~CAC), surface segregation of the additive appears to increase steadily with increase of polymer matrix molecular weight. As we are considering the situation where the additive concentration is below the CAC, we are not concerned with the thermodynamic argument describing the formation of aggregates, but only the thermodynamics of surface adsorption of free additive chains. As already discussed this occurs due to the subsequent reduction in surface energy in addition to the removal of the oleophobic fluoroalkyl groups from the polymer bulk which combined overcome the entropic penalty associated with ordering the additive at the surface.

It is suspected that the origin of the trend seen across the different molecular weight matrices is in fact due to the ratio of additive chain ends to matrix chain ends. Assuming that polymer chains assume a random coil conformation, these

conformations can be characterised by the root mean square end-to-end distance (R_G). Previous work has shown that in the absence of favourable interactions between monomer units and an interface or surface, there is an increase in chain end density at the surface of an ordinary polymer.[22-25] This effect arises because there is a lower loss of conformational entropy associated with a polymer chain end residing at the surface (which can be considered as an impenetrable boundary), when compared with the midsection of the polymer chain residing at the surface, which forces "reflection" of the polymer chain.[22] Therefore polymer chains within one R_G of the surface may adjust their conformation in order to localise their chain ends at the surface.[25]

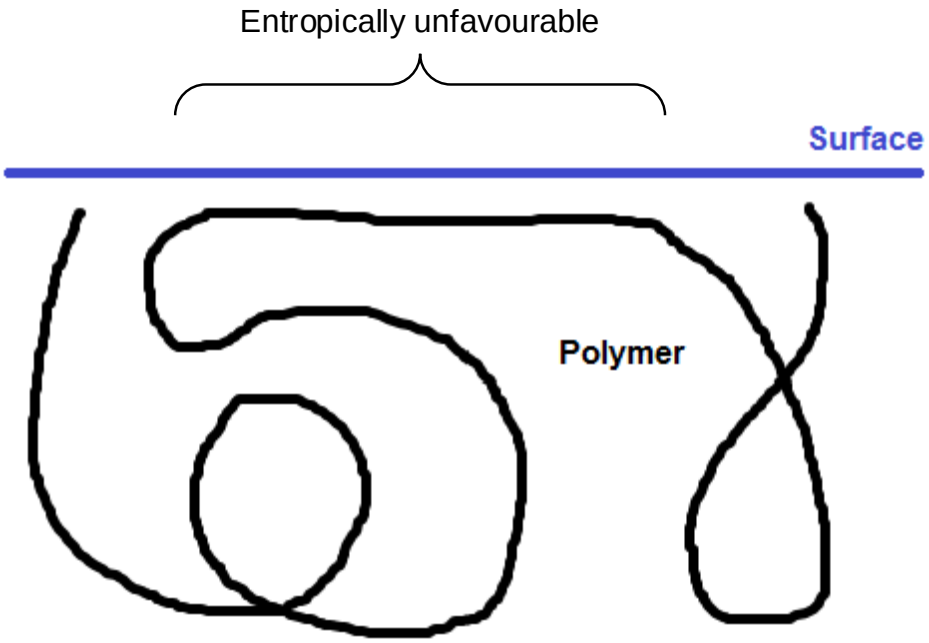

Figure 3.15. Perturbed polymer conformation at the surface.[25]

In addition to this effect, it has been shown that highly branched polymers in a linear polymer matrix,[26,27] and lower molecular weight polymers in a higher molecular weight polymer matrix[28] have a tendency to surface segregate to measurable extent. This is due to the entropic attraction of chain ends to the

surface, and the fact that architecturally complex or significantly lower molecular weight polymers possess a far higher ratio of chain ends per repeat monomer unit than their higher molecular weight bulk polymer counterparts.

An alternative rationalisation for the matrix molecular weight effect seen in Figure 3.12 can be derived from Flory-Huggins theory[29,30] as applied to binary polymer blends in solution.[31,32] Flory-Huggins theory is a mean field approximation, whereby the location of monomer units and solvent molecules is modelled on a regular lattice. All lattice points are assumed occupied by either a monomer unit or solvent molecule, and it is assumed that they are of equal volume. Another important assumption is that there is complete flexibility between monomer units. Ignoring the fluoroalkyl functional end-groups on the additive chains, consider the PVP thin films to be simply a blend of two different molecular weights of otherwise identical PVP. The Gibbs free energy of mixing for a two component polymer blend in which both components are monodisperse is given by Equation 3.4, which is derived from the Flory-Huggins model described above.[33]

$$\frac{G_{mix}}{k_B T} = \frac{\phi_A}{N_A} \ln \phi_A + \frac{\phi_B}{N_B} \ln \phi_B + \chi \phi_A \phi_B \qquad \textbf{3.4}$$

Where ϕ_A and ϕ_B are the volume fractions of polymers A and B respectively, N_A and N_B are the degrees of polymerisation, χ is the Flory-Huggins interaction parameter, k_B is the Boltzmann constant and T is the absolute temperature. In this case, the final term in this equation can be ignored as we are dealing with a blend of two different molecular weights of PVP, and so as both polymer components are chemically identical as far as their repeat structure is concerned, $\chi = 0$. However it can be seen that the other two terms are affected by the degree of polymerisation of each polymer, and hence the M_n, thus the molecular weight of each polymer will have an effect on the Gibbs free energy of mixing.

Flory-Huggins phase diagrams for a specific system can be generated theoretically

or measured experimentally, often by virtue of SANS or SAXS. In their simplest form, these diagrams consist of a so-called 'coexistence curve' which divides the diagram into two regions, one in which the components are mixed and one in which they are phase separated.

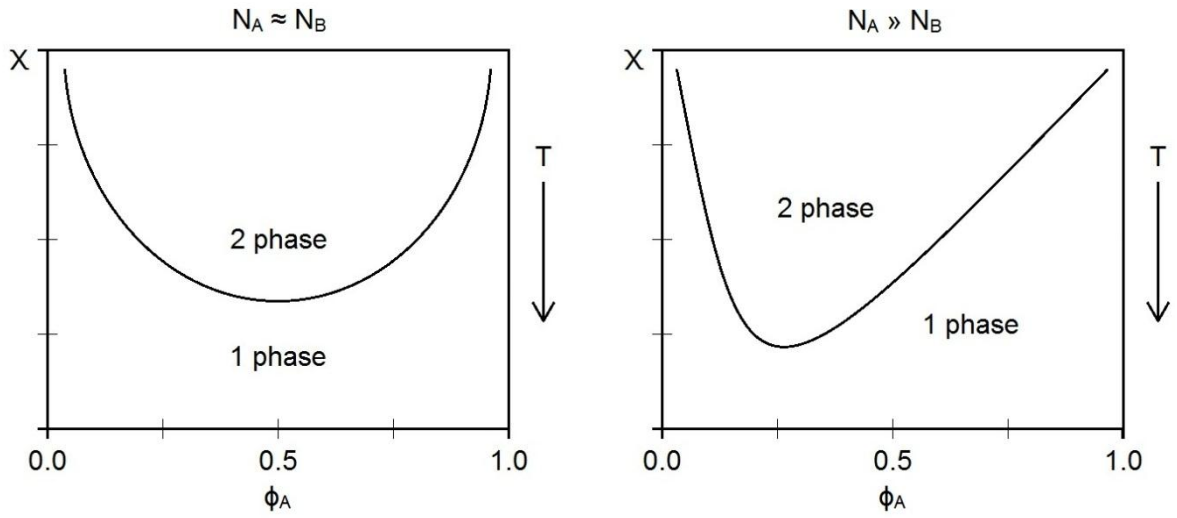

Figure 3.16. Flory-Huggins phase diagrams for binary polymer blends of polymer A and polymer B, where A and B are of similar M_n (left), and A is of significantly higher M_n than B (right). χ is the Flory-Huggins interaction parameter, ϕ_A is the volume fraction of polymer A, and N is the degree of polymerisation of each polymer.

Figure 3.16 shows two example phase diagrams for a binary polymer system in solution: one where the degrees of polymerisation are equal, and one where one polymer is of a significantly higher degree of polymerisation than the other. It can be seen from these diagrams that the difference in degrees of polymerisation, and hence M_n of each polymer, has a significant effect on ΔG_{mix}, and indeed whether or not the blend is mixed or phase separated. Thus it is possible that the trend seen in Figure 3.12 across the range of molecular weight matrices at additive concentrations below the CAC, is attributable to this phenomenon whereby increasing the M_n of the matrix is leading to phase separation of the matrix and the

additive.

It is either one or both of these effects (chain end density / M_n effect on ΔG_{mix}) that is assumed to be responsible for the trend of contact angles for specific concentrations of additive seen below the CAC, to increase slightly with an increase of matrix molecular weight, as seen in Figure 3.12. That is to say that an increase in molecular weight of the polymer matrix relative to that of the low molecular weight polymer additive leads to a slightly enhanced surface segregation of the additive. This subtle effect is unrelated to the additive fluoroalkyl functionality and is a sole consequence of increasing the molecular weight of the matrix.

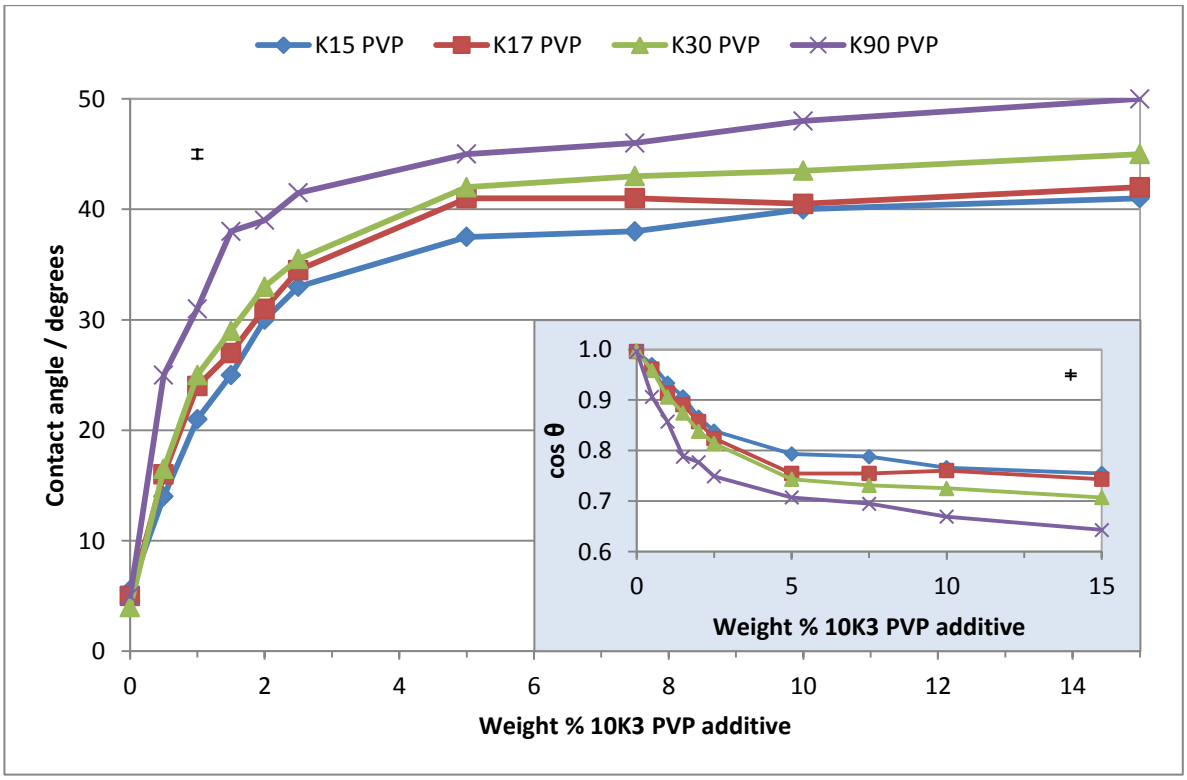

Figure 3.17. Effect of concentration of 10K3 PVP additive on contact angle for blends of additive in PVP matrices of varying molecular weight.

Figure 3.17 shows contact angle data for differing concentrations of the 10,000 g mol^{-1} tri-functional additive (10K3) in the four PVP matrices; K15, K17, K30 and K90. The first point to note is the 20-25% increase in contact angles achieved relative to those obtained with the di-functional additive at both the plateau region of the data and also at lower concentrations of additive. This increased impact on contact angle relative to the di-functional additive is expected due to the larger fluorine content of the tri-functional additive. Again there is a significant increase in contact angle with increasing concentration of additive resulting in a higher surface concentration of fluorine and hence additive. The addition of as little as 0.5 wt. % of additive (in the case of the K90 PVP matrix) resulted in an increase of contact angle from 5° to 25°.

As discussed previously, a plateau in contact angle is observed corresponding to the CAC and the preferential formation of additive aggregates over surface adsorption. However in the case of the tri-functional additive it seems that this occurs at slightly higher concentrations than in the di-functional case, at approximately 3-5 wt. % additive. It seems reasonable to suggest that this is due again to the increased molar fluorine content (50%) relative to that of the di-functional additive. One could argue that the extra fluoroalkyl chain could induce the additives to aggregate at lower concentrations, however it would also lead to a greater thermodynamic drive for surface adsorption due to a greater reduction in surface energy for the same entropic penalty. In this case, below the CAC, surface adsorption would be enhanced relative to the di-functional additive, effectively retarding the bulk concentration of the additive and raising the CAC; that is to say the concentration of additive at which aggregation will start to occur and give rise to the plateau region seen in the data.

Another important feature of this data is the change in contact angles seen across the different molecular weight matrices at lower concentrations of additive, below the CAC. It can clearly be seen that the higher the matrix molecular weight, the larger the observed contact angles are below the CAC. This phenomena has already been discussed and explained in terms of entropic attraction of chain ends to the surface, however it is interesting to note that in the case of the tri-functional

additive as seen here, this increase in contact angle with increasing matrix molecular weight appears to occur not only at low concentrations of additive below the CAC, but at all concentrations of additive. If one were to consider the terminal unit of each fluoroalkyl C_8F_{17} chain (which is in fact an $-OC_3H_6C_8F_{17}$ chain) as a chain end, it would be conceivable this entropic attraction of the tri-functional additive to the surface would be slightly enhanced when compared to that of the di-functional additive.

3.2.2.2 Effect of additive type on contact angle measurements

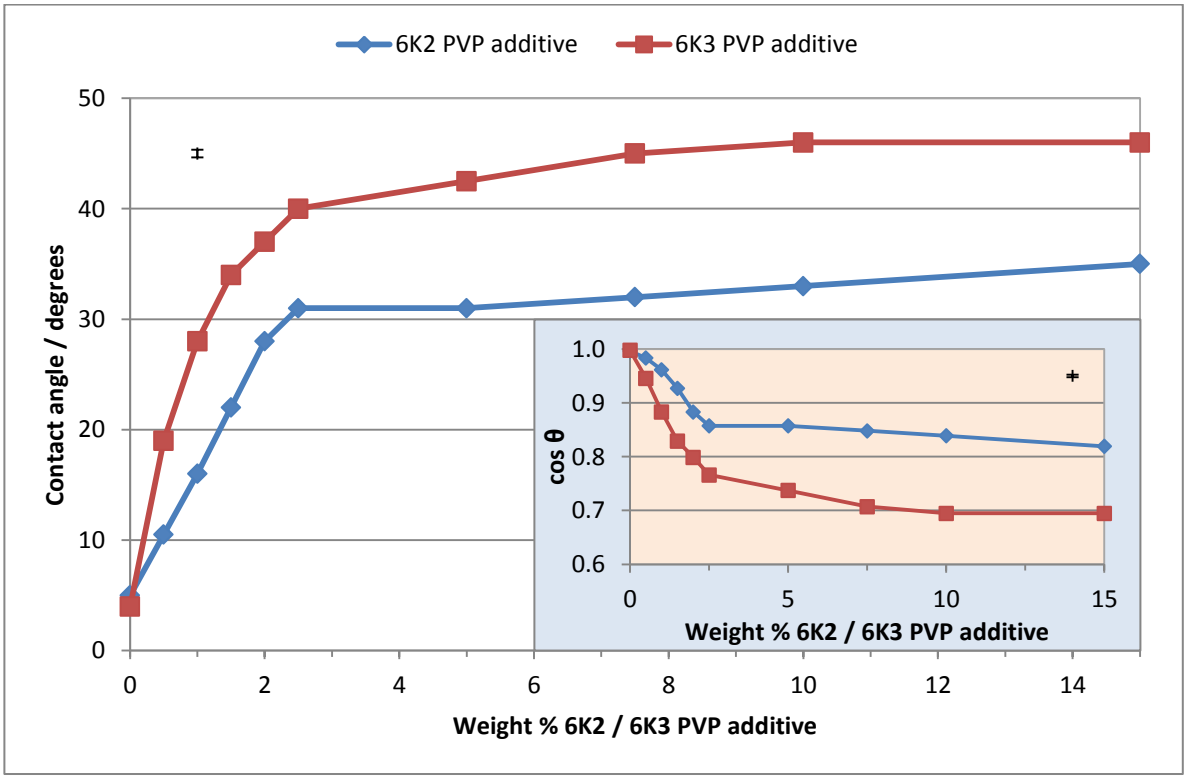

Figure 3.18. Effect of additive type at varying additive concentrations on contact angle, for blends of either di-functional or tri-functional additive in a K15 PVP matrix.

Figure 3.18 shows data providing a direct comparison between a di-functional and

tri-functional additive of the same molecular weight (6,000 g mol^{-1}, 6K2 PVP and 6K3 PVP) in a K15 PVP matrix. All other things being equal it can be seen that the tri-functional additive gives rise to both a significantly increased contact angle at all additive concentrations and also it would appear to reach the plateau region at a slightly higher additive concentration corresponding to the CAC, possibly due to its 50% greater molar fluorine content as previously discussed. This plot serves simply to illustrate the superior performance of TPFPB-PVP over DPFPB-PVP as a surface modifying additive.

3.2.2.3 Effect of additive molecular weight on contact angle measurements

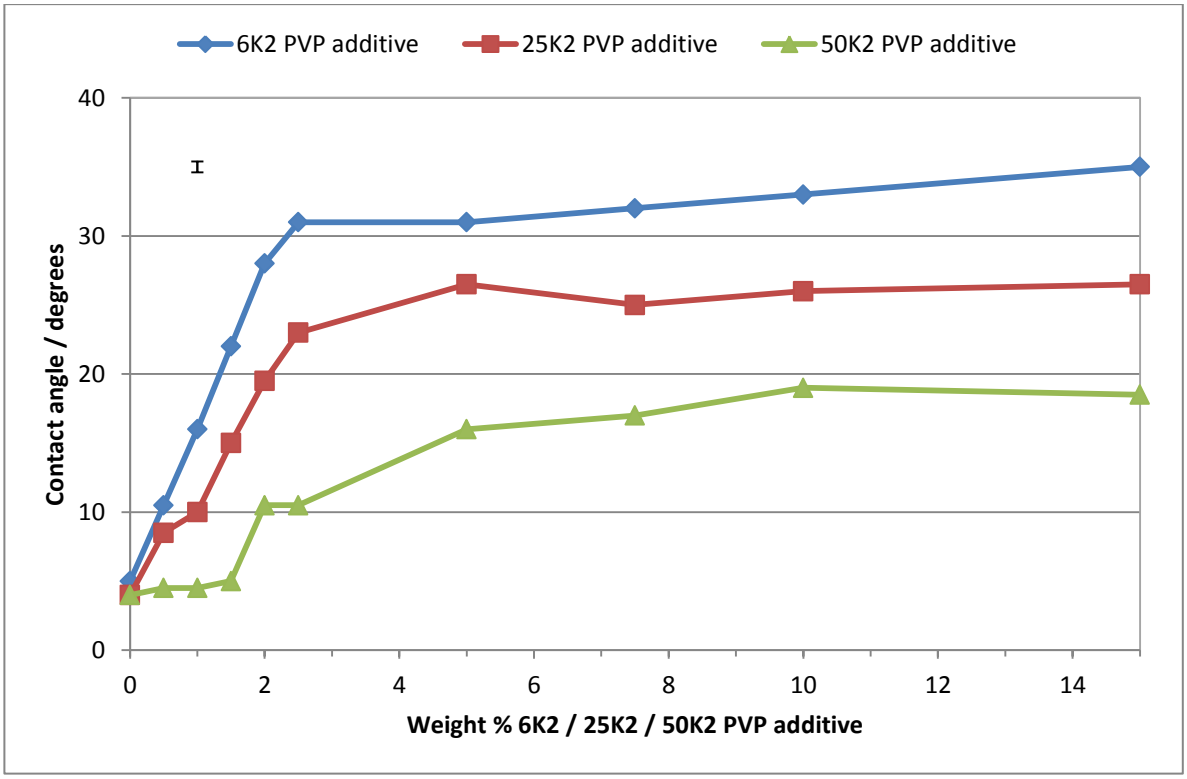

Figure 3.19. Effect of additive molecular weight at varying additive concentrations on contact angle, for blends of one of three molecular weight di-functional additives in a PVP matrix.

In the contact angle data presented in Figure 3.19, it is now the effect of molecular weight of the *additive* that is being compared, with three sets of K15 PVP films containing di-functional additives of 6,000 g mol^{-1}, 25,000 g mol^{-1}, and 50,000 g mol^{-1}. Here we see similar qualitative trends in each set of data pertaining to surface segregation and the CAC as previously discussed, but additionally we see a very obvious trend across the three data sets for the contact angle to decrease with increased molecular weight of the additive.

These observations are consistent with studies on analogous additives and therefore are to be expected.[6,15] Increasing the molecular weight of the additive and hence its hydrodynamic volume during the spin coating process will decrease its rate of diffusion through the polymer matrix. In addition to this effect, increasing the molecular weight of the additive will also reduce the percentage of each additive chain which is comprised of low surface energy fluoroalkyl chains, and by the same token will increase that which is comprised of PVP. Since the low surface energy fluoroalkyl end group is the driving force behind the spontaneous surface segregation and pendant PVP chain is compatible with the PVP matrix, decreasing the percentage composition of the former and increasing that of the latter will increase the compatibility of the additive with the matrix, to the detriment of its ability to surface segregate. A final factor to take into account is that increasing the molecular weight and hence R_G of the polymer additive will decrease the packing density of fluoroalkyl end groups at the surface. These effects combined lead to reduced surface segregation, a reduced fluorine concentration at the polymer surface, hence reduced surface oleophobicity and therefore increasing the molecular weight of the additive will give rise to lower contact angle measurements.

3.2.3 Annealed films

Annealing of the polymer films at temperatures well in excess of the glass transition temperature of PVP should allow reorganisation of the polymer films, and

past work[6,15] has shown that annealing in this fashion can result in enhanced surface segregation of polymer additives, giving rise to increased contact angle measurements. In this work, Hutchings *et al.* made a series of low molecular weight polystyrene additives analogous to the PVP additives presented in this thesis, and these additives were spin coated in bulk polystyrene matrices so as to perform contact angle measurements on the resulting surfaces.

Annealing was shown to be of considerable benefit in terms of enhancing surface properties and increasing measured contact angles. The impact of annealing upon surface segregation also supports the theory that the plateau regions seen in our contact angle data are a result of an equilibrium between free additive molecules and aggregates as opposed to a simple surface saturation effect. It also shows that this equilibrium has not been reached in the short duration of the spin coating process, prior to annealing. If the surface were indeed saturated by additive molecules, the maximum surface concentration would be determined by the size of the pendant polymer chain, or to be more precise its R_G, as this is significantly larger than the end-group. If this were the case one would expect annealing to have little or no effect on the surface concentration of additive (and hence the contact angle) as it would be already saturated. However annealing the polymer films for various amounts of time above the glass transition temperature of polystyrene gave increases in contact angles of 0-5° for all PS additives even at the plateau region (above the CAC) which is indicative of increased surface concentration of additive as a direct result of annealing. Hence simply increasing the concentration of additive in unannealed films leads to aggregation and the observation of a plateau in contact angles, after which the addition of further additive has little or no effect on the surface properties – this does not however result in surface saturation.

This rationale must be approached with a degree of caution however, as annealing could affect the measured contact angles in two additional and somewhat subtler ways. Firstly it could affect the surface topography or roughness of the polymer films which would affect the contact angle by means of changed surface area, or if surface roughness were increased sufficiently, surface features could affect the

shape of drops deposited on the surface giving rise to anomalous results. The Young equation as discussed earlier (Figure 3.10) can be used to describe the equilibrium contact angle, θ, of a drop of liquid on a flat, homogenous surface. However most surfaces are in reality rough, and there are two generally accepted models with which to describe wetting behaviour on a rough surface: the Wenzel[34] model and the Cassie-Baxter[35] model.

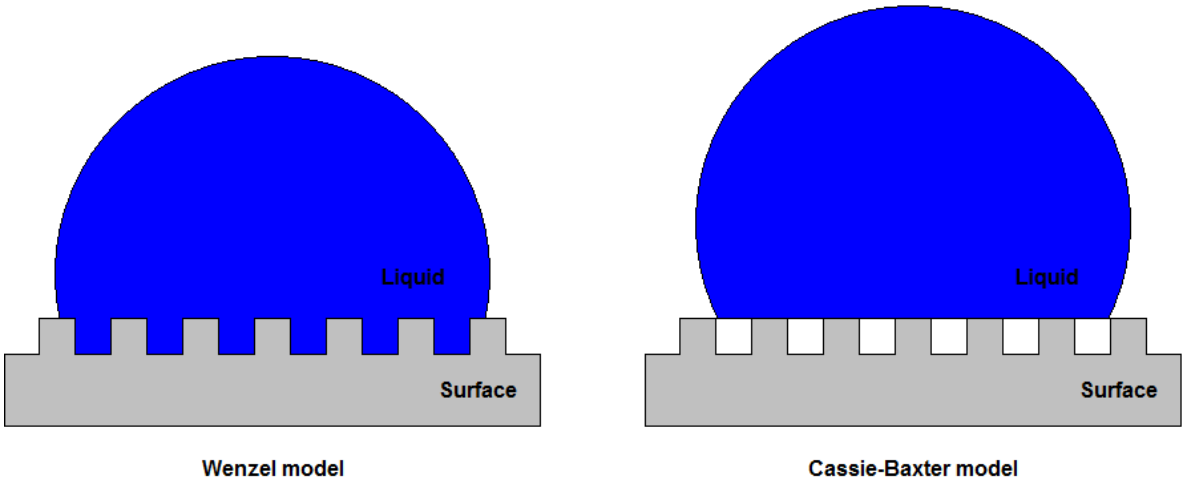

Figure 3.20. Schematics depicting the Wenzel and Cassie-Baxter models of surface wetting.

The Wenzel model assumes that the liquid penetrates into a rough surface, completely wetting it, thus increasing the surface area of the solid-liquid interface relative to that of a perfectly smooth surface. The original Young equation is modified to take into account the surface roughness by introducing a roughness factor, r, which is the ratio of the actual area of liquid-solid contact to the projected area on the horizontal plane. The Wenzel contact angle, θ_r^w, is given by Equation 3.5, where θ_e is the Young equilibrium contact angle.[36]

$$\cos\theta_r^w = r\cos\theta_e \qquad \textbf{3.5}$$

The Cassie-Baxter model assumes that the liquid sits on top of the rough surface, with small pockets of air filling the depressions in the surface. Due to the low resistance of the air pockets, a Cassie-Baxter drop exhibits considerably less contact angle hysteresis than a Wenzel drop, and for the same reason droplet motion will occur more readily. The Cassie-Baxter contact angle, θ_r^c, is given by Equation 3.6, where θ_e is again the Young equilibrium contact angle, ϕ_s is the area fraction on the horizontal projected plane of liquid-solid contact, and r_w is the ratio of the actual area to the projected area of liquid-solid contact.[36]

$$\cos\theta_r^c = r_w \phi_s \cos\theta_e + \phi_s - 1 \qquad \textbf{3.6}$$

Thus if $\phi_s = 1$ (complete wetting of the surface with no air pockets), then $r_w = r$, in which case the Cassie-Baxter equation cancels down to the Wenzel equation. The most relevant point to note however, is that for both Wenzel and Cassie-Baxter models, an increase in surface roughness for a hydrophobic material will lead to an increase in contact angle.

The second possible effect that annealing polymer films could have on observed contact angles is thermal degradation. If any thermal degradation of the polymer matrix or additive were to occur, this could have pronounced effects on the measured contact angles. In order to try and elucidate the exact causes behind the changes observed in our work due to annealing polymer films, we have investigated both the surface topography of the samples by means of atomic force microscopy (AFM), and the thermal stability of both additives and polymer matrices by thermogravimetric analysis (TGA), all of which will be discussed later in this section.

Before contact angle measurements could be measured on annealed polymer films, the T_g of the PVP matrix needed to be measured as well as the thermal stability of the matrix and additive, in order to determine a suitable annealing

temperature. Initially we measured the T_g of K15 PVP by differential scanning calorimetry (DSC) to be 155°C. Having determined the T_g of the polymer matrix we then investigated the thermal stability of K15 PVP in addition to that of the 6K2 PVP additive by means of TGA in order to see how high we would be able to heat the polymer films without risk of thermal degradation. While the situation for a TGA sample and a polymer film of a thickness of approximately 250nm are not directly comparable due to huge differences in surface area to volume ratios, TGA at least gives a rough guide to the temperatures at which the polymer matrices and additives will start to thermally decompose.

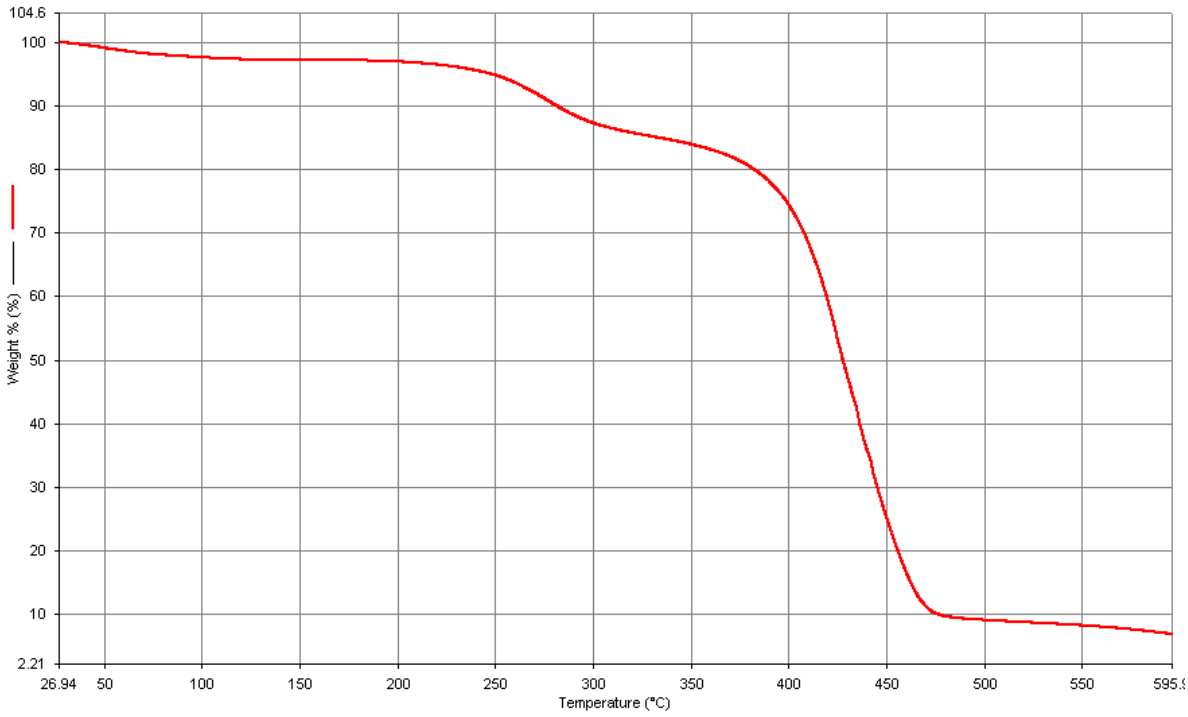

Figure 3.21. TGA data for a 6K2 PVP additive heated from 30°C to 600°C at a rate of 10°C/min under an oxygen-free nitrogen atmosphere.

In Figure 3.21 can be seen TGA data for a 6K2 PVP additive heated at a constant rate of 10°C/min up to a maximum temperature of 600°C. The sample was contained within an oxygen-free nitrogen atmosphere to simulate as closely as

possible the oxygen-free vacuum oven in which PVP samples were to be annealed. As can be seen from the data there is an initial mass loss of approximately 3% corresponding to the loss of water. Despite the fact the additive was stored under vacuum, PVP is hygroscopic and needs more rigorous methods to be applied to it in order to dry it completely. The onset of a degradation step can be seen at approximately 175°C leading to a 10-12% decrease in mass which coincidentally corresponds almost exactly to the mass of the fluoroalkyl end-group and so this was presumed to be the loss of the end-group. Then at approximately 320°C we see complete degradation of the polymer leading to less than 10% of the original mass remaining. From this TGA it was decided to anneal samples at 165°C, roughly midway between the T_g of PVP and the onset of thermal degradation of the end-group.

Having settled on an annealing temperature of 165°C, polymer films comprising of 0-2.5% 6K2 PVP additive in K15 and K90 matrices were prepared and the initial annealing time was set at 1 hour.

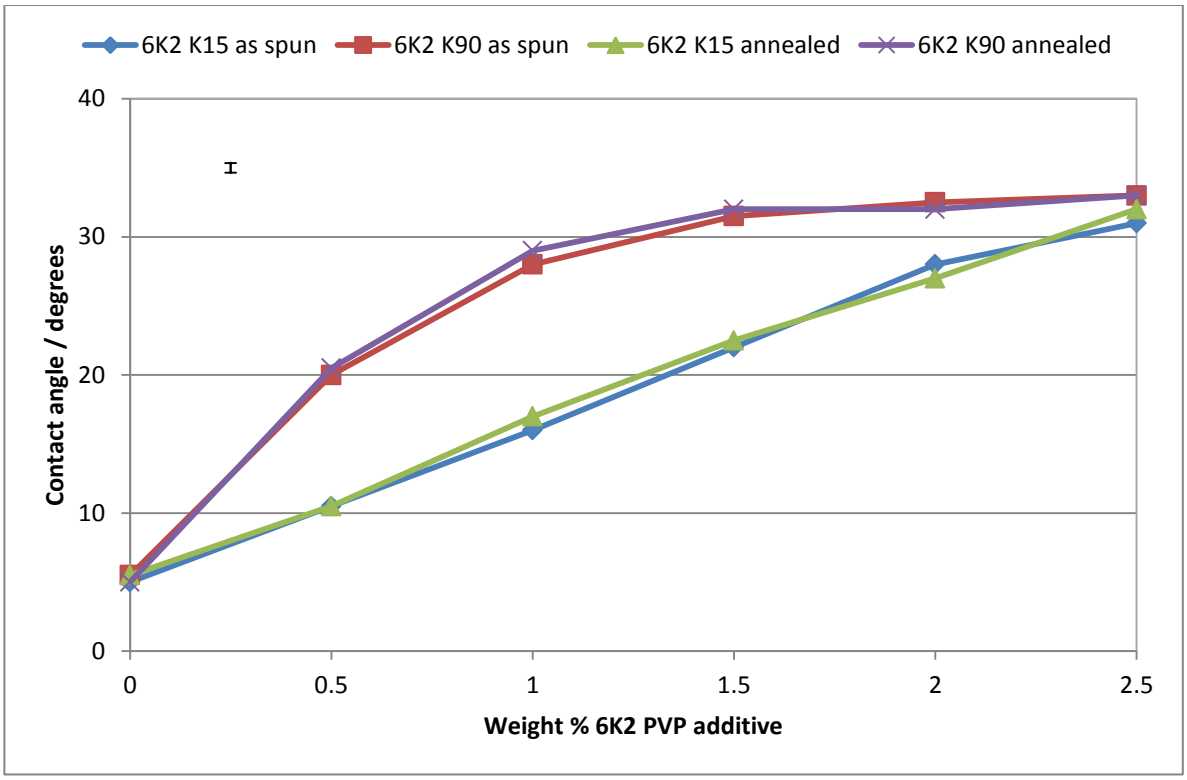

Figure 3.22. Effect of annealing (165°C for 1 hour) polymer blends at varying additive concentrations on contact angle, for blends of 6K2 PVP di-functional additive in either a K15 or K90 PVP matrix.

As can be seen from Figure 3.22, annealing these films at 165°C for 1 hour seems to have little or no effect on the observed contact angle. Though differences between corresponding annealed and unannealed data points are below the threshold of necessarily being statistically significant, one could tentatively suggest that there is a vague trend for the annealed contact angles to be slightly higher by one or two degrees. These results compare unfavourably to past work with analogous polystyrene-based additives[15] in which annealing of polymer films led to significant increases in contact angle, however due to the lower T_g of the polystyrene matrix in question (104°C), the authors were able to anneal at a temperature of T_g+45°C. In the work presented in this thesis, the annealing temperature of 165°C only equates to T_g+10°C as it is more tightly constrained by

the higher T_g of the PVP matrix (155°C) and the onset of thermal degradation of the additive (175°C). As 165°C is an annealing temperature constrained by the thermal stability of the materials involved and not as high above the T_g as would be desirable, it was decided after this initial experiment to increase the annealing time to 12 hours at the same temperature using a fresh set of polymer films.

At the longer annealing time of 12 hours (Figure 3.23) it can clearly be seen that annealing the films is beginning to have a more noticeable effect on the observed contact angle. The most benefit appears to be for additive in the K15 matrix below the CAC. However at the turning point before the onset of the plateau region it would seem that annealing has had a slightly diminishing effect on the observed contact angle. Another important point to note is that in the case of the K15 matrix that there is a 5° increase in contact angle on annealing for the unmodified matrix - 0% 6K2 PVP additive. This is interesting as it immediately suggests that something other than an increase in additive surface concentration is occurring to change the contact angle as in this case there is no additive present. This is not to say that annealing is definitely having no effect on the surface segregation of the additive in measurements where additive is present, but it clearly shows that something else is happening as well, be it a surface degradation effect or a change in surface topology. The observed changes in contact angle may be a result of any combination of these three possible processes, which will be discussed later in this chapter with the TGA and AFM data.

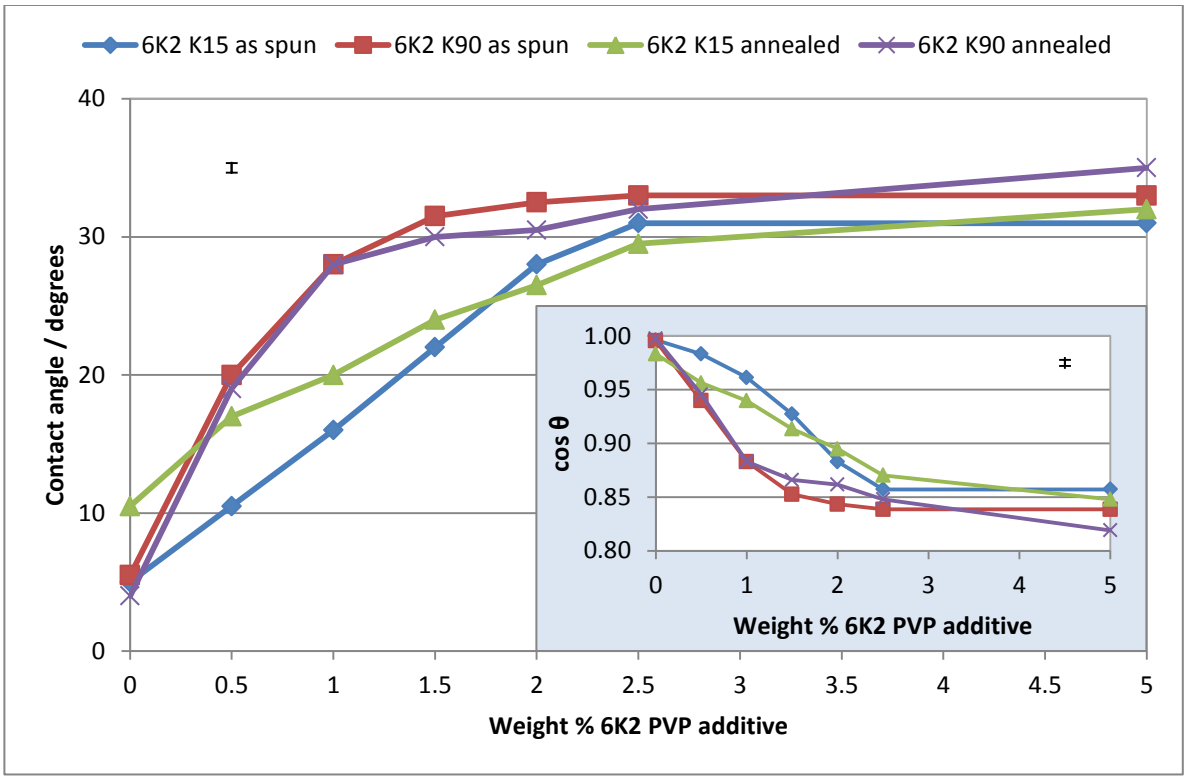

Figure 3.23. Effect of annealing (165°C for 12 hours) polymer blends at varying additive concentrations on contact angle, for blends of 6K2 PVP di-functional additive in either a K15 or K90 PVP matrix.

The effect of annealing for this time and at this temperature is minimal in the case of the additive in the K90 PVP matrix, though while the differences in corresponding annealed and unannealed data points is again not necessarily statistically significant, there would again seem to be a trend for the annealed data points to appear at values of between one and two degrees higher than their unannealed counterparts.

Having observed a clear shift in measured contact angles upon annealing when the additive was present in a matrix of K15 PVP, it was decided to increase the annealing time further in order to ascertain whether or not any additional changes would be seen after 12 hours. Four sets of K15 PVP films were prepared comprising the same concentrations of 6K2 PVP additive as used thus far, and

were subjected to annealing times of 3 days, 6 days, 9 days and 13 days respectively, at a constant temperature of 165°C.

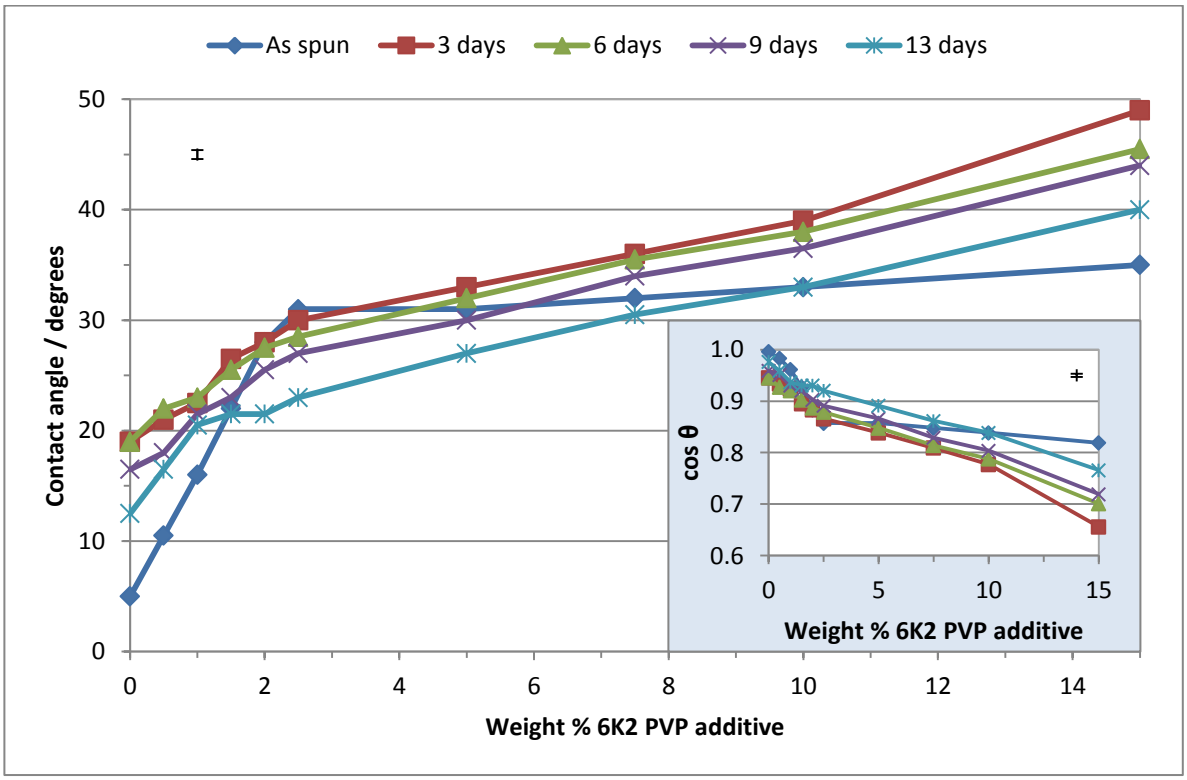

Figure 3.24. Effect of annealing polymer blends with varying additive concentrations at 165°C on contact angle, for blends of 6K2 PVP di-functional additive in a K15 PVP matrix. Weight % additive vs. contact angle for each annealing period (0-13 days).

As can be seen from the data presented in Figure 3.24, an annealing time of three days resulted in qualitatively similar data to that seen for the films annealed for 12 hours, although the increases seen in contact angle at additive concentrations below that of the CAC are significantly larger. Most importantly we see that the largest increase (14°) in contact angle arises as a result of annealing the unmodified matrix, strongly suggesting that any increases in contact angle in the modified films cannot be solely attributed to enhanced surface segregation, but may arise due to a change in surface roughness or thermal degradation.

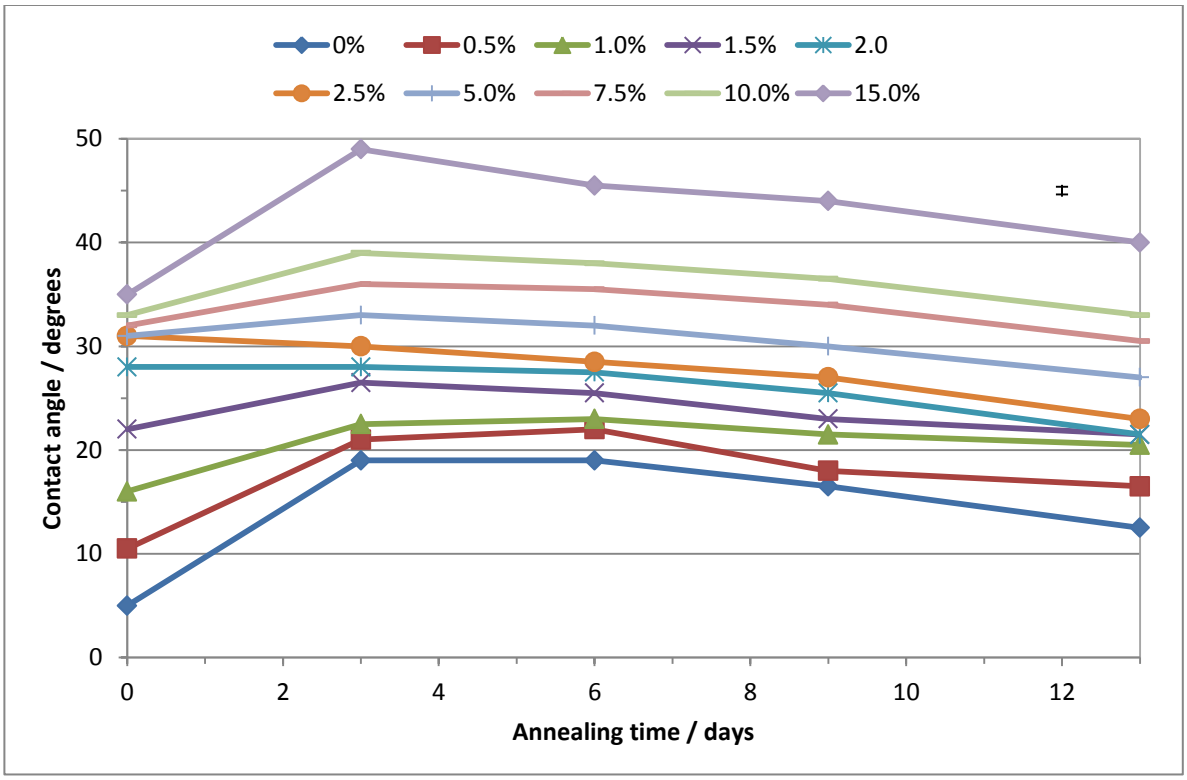

Figure 3.25. Effect of annealing polymer blends with varying additive concentrations at 165°C on contact angle, for blends of 6K2 PVP di-functional additive in a K15 PVP matrix. Annealing time vs. contact angle for each additive concentration (0-15%).

After three days however we see a steady decline in observed contact angles at all additive concentrations, as shown in Figure 3.25, which would further suggest that over longer periods of time some form of thermal degradation is occurring. Initial TGA investigations to establish the thermal stability of both additives and matrix, were carried out for no longer than 1 hour and therefore provide insufficient evidence of these materials' thermal stability on such prolonged time scales. Additionally TGA data does not directly apply to the situation of a 250 nm thick film due to the enormous surface area to volume ratio of such a film relative to that of a simple solid sample. Another possibility is that the temperature in the vacuum oven used to anneal the samples was not completely uniform, and some samples were annealed at temperatures of slightly above or below 165°C. Clearly any

variation in temperature would affect the annealing studies and in particular any samples which experienced temperatures in excess of 165^{o}C would be more prone to thermal degradation. In order to investigate this possibility annealing studies were repeated on a subset of the samples used to generate the data shown in Figure 3.24.

It can be seen in Figure 3.24 that each data set can be broadly defined by three concentrations of additive; 0%, 2.5% and 15%. Therefore fresh samples of 6K2 / K15 PVP films were prepared, containing these three weight percentages of additive. As far fewer samples were investigated in this repeat trial, the films could be placed in close proximity to one another, occupying only a small space in the centre of the vacuum oven and therefore minimising the risk of individual films experiencing varying annealing temperatures.

The results of this repeated annealing study can be seen in Figure 3.26. It would appear that variations in temperature within the vacuum oven are indeed responsible for at least some of the trends seen in the original data in Figure 3.24 from 3 days to 13 days. This would make sense as the samples were placed in the oven in the order that they were to be removed, therefore the “3 day” samples were placed at the front of the oven while the “13 day” samples were placed at the back.

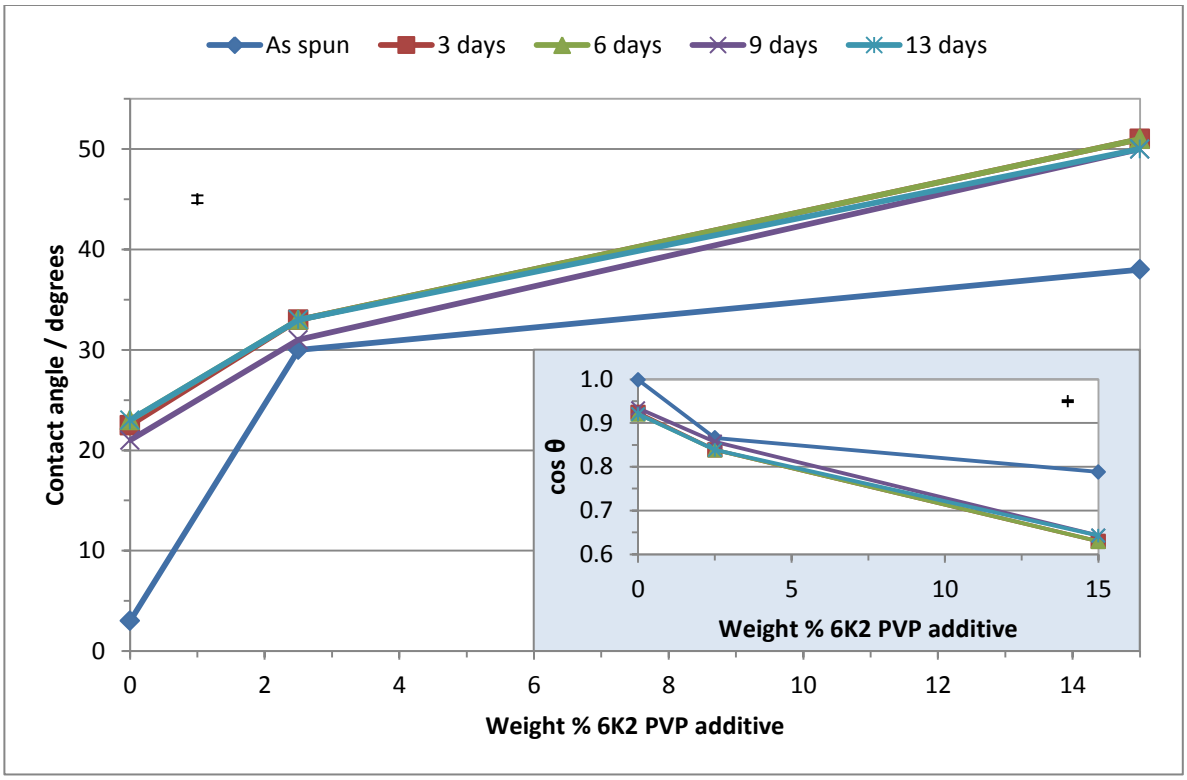

Figure 3.26. Plot of weight % additive against contact angle for the 6K2 PVP di-functional additive in a K15 matrix, for both unannealed films and films annealed at 165°C for periods of 3 days, 6 days, 9 days and 13 days. This data represents repeat experiments from selected data points in Figure 3.24.

However in the repeat data we see that annealing at 165°C for three days has an impact on surface properties, but prolonged annealing beyond that time has no further significant effect on contact angles. However, we can still observe that the largest impact of annealing is on the unmodified matrix where the contact angle increases from 3° to 21-23°, suggesting that factors other than surface segregation are affecting the contact angle measurements. Subsequently a series of prolonged TGA experiments were carried out to verify the thermal stability of both the additive and matrix at 165°C for up to three days. In addition to these experiments, a series of AFM measurements were also performed to try and elucidate, if any, the effect of annealing on the surface topography of the polymer films.

3.3 Atomic Force Microscopy (AFM) and Thermogravimetric Analysis (TGA)

3.3.1 Investigation of surface topology of both unannealed and annealed polymer films

Atomic Force Microscopy (AFM)[37] is a powerful surface imaging technique whereby a fine probe attached to a cantilever is scanned across a sample surface in order to provide detailed topographical information. It also has important application in the determination of force-versus-distance curves which give valuable insight into surface properties such as elasticity, hardness, adhesion and surface charge densities.[38] AFM is capable of imaging both conducting and insulating surfaces, with nanometre lateral and sub-angstrom vertical (atomic) resolution. The probe-surface interaction is observed and recorded by the reflection of a laser beam off the reverse side of the cantilever, and into a split photodiode detector (Figure 3.27). The sample is mounted on a piezoelectric scanner, and with the use of a feedback loop, the probe-surface interaction is kept constant by moving the sample up and down while it scans forwards and backwards past the probe. For each *x*, *y* coordinate of the sample, its height (*z* coordinate) is recorded and a three dimensional digital representation of the surface is constructed in this way.[39]

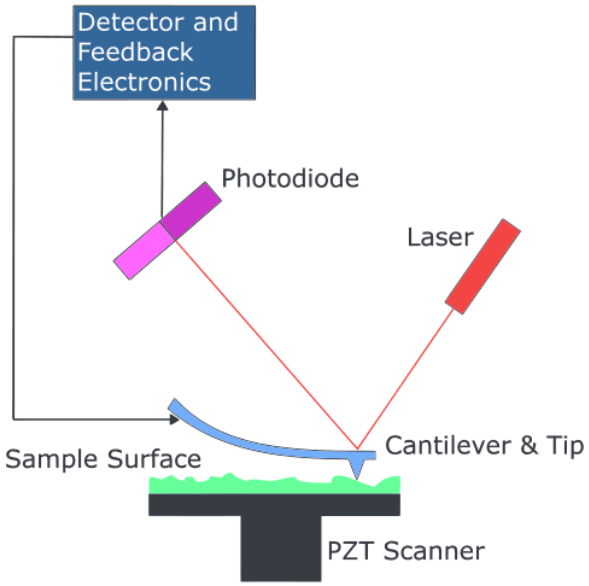

Figure 3.27. Simple block diagram showing the basic components of an Atomic Force Microscope.[40]

When applied as a surface imaging technique, AFM can be performed in a variety of modes, the most common being 'contact' mode and 'tapping' mode. Contact mode is essentially as described above, where a constant probe-surface interaction is maintained by virtue of a feedback loop and vertical movements of the sample, and for each *x*, *y* coordinate of the sample, the *z* coordinate is recorded and used to create a detailed digital image of the surface. Tapping mode, as used in the work presented in this thesis, involves the oscillation of the probe at or near the cantilever's resonance frequency, and rather than maintaining constant contact with the surface, the probe is tapped on the surface during the otherwise similar scanning procedure. The use of an oscillating probe eliminates lateral forces between probe and sample that are otherwise present in contact mode, reducing the possibility of damage being caused to the sample, and allowing the imaging of soft or fragile surfaces.

In this work, AFM was used in an attempt to determine whether surface roughness

and its possible alteration upon annealing, could have a part to play in the contact angle data for annealed polymer films presented earlier. As can be seen in Figures 3.24 and 3.26, it would appear that the greatest increases in contact angle due to annealing occur in those polymer films comprising 0% additive. This is counterintuitive as it was expected that the very presence of additive and its concentration would be the principle cause of any contact angle increases achieved through annealing.

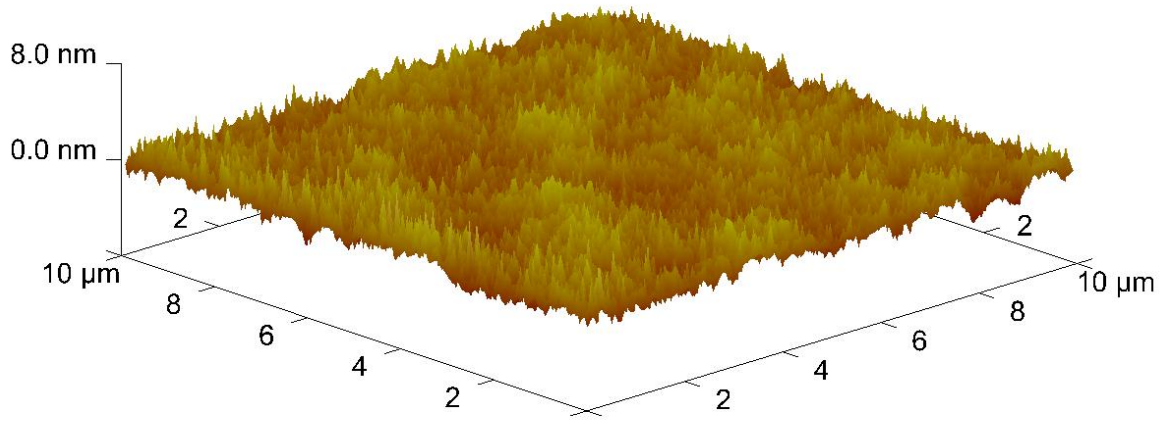

Figure 3.28. Three dimensional representation of AFM data showing the topography of the surface (10µm^2) of a PVP film comprising 2.5 weight % 6K2 additive in a K15 PVP matrix.

A typical atomic force micrograph of an unannealed polymer blend is shown in Figure 3.28. As can be seen from the vertical scale, this film (as with all others) is exceptionally smooth possessing features deviating no further than a few nanometres from the mean plane.

AFM was used to calculate the surface roughness, R_q, of various polymer blends containing 0%, 2.5% or 15.0% 6K2 PVP additive, annealed for times of between 0 and 13 days. R_q is defined as the root mean square of height deviations taken from the mean image data plane, and is given by Equation 3.7.

$$R_q = \sqrt{\frac{\sum z_i^2}{N}} \qquad \textbf{3.7}$$

Each sample (a polymer thin film prepared as for previous contact angle measurements) was cut to size and mounted on an AFM stub. Six, 10μm^2 areas were chosen at random and scanned with the AFM, a value for R_q calculated for each and then the average was taken to give a final value of R_q for the sample. The data from these AFM measurements is presented in Figure 3.29.

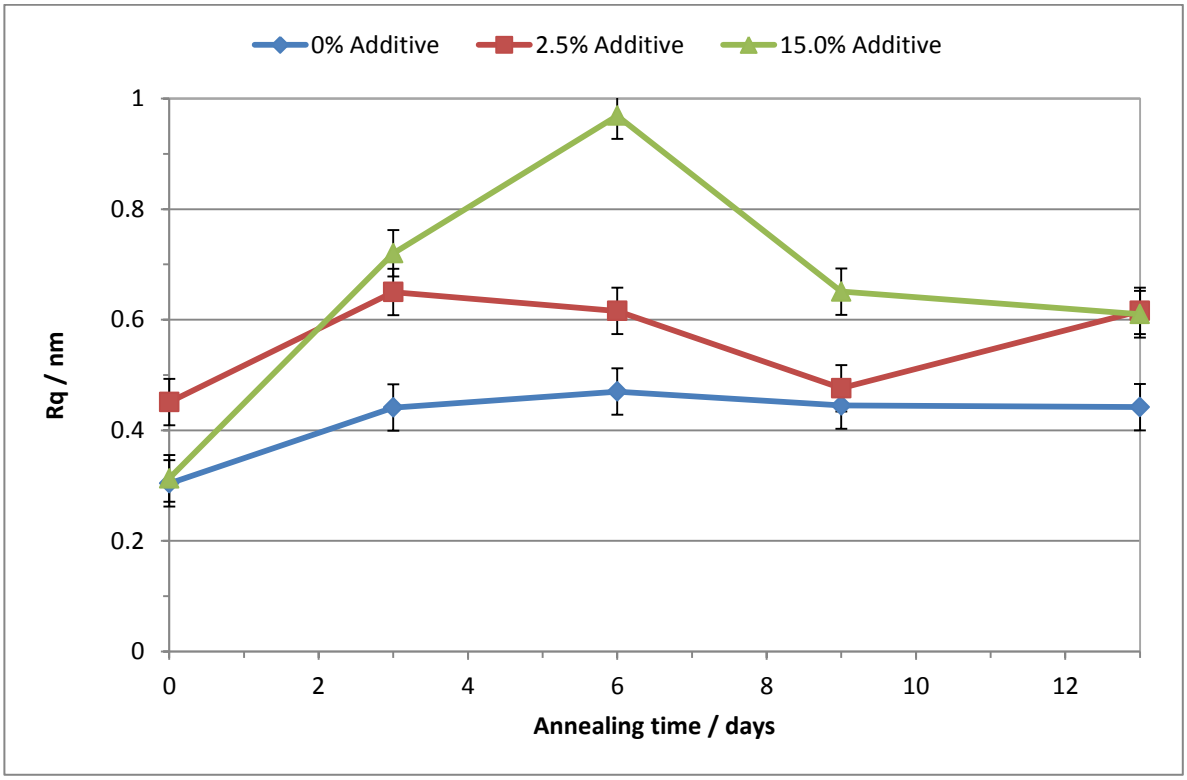

Figure 3.29. Plot of annealing time against R_q (a measurement of surface roughness) in a bid to show the effect of annealing on the topology of a selection of polymer films containing either 0%, 2.5% or 15.0% 6K2 PVP additive.

The first important point to note is the exceptional smoothness of these films, both

annealed and unannealed, with no R_q measurement reaching even a single nanometre (bearing in mind that a nanometre is approximately only seven times the length of a typical carbon-carbon single bond). While in all three blends the unannealed (0 days) polymer film has the lowest R_q, it is in fact the concentration of additive present that appears to have the more significant effect on surface roughness than the annealing process does. That the concentration of additive affects the surface roughness is perhaps unsurprising given the very small R_qs involved and the comparatively significant size of the additive end groups present at the surface, but it does highlight the minimal effect that annealing appears to have on surface roughness. In the 0% additive films, annealing over periods of between 0 and 13 days leads to fluctuations in R_q of no more 0.17nm, and the most significant variation in R_q seen in any of the blends over all of the annealing periods is 0.67nm. We have found no evidence in the literature that variations in surface roughness on this scale could have as pronounced an effect upon contact angle as can be seen in the results shown for 0% additive films in Figure 3.26. Additionally, any variations in surface roughness seen in Figure 3.29 do not correlate at all with the contact angle measurements shown in Figure 3.26. Therefore this work performed with AFM has shown that the annealed contact angle measurements shown in Figures 3.24 and 3.26 are not a result of changes in surface roughness due to the annealing process, as no significant changes have been observed.

3.3.2 Thermal stability of end-functionalised additive at 165°C for prolonged time period

Thermogravimetric Analysis (TGA) is an analytical method used to measure sample mass as a function of temperature.[41,42] The temperature can be controlled precisely and extremely accurate dynamic weighing of the sample allows the thermal stability of a material to be tested. TGA can be used to determine if a sample is stable at a specific temperature, or the temperature can be increased steadily to give a degradation profile (a plot of sample mass vs. temperature) from room temperature to that of sample combustion. These experiments can be performed in air, or under an inert atmosphere. Additionally TGA can be used to measure the moisture or solvent content of a sample, and also to measure the percentage of non-combustible material in a sample, for example a thermally stable constituent in a composite material.

In this work TGA has been used to determine the thermal stability of the DPFPB-PVP di-functional additive, 6K2 PVP, at the annealing temperature of 165°C over a prolonged time period. Earlier TGA of this material (Figure 3.21) showed the onset of thermal degradation at 175°C when heating the sample at a rate of 10°C/min, and 165°C was chosen as a safe annealing temperature, which is still only 10°C above the T_g of the polymer. However as the annealing process has been performed for time periods of up to 13 days, these longer scale TGA experiments were performed in order to ascertain whether thermal degradation could be the cause of the unexpected contact angle measurements for annealed samples as shown in Figure 3.26.

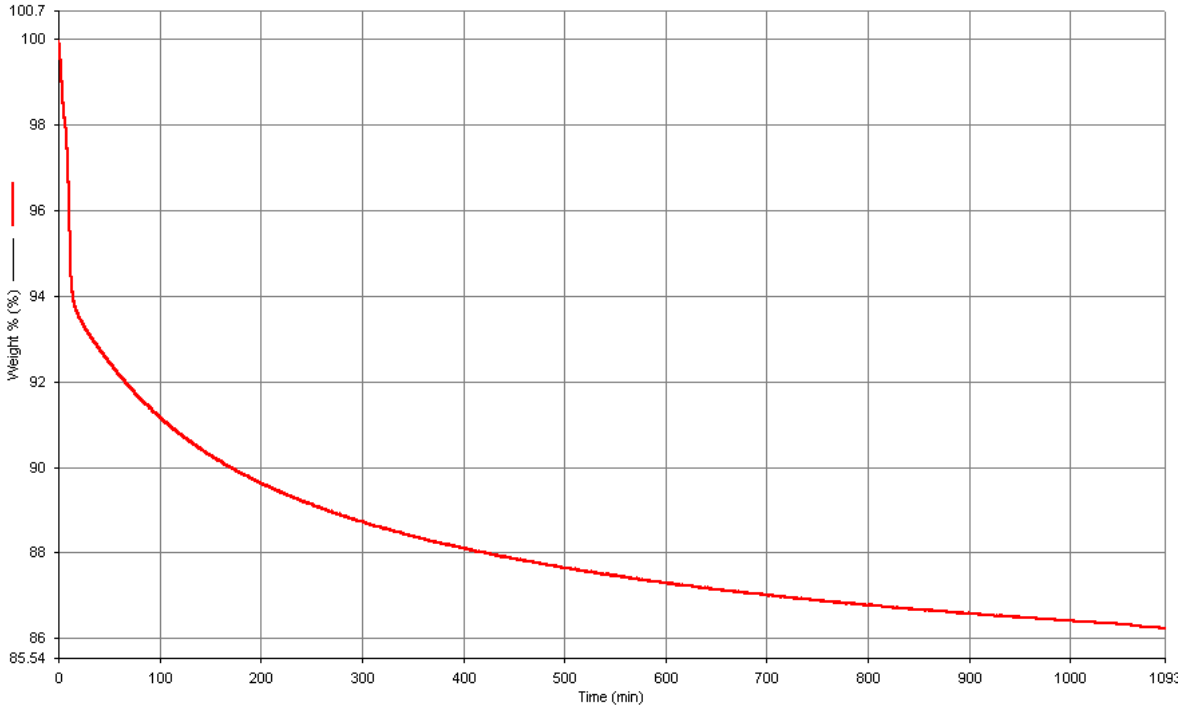

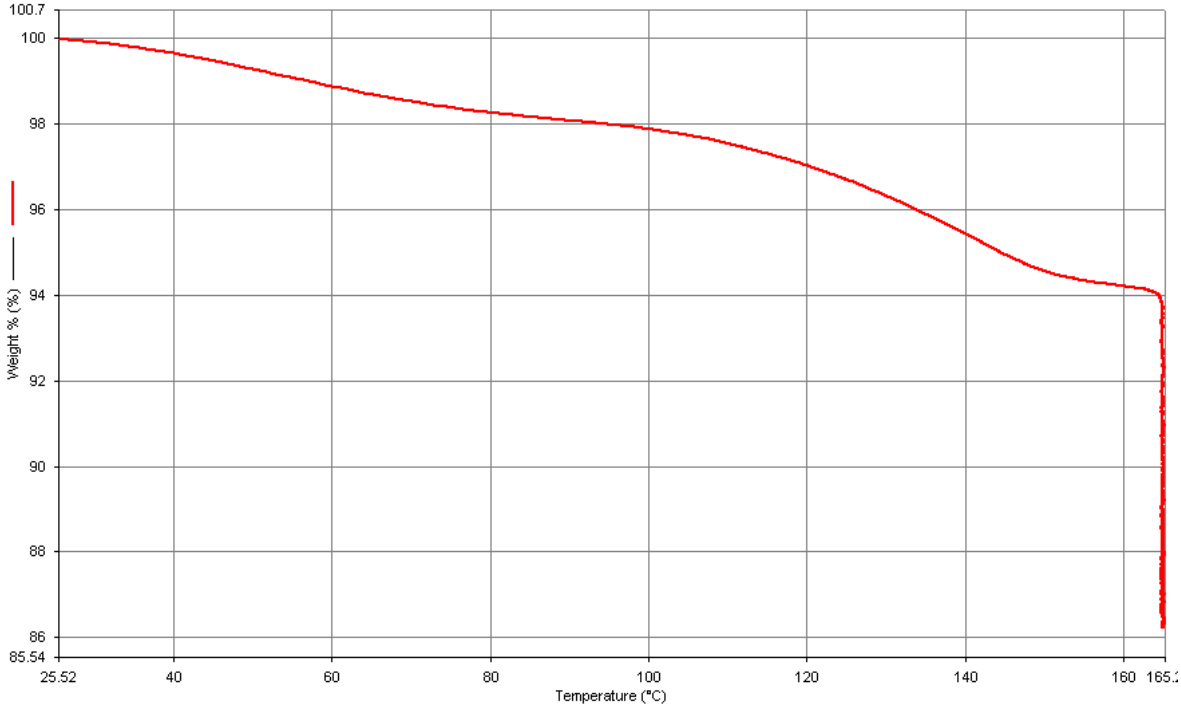

Figure 3.30. TGA data (sample weight vs. time and sample weight vs. temperature) for a 6K2 PVP additive heated to a steady 165°C under an oxygen-free nitrogen atmosphere for 18 hours.

Shown in Figure 3.30 is TGA data for the 6K2 PVP additive heated at 10°C/min to a steady temperature of 165°C which was maintained for a period of 18 hours. The first plot showing sample mass vs. time clearly indicates that mass loss continues to occur throughout the full 18 hours of the experiment. The second plot is of sample mass against temperature for the same experiment, and shows that during the heating of the sample to 165°C there is a mass loss of 6%; however a further 8% is lost after reaching and being held at 165°C. There is also an inflection in the curve between 0 and 165°C indicating two separate mechanisms by which this mass loss is occurring. The first is most certainly moisture loss, however it is possible that the second step (onset at 85°C) in addition to the 8% mass loss after reaching 165°C is due to either further moisture loss, of water bound to the polymer by a different mechanism than that lost below 85°C, or it is due to thermal degradation of the sample. Given the AFM results discussed in the previous section, and in light of this data, it is most likely that some form of thermal degradation of the 6K2 PVP additive is occurring, and it is this process which is responsible for the contact angle measurements shown for annealed polymer blends in Figure 3.26.

3.4 Rutherford Backscattering experiments

3.4.1 Introduction to Ion Beam Analysis and Rutherford Backscattering

Figure 3.31. Picture of the NEC 5SDH Pelletron accelerator used to perform RBS experiments.

Ion beam analysis (IBA)[43,44] encompasses a range of analytical techniques all involving the use of high energy (MeVs) ion beams in order to obtain quantitative data pertaining to the elemental composition of solid surfaces. Depth resolution is typically in the range of nanometres to a micron, and in addition to analysing near surface elemental composition, certain techniques can be used to provide elemental depth profiles. The use of any particular technique is determined predominantly by the mass of the target nuclei relative to that of the incident ions being accelerated into the surface, and also relative to that of the majority of the other nuclei within the sample.

When an ion beam with an energy of the order of MeVs is incident upon a solid surface, the vast majority of accelerated ions are embedded into the sample and are not backscattered at all, owing to the relatively small probability of a direct collision with a nucleus. However, when a high energy ion does collide with a nucleus, there are three possible outcomes. The first two possibilities arise from the situation where the ion collides with a target nucleus at the surface which leads to what can be considered as an elastic collision (energy is neither lost nor gained).

Technically this collision does not actually involve direct contact between the accelerated ion and target nucleus, but energy is transferred through Coulombic repulsion between them when they come in close proximity to each other. However this interaction can be modelled accurately as an elastic collision using classical mechanics.

If the accelerated ion is of a lower mass than the target nucleus, the ion would simply be deflected back in the general direction of the ion source having lost a certain amount of energy through transfer of momentum to the target nucleus. These “backscattered” ions and their corresponding energies can then be detected by a stationary solid state detector placed at a specific angle to the incident ion beam and this is the basis for Rutherford Backscattering analysis (RBS).[43,44] The energy of a backscattered ion (having come originally from a monoenergetic ion beam of known energy) is dependent upon the mass of the target nucleus with which the collision occurred – the larger the nucleus the higher the energy of the backscattered ion.

If the accelerated ion is of a greater mass than the target nucleus, then the ion will no longer be backscattered as this is not kinematically allowed, but it will continue travelling away from the ion source and into the sample surface. The lower mass target nucleus however will be recoiled and ejected from the sample also in a forward direction with respect to the ion beam, and it is this effect that is the basis of Elastic Recoil Detection analysis (ERD).[45,46] Kinematics is simply the branch of mechanics which describes the motion of bodies (or in this case particles) without consideration for the forces that give rise to their motion i.e. how they interact with each other taking into account the conservation of both momentum and kinetic energy. An easy way to visualise the difference between RBS and ERD is simply to imagine firing a snooker ball at a few metres per second along a flat surface towards a bowling ball versus firing the bowling ball in the same fashion towards a snooker ball. In the first instance the snooker ball would be deflected away from the bowling ball which would hardly move (backscattering) however in the second instance the snooker ball would be shot forwards and the bowling ball would continue forwards as well (elastic recoil).

The third and most likely possibility is that the accelerated ion will not collide with a target nucleus at the surface at all, but will travel into the surface gradually losing energy through low energy collisions with electrons. At some point an elastic collision with a nucleus will occur and the ion will be backscattered and exit the sample again in the general direction of the ion source. It is this third process that allows RBS to provide an elemental depth profile as the lower energy of the backscattered ion relative to that of one which did not penetrate into the sample is measurable and the depth to which it penetrated can be calculated. Though energy is lost in discreet interactions with electrons, the process can be considered continuous and the total energy lost is a direct result of the total distance travelled through the solid sample summed with the energy lost by a single elastic collision with a target nucleus within the solid.

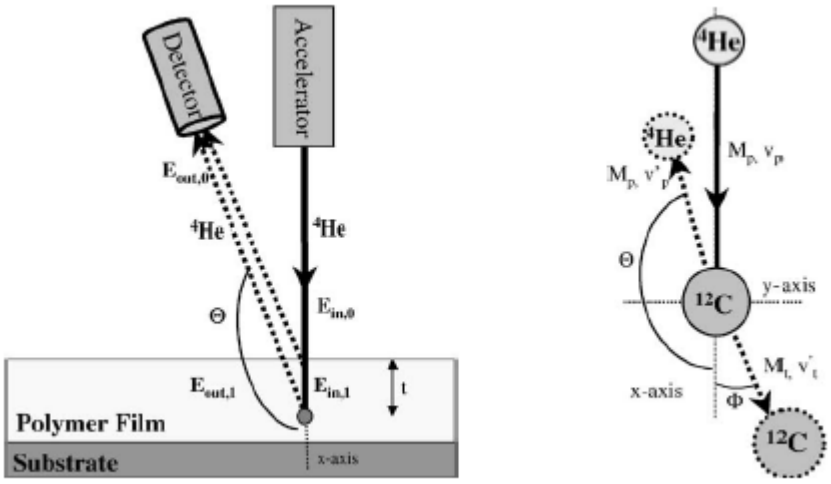

Figure 3.32. Diagrams depicting the experimental configuration for RBS (left) and an elastic collision between a moving particle and a stationary particle (right) where solid lines refer to the situation "pre-collision", and dotted lines "post-collision". Masses and velocities are designated by M and v respectively and all quantities refer to a laboratory frame of reference.[43]

In RBS, the loss of energy in ions backscattered from the surface is a direct consequence of momentum transfer from the high energy ion to the target nucleus during the collision event. With lighter elements that are closer in atomic mass to the accelerated ions, the amount of momentum transfer is significant and therefore leads to a correspondingly significant reduction in the energy of the backscattered ions allowing for these elements to be easily identified. As the differences in mass between these small nuclei as a percentage of their total mass is significant relative to the mass of the accelerated ion, different elements will give rise to measurably different backscattering energies and these elements can easily be resolved from one another. However with elements of a much greater atomic mass than the accelerated ions, far less momentum is transferred during collision events leading to backscattered ions with energies that are much closer to both that of the original ion beam and also to each other. The extent to which each element affects the energy of backscattered ions detected at a specific angle, θ, from the direction of the ion beam is known as the "kinematic scattering factor" and is given by Equation 3.8:

$$K = \left[\frac{M_p \cos\theta + \sqrt{M_t^{\,2} - M_p^{\,2} \sin^2\theta}}{M_p + M_t} \right]^2 \qquad \textbf{3.8}$$

Where K is the kinematic scattering factor, M_p is the mass of the accelerated ion, M_t is the mass of the target nucleus with which the collision occurred, and θ is the angle at which the detector is placed relative to the direction of the ion beam (i.e. only ions that are backscattered at this precise angle are detected). The energy of a backscattered ion arising from a specific element can then be calculated using the kinematic factor as in equation 3.9 and hence counts with this energy are attributable to collision events involving that element.

$$E_{out} = K \times E_{in} \qquad \textbf{3.9}$$

Where E_{out} is equal to the energy of the backscattered ion and E_{in} is the energy of the ion before the collision, i.e. the beam energy.

This means that RBS is much more sensitive to lighter elements, easily distinguishing between nuclei with a difference in mass of only one or two atomic mass units, but cannot always resolve heavier elements from each other as the energies of backscattered ions arising from collisions with these nuclei are all much more similar.

When considering the energy of a backscattered ion that has penetrated the surface and lost energy through interaction with electrons as well as a nuclear collision, the energy can also be described in terms of the kinematic scattering factor as in Equation 3.10:

$$E_{out} = K(E_{in} - E_1) - E_2 \qquad \textbf{3.10}$$

Where E_1 is the energy lost by the accelerated ion on the inward path through the sample and E_2 is the energy lost on the outward path.

Another factor to consider is the change in probability of an ion being backscattered when we vary the atomic mass and therefore size of the target nuclei which is related to the differential scattering cross section given in Equation 3.11:

$$\sigma(\theta) = \left(\frac{Z_p Z_t e^2}{4E_{in}} \right)^2 \frac{4}{\sin^4\theta} \left[\frac{\left\{ \left[1 - \left((M_p/M_t) \sin\theta \right)^2 \right]^{1/2} + \cos\theta \right\}^2}{\left[1 - \left((M_p/M_t) \sin\theta \right)^2 \right]^{1/2}} \right] \qquad \textbf{3.11}$$

Where σ is the differential scattering cross section which represents the area that the nucleus of the element in question presents to the accelerated ion that will result in a backscattering event. Z_p and Z_t are the atomic numbers of the accelerated ion and target nucleus respectively, and e is the charge of an electron.

More simply the probability of a backscattering event being observed at a certain angle relative to the direction of the ion beam is as an approximation proportional to the square of the atomic number of the target nucleus. In other words heavier elements have larger nuclei and are therefore more likely to be involved in collisions with accelerated ions. So RBS is actually more sensitive to heavier elements in terms of detecting their backscattered ions which are more numerous and of a higher energy than those from lighter elements, but as already discussed, RBS is less sensitive to heavier elements in terms of being able to resolve their signals from one another and hence identify and distinguish between them.[43]

In our work and with most work involving polymer analysis, $^{4}He^{++}$ is a suitable incident ion as it allows RBS from any elements heavier than itself (ruling out only hydrogen, though this can be used for tandem RBS / ERD experiments) and results in good resolution between many of the elements you might expect to see in a normal polymer and that we indeed see in our polymers (^{12}C, ^{14}N, ^{16}O, ^{19}F etc). Certainly all of the elements that we are concerned with in this work are easily resolvable by RBS with $^{4}He^{++}$, most notably ^{19}F, which being a significantly heavier element than those contained within the rest of the polymer backbone leads to a separate and easily identifiable peak allowing facile calculation of ^{19}F concentration at the polymer surface.

In our use of RBS we have been principally concerned with the quantitative detection of ^{19}F at the polymer surface as a measure of the efficiency of our low molecular weight fluorinated PVP additive to spontaneously surface segregate. As we are interested only in detecting ^{19}F at the surface and not in the bulk, it is not desirable to have incident $^{4}He^{++}$ ions penetrating the surface of the sample (the majority of which ordinarily would) and leading to more complicated spectra. In order to analyse only the top few nanometres of the surface, the sample is placed

in such a fashion that that the ion beam contacts with it at a “grazing” angle of only a few degrees from the direction of the beam in order to take advantage of the effect known as “blocking”. This term refers to the fact that each nucleus within the sample surface casts what can be effectively considered as a shadow behind it, relative to the direction of the incident ion beam. Any ion that hits a nucleus will be backscattered and therefore no ions will continue to penetrate the sample in the space directly behind that nucleus. Any ions that travel in close proximity to the positive nucleus but do not collide with it will be repelled slightly as they pass it due to their own positive charge and their trajectory will be bent away from the nucleus. This leads to a cone shaped shadow behind each nucleus which no ions can reach and this is referred to as “blocking”. If the ion beam is perpendicular to the surface then as there is a relatively large amount of space between each of the nuclei, the accelerated ions can penetrate dozens of nanometres into the surface before a collision occurs or they become embedded in the sample. However if the sample is rotated with respect to the ion beam so that it hits the surface at a grazing angle of approximately five degrees, the ion beam will penetrate more or less the same distance into the material in the direction of the beam, but barely at all in the direction perpendicular to the surface itself. In this way blocking can be taken advantage of allowing us to obtain RBS data corresponding only to the top few layers of atoms at the very surface of the sample.

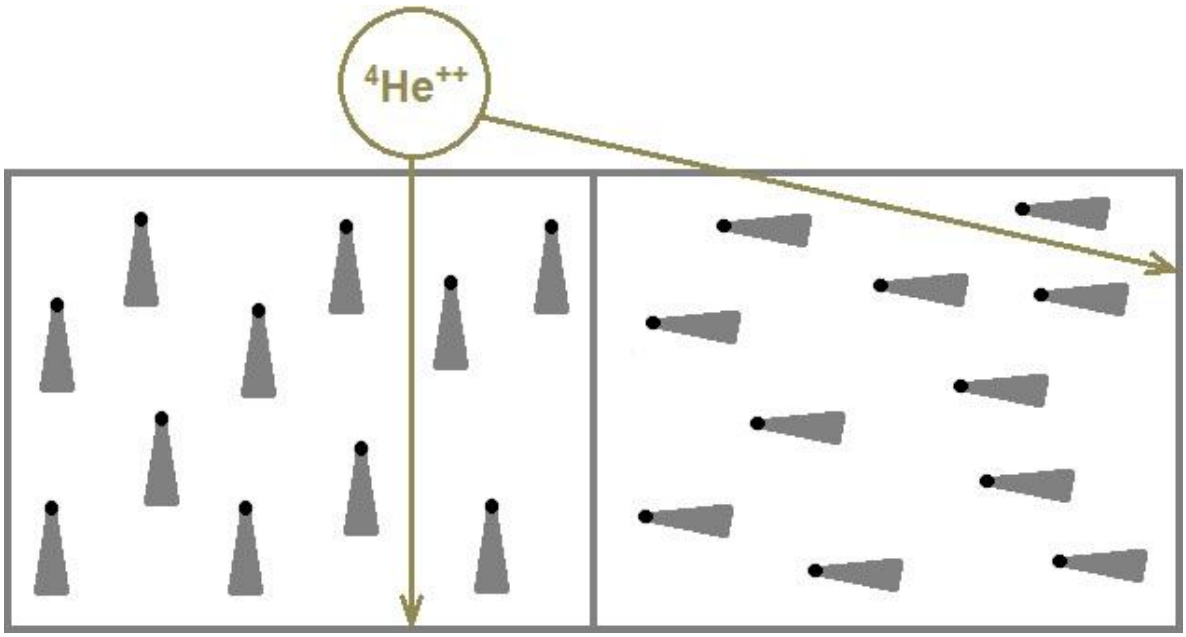

Figure 3.33. Diagram depicting the effects of "blocking" with a $4He^{++}$ ion beam incident upon a solid surface and then at a grazing angle. The black dots represent nuclei within the solid sample and the grey cones show the effective "shadow" cast by each nucleus relative to the ion beam.

3.4.2 Rutherford Backscattering data and discussion

Grazing angle RBS has been used to provide a more quantitative measure of the amount of fluorine at the surface of our modified polymer films, and can therefore give us a good approximation of the surface concentration of fluorinated end-groups. In the case of PVP, RBS is particularly sensitive to the presence of fluorine due to its greater mass and hence greater differential scattering cross section than that of all of the other constituent elements of the polymer. Being able to measure the amount of fluorine specifically in the near surface layer of the polymer films provides us with another good indicator of how the surface adsorption of the fluorinated polymer additive is affected by its concentration and is a useful complementary analytical technique to the contact angle measurements already discussed.

Halogenated organic materials and some polymer surfaces are known to be susceptible to beam damage and as such the beam charge was restricted to 2 μC, with twelve measurements being taken from twelve different spots in order to minimise the exposure of any particular point on the surface to the ion beam. For each sample, the cumulative data collected from these twelve measurements was then imported into SIMNRA,[47] a piece of dedicated software designed to simulate back or forward-scattering spectra for ion beam analysis with MeV beams, and the data was manually fitted to a simulation. The software was then used to integrate the higher energy peak attributable to ^{19}F and a value for the surface concentration of ^{19}F was obtained in atoms cm^{-2}.

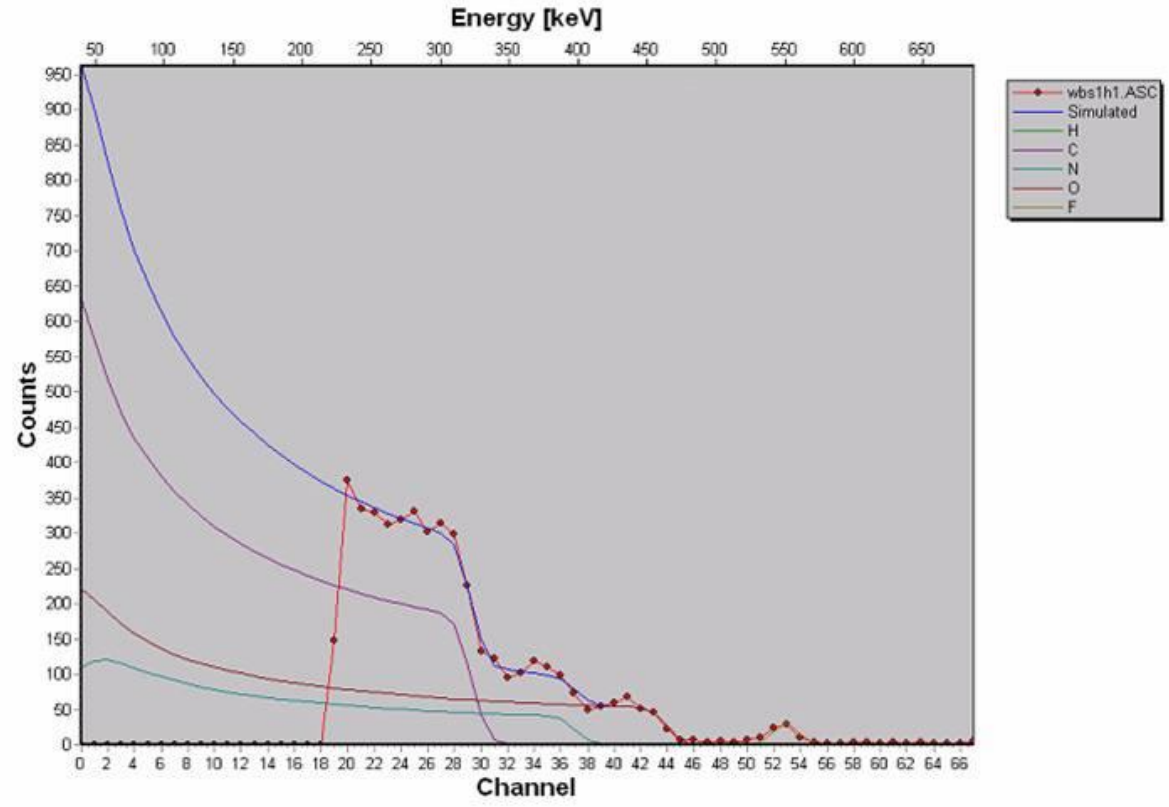

Figure 3.34. SIMNRA screenshot of raw data from an RBS experiment (wbs1h1.ASC data for 1.0% 6K2 PVP / K15 PVP polymer blend) fitted to a simulation. The higher energy peak at 550keV is attributable to ^{19}F and the software is used to calculate its surface concentration.

RBS experiments were performed on a set of K15 PVP films containing a range of percentages of a 6K2 PVP additive with a view to analysing the effect of both additive concentration and additive type on surface adsorption.

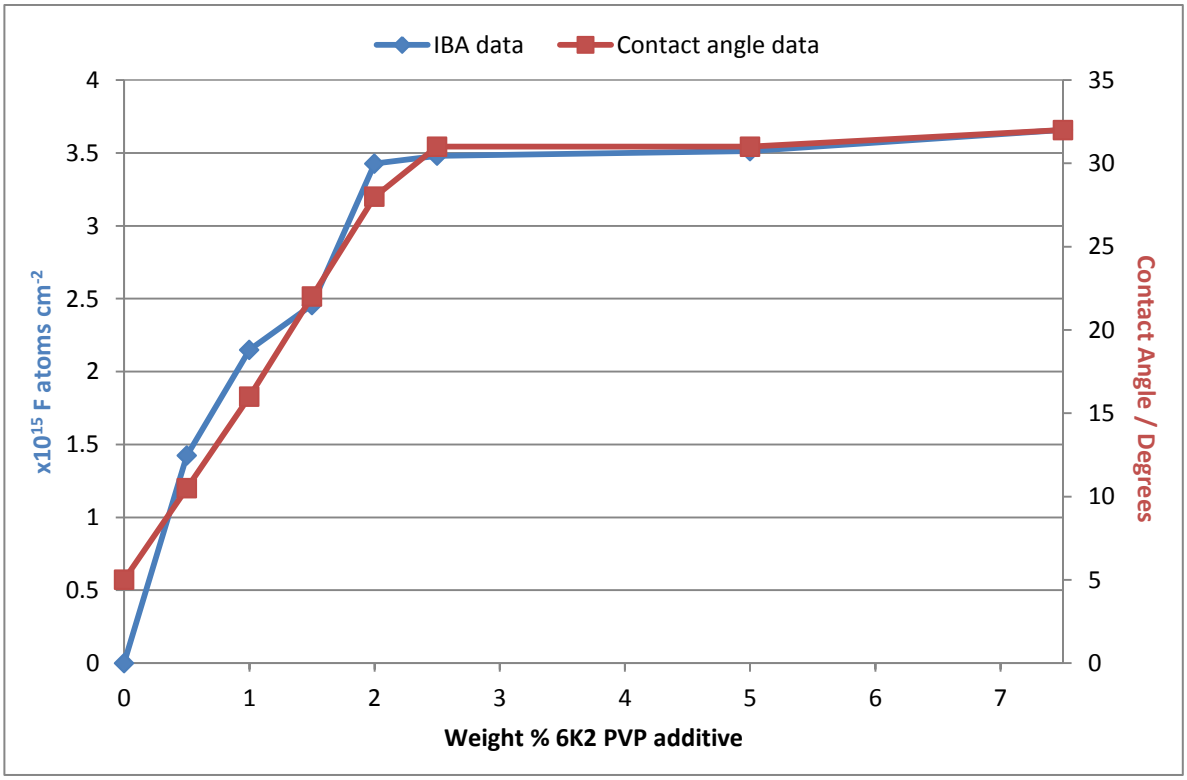

Figure 3.35. Plot of weight % 6K2 additive in a K15 PVP matrix against the number of fluorine atoms per square centimetre of surface. Red data set and right hand y axis show contact angle measurements for the same set of polymer films.

In Figure 3.35 is shown data obtained from RBS experiments carried out on K15 PVP films containing several different concentrations of 6K2 PVP additive. The characteristic shape of the data obtained in all of the "as-spun" contact angle measurements from the previous section (equivalent 6K2 PVP / K15 PVP measurements shown in red using the right hand y axis) can instantly be seen

mirrored in this RBS data, with a steady increase in fluorine surface concentration up to 2.5% additive concentration whereupon a plateau region is reached. This plateau region corresponds to maximum obtainable surface concentration of additive which is determined by the Critical Aggregation Concentration (CAC) as previously discussed (see Figure 3.13).

It can again be seen that very small quantities of additive (as little as 0.5 wt. %) have a pronounced effect on the fluorine content at the surface and hence the surface properties of otherwise unmodified PVP. This data also proves conclusively the presence of our functionalised polymer additive, specifically at the surface of the polymer film. It also confirms observations made from contact angle measurements regarding the additive's behaviour in terms of spontaneous surface segregation with respect to its concentration, as the additive is the only possible source of fluorine in any of the samples.

3.5 References

[1] Downie, I. M.; Holmes, J. B.; Lee, J. B.; *Chem. Ind. (London)*, **1966**, 900

[2] Appel, R.; *Angew. Chem. Int. Ed. (English)*, **1975**, *14*, 801

[3] Williamson, A.; *Philos. Mag.*; **1850**, *37*, 350

[4] 'Appel Reaction', *Organic Chemistry Portal*, <http://www.organic-chemistry.org/namedreactions/appel-reaction.shtm> (15th August 2011)

[5] 'Williamson Synthesis', *Organic Chemistry Portal*, <http://www.organic-chemistry.org/namedreactions/williamson-synthesis.shtm> (15th August 2011)

[6] Narrainen, A. P.; Hutchings, L. R.; Ansari, I.; Thompson, R. L.; Clarke, N.; *Macromolecules*, **2007**, *40*, 1969

[7] Mougin, N.; *U. S. Patent 20060088487*, **2005**

[8] Hudson, J. B.; *Surface Science: An Introduction*, Wiley-Interscience, **1998**, 63–65

[9] Tadmor, R.; *Langmuir*, **2004**, *20*, 7659

[10] Young, T.; *Philos. Trans. R. Soc. London*, **1805**, *95*, 65

[11] Masahide, T.; Pieracci, J. P.; Belfort, G.; *Langmuir*, **2001**, *17*, 4312

[12] Ansari, I. A.; Clarke, N.; Hutchings, L. R.; Narrainen, A. P.; Terry, A. E.; Thompson, R. L.; Webster, J. R. P.; *Langmuir*, **2007**, *23*, 4405

[13] Turberg, M. P.; Brady, J. E.; *J. Am. Chem. Soc.*, **1988**, *110*, 7797

[14] Binks, B. P.; Fletcher, P. D. I.; Kotsev, S. N.; Thompson, R. L.; *Langmuir*, **1997**, *13*, 6669

[15] Hutchings, L. R.; Norazilawati, M. S.; Thompson, R. L.; *Polym. Chem.*, **2011**, *2*, 851

[16] Davies, D. G.; Bury, C. R. J.; *J. Chem. Soc.*, **1930**, 2263

[17] Grindley, J.; Bury, C. R. J.; *J. Chem. Soc.*, **1929**, 679

[18] Mukerjee, P.; Mysels, K. J.; *Critical Micelle Concentration of Aqueous Surfactant Systems*, National Bureau of Standards: Washington DC, **1970**

[19] deGennes, P. G.; *Scaling Concepts in Polymer Physics*, Cornell University Press, **1979**

[20] Shinoda, K.; Yamaguchi, N.; Anders, C.; *J. Phys. Chem.*, **1989**, *93*, 7216

[21] Kunleda, H.; Shinoda, K.; *J. Phys. Chem.*, **1976**, *80*, 2468

[22] Welp, K. A.; Wool, R. P.; *Macromolecules*, **1999**, *32*, 5127

[23] Botelho do Rego, A. M.; Lopes da Silva, J. D.; *Macromolecules*, **1993**, *26*, 4986

[24] Zhao, W.; Zhao, X.; Rafailovich, M. H.; Sokolov, J.; *Macromolecules*, **1993**, *26*, 561

[25] Schaub, T. F.; *Chain End Segregation at Polymer Thin Film Surfaces*, **1995**, MSc Thesis, Massachusetts Institute of Technology

[26] Minnikanti, V. S.; Archer, L. A.; *J. Chem. Phys.*, **2005**, *123*, 144902

[27] Wu, D. T.; Fredrickson, G. H.; *Macromolecules*, **1996**, *29*, 7919

[28] Minnikanti, V. S.; Qian, Z.; Archer, L. A.; *J. Chem. Phys.*, **2007**, *126*, 144905

[29] Huggins, M. L.; *J. Chem. Phys.*, **1941**, *9*, 440

[30] Flory, P. J.; *J. Chem. Phys.*, **1941**, *9*, 660

[31] Eichinger, B. E.; Mumby, S. J.; Qian, C.; *Macromolecules*, **1991**, *24*, 1655

[32] Forrest, B. M.; Toral, R.; *Journal of Statistical Physics*, **1994**, *77*, 473

[33] Balsara, N. P.; Nedoma, A. J.; Robertson, M. L.; Wanakule, N. S.; *Macromolecules*, **2008**, *41*, 5773

[34] Wenzel, R. N.; *Ind. Eng. Chem.*, **1936**, *38*, 988

[35] Cassie, A. B. D.; Baxter, S.; *Trans. Faraday Soc.*, **1944**, *40*, 546

[36] Patankar, N. A.; *Langmuir*, **2004**, *20*, 7097

[37] Binnig, G.; Quate, C. F.; *Phys. Rev. Lett.*, **1986**, *56*, 930

[38] Butt, H.-J.; Cappella, B.; Kappl, M.; *Surface Science Reports*, **2005**, *59*, 1

[39] Ngwa, W.; Luo, W.; Kamanyi, A.; Fomba, K. W.; Grill, W.; *Journal of Microscopy*, **2005**, *218*, 208

[40] Image source: 'Atomic Force Microscopy', *Wikipedia*, <https://secure.wikimedia.org/wikipedia/en/wiki/File:Atomic_force_microscope_block_diagram.svg> (23rd September 2011)

[41] Kellum, G. E.; Smith, R. C.; *Anal. Chem.*, **1967**, *39*, 341

[42] Mansfield, E.; Kar, A.; Quinn, T. P.; Hooker, S. A.; *Anal. Chem.*, **2010**, *82*, 9977

[43] Composto, R. J.; Walters, R. M.; Genzer, J.; *Mater. Sci. Eng. R*, **2002**, *38*, 107

[44] Nastasi, M.; Tesmer, J. R.; *Handbook of Modern Ion Beam Materials Analysis*, Materials Research Society, **1995**

[45] L'Ecuyer, J.; Brassard, C.; Cardinal, C.; Chabbal, J.; Deschênes, L.; Labrie, J. P.; Terreault, B.; Martel, J. G.; St.-Jacques, R.; *J. Appl. Phys.*, **1976**, *47*, 381

[46] Arnold Bik, W. M.; Habraken, F. H. P. M.; *Rep. Prog. Phys.*, **1993**, *56*, 859

[47] Mayer, M.; *SIMNRA User's Guide*, Max-Planck-Institut für Plasmaphysik, **2002**

Chapter 4
Additive Effects on GDL Performance

Preliminary investigation into the effects of novel end-functionalised PVP additives on Gas Diffusion Layer performance under simulated fuel cell operating conditions

4.1 Introduction

The work presented in this chapter is a collaboration between myself and Rosemary Fisher at Technical Fibre Products Ltd., under the supervision of Dr Lian Hutchings (Durham University) and Dr Michael Jeske (Technical Fibre Products Ltd.). The preparation of all Low Cost Substrates was performed by myself in the Technical Fibre labs in Kendal, while the water uptake and durability tests that were carried out over a period of approximately three months were performed by Rosemary, as was the subsequent data analysis.

Having tested the novel low molecular weight, end-functionalised polymer additives under laboratory conditions, predominantly by means of contact angle measurements on thin films and Rutherford Backscattering Ion Beam Analysis as discussed extensively in the previous chapter, it was decided to perform some tests more directly linked to the intended application of these materials. It has been shown that these materials are highly efficient at modifying the surface energy, and hence oleophobicity and hydrophobicity, of their corresponding bulk polymer, poly(*N*-vinyl pyrrolidone) (PVP). However, given the intended application for these materials and the industrial funding backing the project, there was a need to try and ascertain how these materials might perform in the Gas Diffusion Layer (GDL) of a Polymer Electrolyte Membrane Fuel Cell (PEMFC), specifically under the operating conditions of such a fuel cell.

In order to gain an insight into the ability of the novel polymer additives to modify the operating characteristics of a GDL, a series of mock GDLs was made, termed Low Cost Substrates (LCSs). These LCSs were made from a base sheet of carbon fibre paper, to which was applied an aqueous suspension containing graphite, unfunctionalised PVP, DPFPB-PVP (6K2 PVP) or TPFPB-PVP (6K3 PVP) end-functionalised PVP additive, and either polytetrafluoroethylene (PTFE) or Fluorinated Ethylene Propylene (FEP). The suspension was applied by laying a sheet of porous carbon fibre paper on a clean, flat surface, and pouring the aqueous solution onto the sheet before rolling it evenly over the sheet with a hand

roller. The sheet was then allowed to air dry before being fired at a predetermined temperature and time, the resulting LCSs roughly approximating the composition of a real GDL at a fraction of the cost.

The LCSs were then used to test the effects of the new additives on both LCS water uptake and durability (mechanical strength) under PEMFC operating conditions. A series of LCSs were prepared in order to test the effects of each additive on water uptake and durability, when used with either PTFE or FEP, and fired for varying temperatures and times. Statistically based experimental design was employed due to the large number of variables being tested (concentration of additive, PTFE / FEP, firing time and firing temperature), which would otherwise need to be tested one at a time whilst keeping additional variables constant. In addition to being inefficient, a one-by-one approach would also ignore any effects arising from possible variable-variable interactions, giving rise to potentially misleading results. Given this disadvantage and the finite amount of additive available this would not have been practical, and so the composition of each LCS in terms of quantities of each component in the solution, as well as the firing times and temperatures, were generated by StatGraphic[1] experimental design software using a Design of Experiment (DoE) approach (Box-Behnken design[2]), in order to give the most statistically significant results from a limited number of samples.

Each LCS was accurately weighed and its tensile strength measured using a Testometric AX-250 tensile tester. They were then submerged completely in water in sealed containers and placed in an oven where they were heated to a constant temperature of 80°C. The samples were then held at 80°C for 2000 hours, being removed from the oven periodically to be weighed (in order to measure water uptake of the sample) and for parallel 15cm x 15mm strips to have their tensile strength measured (as a measure of durability). As a temperature of 80°C in water closely approximates the conditions a GDL would be subjected to in a functioning PEMFC, it was hoped that these tests would give an indication of the benefits or otherwise of incorporating the novel end-functionalised polymer additives into a GDL.

4.2 Results and Discussion

4.2.1 Di-functional additive: 6K2 PVP

The experimental parameters of the DoE were as follows:

PTFE-based LCSs:

- Additive concentration: 0 – 20%
- Firing temperature: 300 – 380°C
- Firing time: 30 – 120 minutes

FEP-based LCSs

- Additive concentration: 0 – 20%
- Firing temperature: 280 – 320°C
- Firing time: 30 – 300 minutes

These experimental parameters were inputted into the aforementioned StatGraphic software package, and it was used to generate the sample sets displayed in Table 4.1 (a set of sample compositions for each PTFE-containing LCSs and FEP-containing LCSs). The corresponding LCSs were then prepared and as previously discussed, water uptake and durability tests were performed at various time intervals while the samples were being subjected to simulated fuel cell operating conditions.

Table 4.1. Sample compositions for PTFE-based (#1-15) and FEP-based (#16-30) Low Cost Substrates generated by StatGraphic using Box-Behnken experimental design. All samples contain the same overall concentration of PVP, including both matrix (PVP) and additive (6K2 PVP).

	Sample Composition – 6K2 PVP & PTFE / FEP based LCSs							**Firing info**			
#	**KS4 Graphite / g**	**AquaDAG / g**	**PVP / g**	**PTFE or FEP / g**	**Weight % 6K2 PVP**	**Mass 6K2 PVP / g**	**Water / g**	**PTFE-based samples**		**FEP-based samples**	
								Temperature / °C	**Firing time / min**	**Temperature / °C**	**Firing time / min**
1 / 16	3.1	11	2.6	0.65	0	0	15	380	75	280	115
2 / 17	3.1	11	2.6	0.65	0	0	15	300	75	300	200
3 / 18	3.1	11	2.6	0.65	0	0	15	340	120	320	115
4 / 19	3.1	11	2.6	0.65	0	0	15	340	30	300	30
5 / 20	3.1	11	2.34	0.65	10	0.08	15	300	120	280	200
6 / 21	3.1	11	2.34	0.65	10	0.08	15	380	120	300	115
7 / 22	3.1	11	2.34	0.65	10	0.08	15	380	30	320	30
8 / 23	3.1	11	2.34	0.65	10	0.08	15	340	75	280	30
9 / 24	3.1	11	2.34	0.65	10	0.08	15	300	30	320	200
10 / 25	3.1	11	2.34	0.65	10	0.08	15	340	75	300	115
11 / 26	3.1	11	2.34	0.65	10	0.08	15	340	75	300	115
12 / 27	3.1	11	2.08	0.65	20	0.16	15	340	30	300	30
13 / 28	3.1	11	2.08	0.65	20	0.16	15	380	75	300	200
14 / 29	3.1	11	2.08	0.65	20	0.16	15	340	120	280	115
15 / 30	3.1	11	2.08	0.65	20	0.16	15	300	75	320	115

Having performed these experiments, the results were then fed back into the StatGraphic software package in order to generate several important sets of data, these being:

1. **A standardised Pareto chart.** This displays the statistical significance of individual variable effects on a specific outcome (in this case water uptake or durability), in decreasing order of significance. In this work a line is also displayed showing a 5% statistical significance, variables below which are considered statistically insignificant in comparison to those above.
2. **A main effects plot.** This displays the effect of each statistically significant variable upon the specific outcome, while holding all other variables at their middle point. The overall difference for each variable in the lowest measurement and highest measurement of the outcome is referred to as the "main effect" of that variable.
3. **A response surface plot.** This displays a three dimensional wire frame surface representing the effect of any two variables on a specific outcome, and is very useful for calculating the optimum combination of these variables to achieve the desired outcome (in the case of this work, minimum water uptake or maximum durability). This plot comes with an associated R squared value which is a measure of confidence – the nearer this value is to 100%, the more certain the data.

The results for the PTFE-based LCS incorporating the 6K2 PVP additive are shown in Figures 4.01 and 4.02.

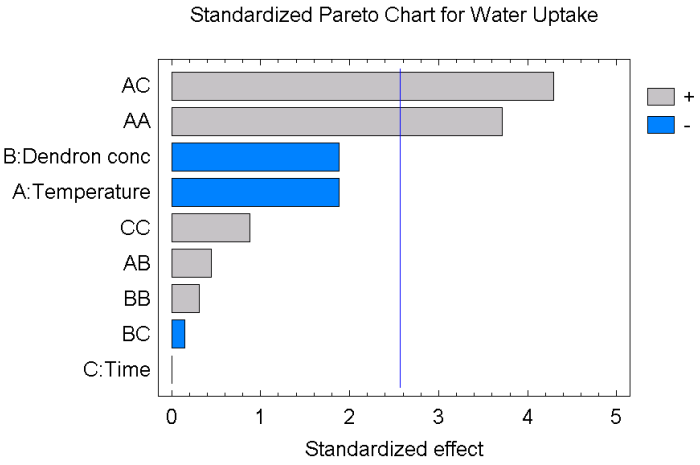

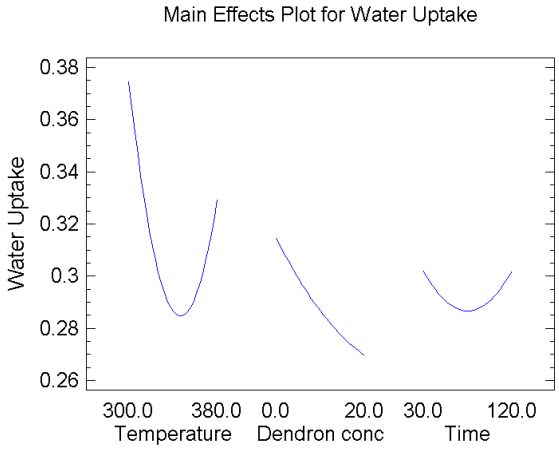

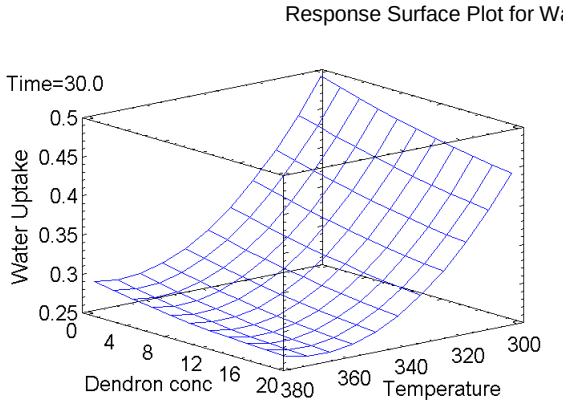

R squared = 88%

Optimum parameters:

- Dendron conc = 20%
- Firing temp = 367°C
- Firing time = 30 min

Predicted water uptake: 0.26 cm^3 / g

Figure 4.01. StatGraphic data for water uptake tests (water uptake measured in cm^3 / g) performed on PTFE-based LCSs, where "dendron" refers to the di-functional additive, 6K2 PVP.

The first point to note is that although the concentration of additive (dendron conc) is indicated to be statistically insignificant in the standardised Pareto chart, this is only in comparison to the effect of temperature, which as can be seen in all three charts, is the dominant factor in determining water uptake. However, as can be seen in the main effects plot, water uptake decreases steadily with increased additive concentration, and all other things being equal, an additive concentration of 20% results in a 14% decrease in water uptake compared to 0% additive concentration. The response surface plot (with the firing time fixed at the optimum of 30 minutes) shows with a good degree of confidence that increased additive concentration results in a lowering of water uptake at all firing temperatures, but that the optimum result is obtained at a firing temperature of 367°C with a maximum additive concentration of 20%.

Shown in Figure 4.02 is the StatGraphic generated data for the durability tests performed on the same 6K2 PVP / PTFE LCSs. Again we see that firing temperature is the major factor involved in determining durability, however, the di-functional additive also has an effect, with higher durability being achieved at low and high concentrations of additive. The main effects plot shows that in fact a 0% additive concentration should lead to a slightly higher durability than 20%, however the difference being small, one could argue that the benefits displayed in water uptake behaviour are worth the cost in terms of durability.

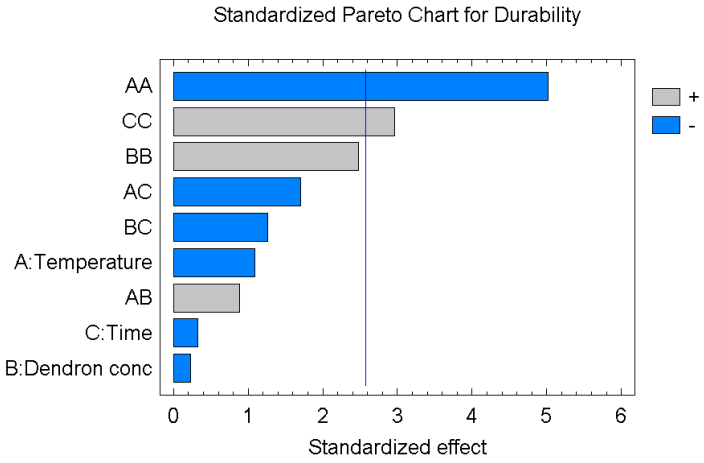

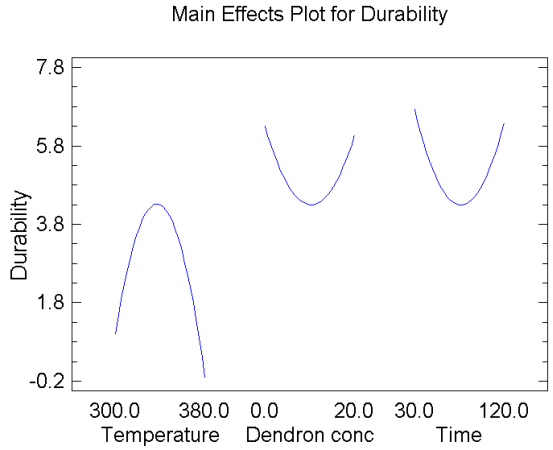

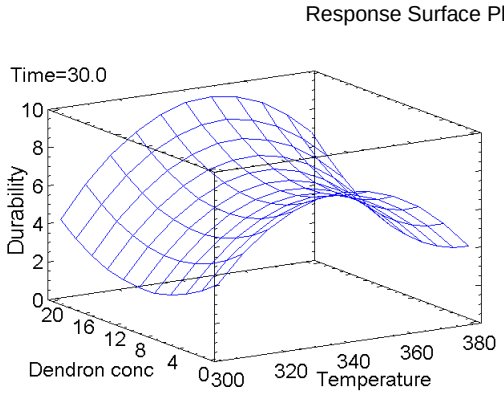

R squared = 91%

Optimum parameters:

- Dendron conc = 20%
- Firing temp = 367°C
- Firing time = 30 min

Predicted durability: 9.5 N / 15mm

Figure 4.02. StatGraphic data for durability tests (durability measured in N / 15mm) performed on PTFE-based LCSs, where "dendron" refers to the di-functional additive, 6K2 PVP.

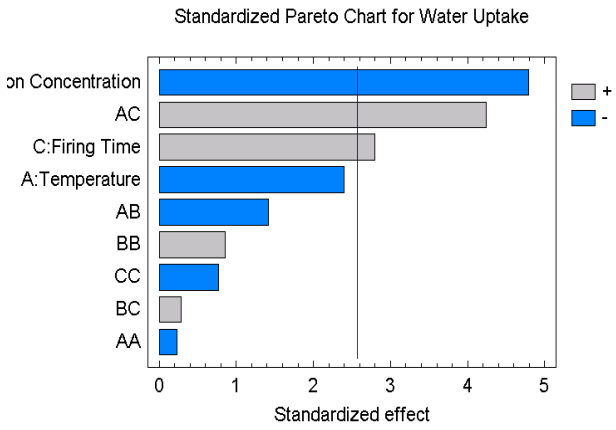

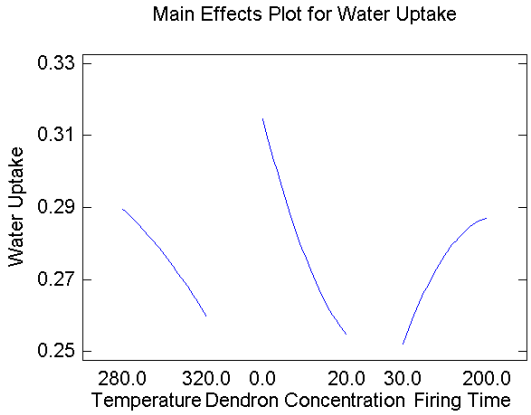

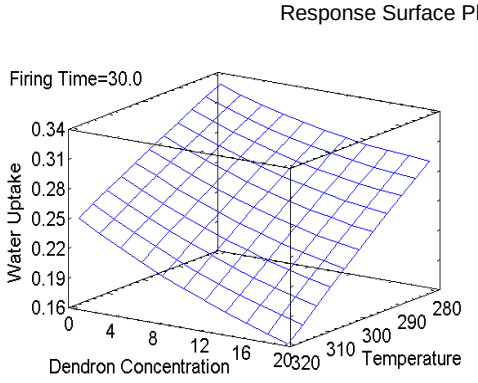

R squared = 92%

Optimum parameters:

- Dendron conc = 20%
- Firing temp = 318°C
- Firing time = 30 min

Predicted water uptake: 0.16 cm^3 / g

Figure 4.03. StatGraphic data for water uptake tests (water uptake measured in cm^3 / g) performed on FEP-based LCSs, where "dendron" refers to the di-functional additive, 6K2 PVP.

Shown in Figures 4.03 and 4.04 is a parallel set of data for the FEP-based LCSs as opposed to PTFE, still for the di-functional 6K2 PVP additive. Figure 4.03 shows the StatGraphic data for water uptake, and immediately one can see that the additive has a far greater beneficial effect on water uptake when used with FEP. The standardised Pareto chart shows that it is now the additive concentration alone that is the most statistically significant variable when considering water uptake, followed by firing temperature and time. The main effect of additive concentration shown in the main effects plot is 0.06 cm^3 / g, which corresponds to a 20% decrease in water uptake between 0% and 20% additive concentration. However, when combined with the optimum firing time and temperature as shown in the response surface plot with a high associated degree of confidence, a 20% additive concentration yields a predicted water uptake of 0.16 cm^3 / g. This corresponds to a 36% reduction in water uptake compared to the otherwise identical situation in the absence of any 6K2 PVP additive.

Figure 4.04 shows the StatGraphic data for the durability tests performed on the 6K2 PVP / FEP LCSs. The additive concentration is still a significant variable, and the main effect of additive concentration is significantly beneficial, with a steady increase of durability with additive concentration from 0 – 20%, corresponding overall to a 13% increase in tensile strength, which is significantly higher than in the case of the PTFE-based LCSs. The response surface plot indicates a steady increase in durability with additive concentration at all firing temperatures, however for the first time, this statistical data comes with a low confidence level of 41% and so while the trend should be considered a positive result, there is little point in discussing this data quantitatively.

Overall our initial work in this area has shown positive results using the di-functional additive with PTFE, but especially with FEP where it has demonstrated a significant benefit in terms of water uptake. It has also shown promising results when considering tensile strength, however more experiments need to be done in order to clarify the additives effect in this regard.

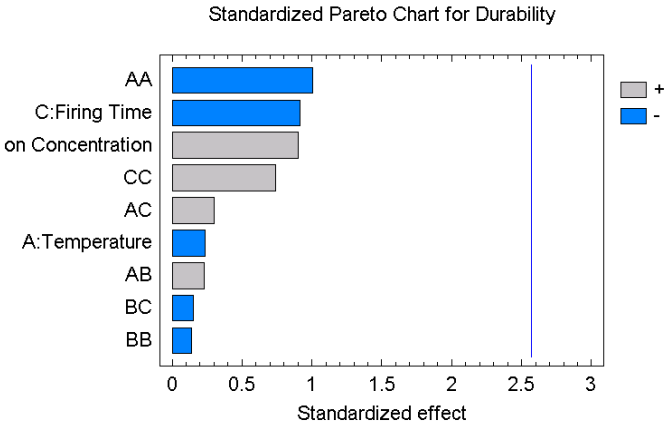

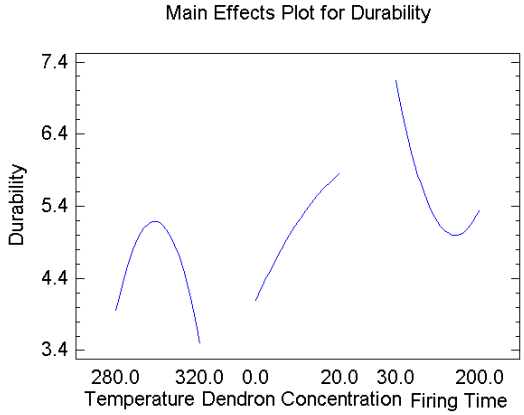

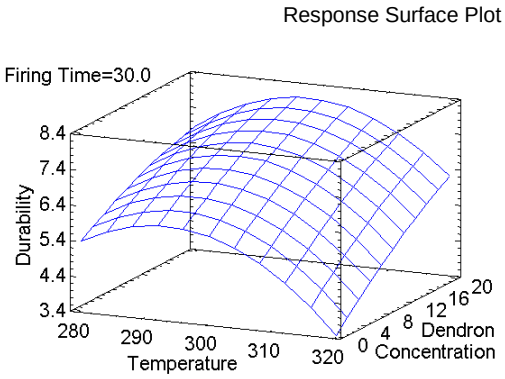

R squared = 41%

Optimum parameters:

- Dendron conc = 20%
- Firing temp = 297°C
- Firing time = 30 min

Predicted durability: 9.0 N / 15mm

Figure 4.04. StatGraphic data for durability tests (durability measured in N / 15mm) performed on FEP-based LCSs, where "dendron" refers to the di-functional additive, 6K2 PVP.

4.2.2 Tri-functional additive: 6K3 PVP

Due to time constraints, in part due to the difficulties encountered with manufacturing this material successfully, and initially on a large enough scale, experimentation with the tri-functional additive and its incorporation into LCSs was more limited. Instead of using a DoE approach as with the di-functional additive, a more precursory investigation was done, using a fixed concentration of additive (20% by mass of total PVP content) in a FEP-based LCS, and comparing the results of water uptake and durability tests over a 2000 hour period with an otherwise identical LCS containing no additive.

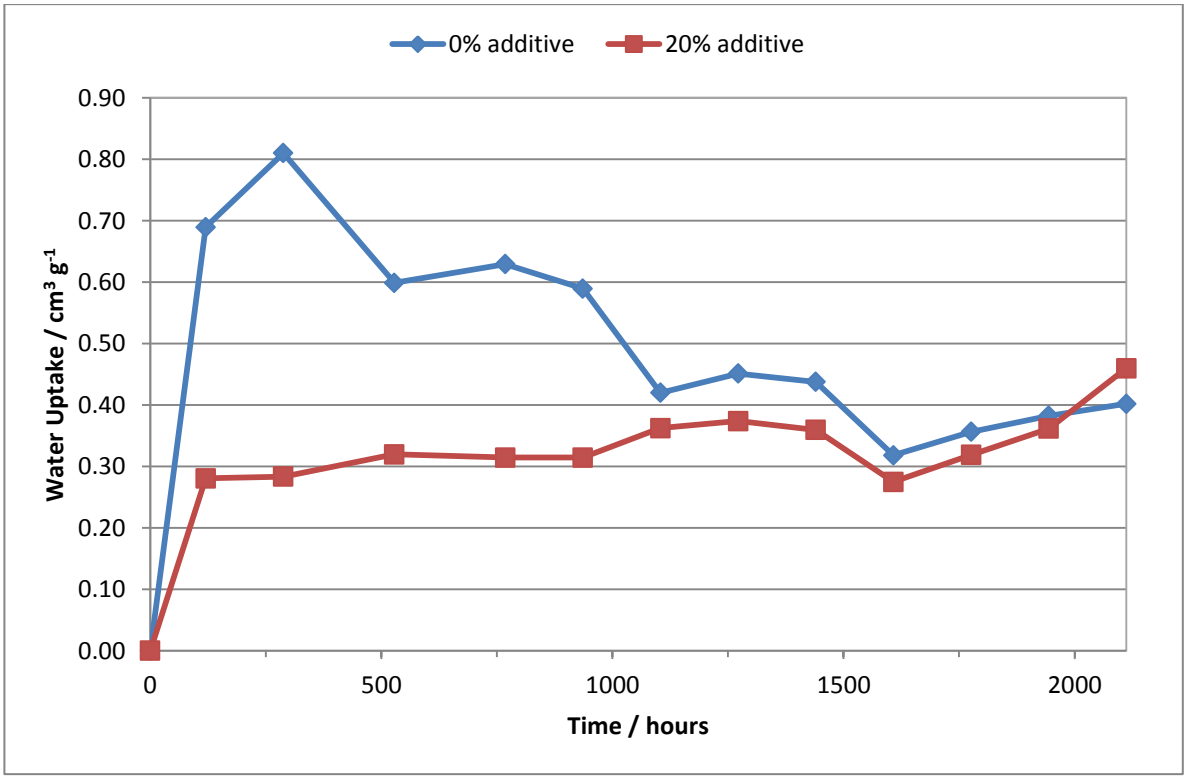

Figure 4.05. Water uptake data for FEP-based LCSs containing either 0% or 20% 6K3 PVP tri-functional additive, submerged in water at 80°C over a period of 2112 hours.

The water uptake data shown in Figure 4.05 displays clearly a large benefit in the presence of the tri-functional additive, especially below 1000 hours where water uptake is reduced by up to 65% by the presence of additive. While the water uptake of the additive-free LCS eventually comes down nearer to that of the additive-containing LCS, the 20% additive LCS's water uptake remains relatively constant throughout the entire 2000 hour period, which would suggest that if it were a real GDL it would perform more consistently.

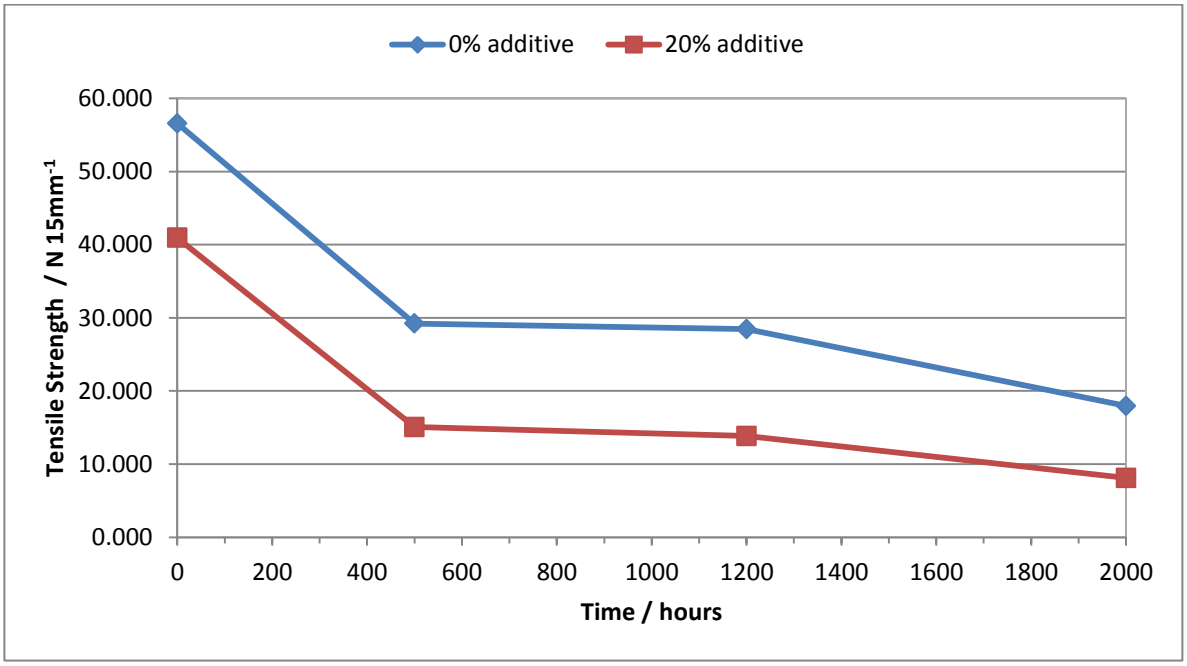

Figure 4.06. Tensile strength data for FEP-based LCSs containing either 0% or 20% 6K3 PVP tri-functional additive, submerged in water at 80°C over a period of 2000 hours.

Figure 4.06 shows the durability data for the same set of LCSs. While in both cases there is a regular decline in tensile strength over the testing period, it would appear that in this case, the tri-functional additive has a slightly negative effect on the durability of the sample.

4.3 Conclusions from preliminary LCS water uptake / durability study

This preliminary work has demonstrated that our novel end-functionalised PVP additives impart significant benefit in terms of reducing water uptake of the LCS under simulated PEMFC operating conditions, especially when used with FEP rather than PTFE. Additionally we have shown that the presence of additive appears to have a beneficial effect on the consistency of water uptake over time. Durability experiments have yielded slightly more questionable results, with some formulations displaying slight benefit in terms of mechanical strength while others display slight deficit.

However, in this more complex system we have had to re-evaluate the role of the end-functionalised PVP additives. The trends seen in the DoE-based study on 6K2 PVP where the most promising results in terms of water uptake are seen in the FEP-based samples, are not entirely consistent with our previous research. For example it would appear that the most benefit is obtained from the presence of this additive when it is at its maximum concentration (in this set of experiments) of 20% (weight fraction of the overall PVP component of the formulation). This is not consistent with our contact angle and Rutherford backscattering investigations, where we see the surface segregation of this additive increase with concentration until a plateau effect is seen at the critical aggregation concentration (CAC) which is typically at about 2.5% additive.

This observation has prompted us to speculate that in this more complex (than a simple blend of unfunctionalised and functionalised PVP) system, the benefit derived from the presence of the additive is in fact not due to it behaving as a surface modifying additive, but more as a surfactant, helping to compatibilise the fluoropolymer with the aqueous phase and the PVP. If the additive was behaving in such a way it could lead to improved dispersion of the fluoropolymer component of the formulation, and result in enhanced LCS properties. However, more work will need to be undertaken with these materials in order to verify this hypothesis.

4.4 References

[1] *STATGRAPHICS® Centurion XVI User Manual*, StatPoint Technologies Inc., **2009**

[2] Box, G. E. P.; Behnken, D. W.; *Technometrics*, **1960**, *2*, 455

Chapter 5
Experimental

5.1 Analytical techniques and instrumentation

5.1.1 Nuclear Magnetic Resonance Spectroscopy (NMR)

^{1}H NMR analysis was performed using a Bruker Avance-400 spectrometer at 400 MHz using $CDCl_3$ (100%, 99.96 atom % D, Sigma-Aldrich) as a solvent.

5.1.2 Size Exclusion Chromatography (SEC)

In the case of polystyrene, molecular weight data was obtained using Size Exclusion Chromatography (SEC) on a Viscotek TDA 302 with refractive index, viscosity and light scattering detectors and 2 x 300 ml PLgel 5 µm mixed C columns. Tetrahydrofuran was used as the eluent at a flow rate of 1.0 ml/min and at a constant temperature of 35°C. The light scattering detector was calibrated with a narrow molecular weight polystyrene standard purchased from Polymer Laboratories using a value of 0.185 ml/g for the dn/dc of polystyrene.

In the case of PVP, a separate setup was used to obtain SEC data using identical hardware though using dimethylformamide (DMF) was used as the eluent at a flow rate of 1.0 ml/min and at a constant temperature of 35°C. The light scattering detector was calibrated with a narrow molecular weight polystyrene standard purchased from Polymer Laboratories using a value of 0.990 ml/g for the dn/dc of PVP calculated using an accurate solution of PVP.

5.1.3 Thin Film Analysis

Film thicknesses were measured using a Sentech SE400 Ellipsometer (up to 200 nm film thickness) and a Sentech FTP500 White Light Interferometer (above 150 nm film thickness).

Contact angles were measured using a Ramé-Hart NRL contact angle goniometer (model number 100-00-230).

All AFM measurements were performed using a Digital Instruments Nanoscope IV scanning probe microscope.

5.2 Materials

5.2.1 Cumyl dithiobenzoate synthesis and RAFT polymerisation of styrene

Sulphur (powder, 99.98%, Sigma-Aldrich), sodium methoxide (≥97%, Fluka), benzyl chloride (99%, Sigma-Aldrich), α-methylstyrene (99%, Sigma-Aldrich) and *p*-toluenesulfonic acid (98.5%, Sigma-Aldrich) were used as received. Tetrahydrofuran (Analytical Grade, Fisher Scientific), methanol (Analytical Grade, Fisher Scientific), diethyl ether (Lab Reagent Grade, Fisher Scientific), hexane (Analytical Grade, Fisher Scientific) and 1,4-dioxane (ACS reagent, Sigma-Aldrich) were used as received, and in any instance of water being used it was deionised. Styrene (99+%, Sigma-Aldrich) was freshly distilled over calcium hydride under high vacuum before use. Azobisisobutyronitrile (98%, Acros Organics) was recrystallised from 1:1 chloroform / methanol.

5.2.2 DPCM synthesis and all RAFT polymerisations of N-vinyl pyrrolidone

Benzene (HPLC grade, Sigma-Aldrich), sodium amide (95%, Sigma-Aldrich), diphenylamine (99+% A.C.S. Reagent, Sigma-Aldrich), carbon disulfide (99.9%, Acros Organics) and diethyl chloromalonate (95%, Sigma-Aldrich) were used as received. A 100 ml stock sample of pure *N*-vinyl pyrrolidone (99+%, Sigma-Aldrich) was prepared by vacuum distillation (BP=92-95˚C@11mm/Hg) and stored under dry nitrogen in a freezer. 1,4-dioxane (ACS reagent, Sigma-Aldrich) was freshly vacuum distilled over calcium hydride prior to use, and in any case of water being used it was deionised. Azobisisobutyronitrile (98%, Acros Organics) was recrystallised from 1:1 chloroform / methanol.

5.2.3 G-1 DPCM synthesis (dendritic CTA)

Acetone (Analytical Grade, Fisher Scientific) was dried over 3 Å molecular sieves under a blanket of dry nitrogen overnight before use. Dichloromethane (Analytical Grade, Fisher Scientific), toluene (HPLC Grade, 99.5%, Fisher Scientific) and hexane (Analytical Grade, Fisher Scientific) were used as received. Benzene (HPLC grade, 99.9+%, Sigma-Aldrich) was freshly distilled over calcium hydride before use. Benzyl bromide (98%, Aldrich) was used as received. 3,5-dihydroxybenzyl alcohol (99%, Aldrich), potassium carbonate (≥98%, Aldrich) and 18-crown-6 ether (≥99.5%, Aldrich) were dried in a vacuum oven and stored in a vacuum desiccator. Anhydrous pyridine (99.8%, Aldrich), thionyl chloride (99+%, Aldrich), sodium amide (95%, Aldrich), diphenylamine (99+% A.C.S. Reagent, Aldrich) and carbon disulfide (99.9%, Acros Organics) were used as received.

5.2.4 TPFPB-DPCM and DPFPB-DPCM synthesis (fluorinated CTAs)

Tetrahydrofuran (HPLC Grade, Fisher Scientific) was dried over a sodium wire with benzophenone indicator and freshly distilled prior to use. Dichloromethane (Analytical Grade, Fisher Scientific) was used as received unless referred to as “dry” in which case it was freshly distilled over calcium hydride. Acetone (Analytical Grade, Fisher Scientific) was dried over 3 Å molecular sieves under a blanket of dry nitrogen overnight before use, ethyl acetate (Analytical Grade, Fisher Scientific) was used as received and in any instance of water being used it was deionised. 3-perfluorooctyl-1-propanol (FluoroChem), carbon tetrabromide (99%, Sigma-Aldrich), triphenylphosphine (Sigma-Aldrich), 3,5-dihydroxybenzyl alcohol (99%, Sigma-Aldrich), methyl 3,4,5-trihydroxybenzoate (98%, Sigma-Aldrich), potassium carbonate (≥98%, Sigma-Aldrich), 18-crown-6 ether (≥99.5%, Sigma-Aldrich) and diphenylamine (99+% A.C.S. Reagent, Sigma-Aldrich) were dried for a minimum of 24 hours in a vacuum oven at room temperature prior to use. Lithium

aluminium hydride (95% pellets, Sigma-Aldrich) and carbon disulfide (99.9%, Acros Organics) were used as received. Sodium hydride (60% dispersion in mineral oil, Sigma-Aldrich) was washed with dry hexane (dried over calcium hydride and distilled under high vacuum) using specialist apparatus on a high vacuum / nitrogen line in order to remove mineral oil. Once washed, sodium hydride was weighed and transferred into reaction vessels under a dry nitrogen atmosphere in an MBraun MB150B-G glove box.

5.3 Synthesis of CTAs and RAFT polymerisations

5.3.1 Cumyl dithiobenzoate synthesis

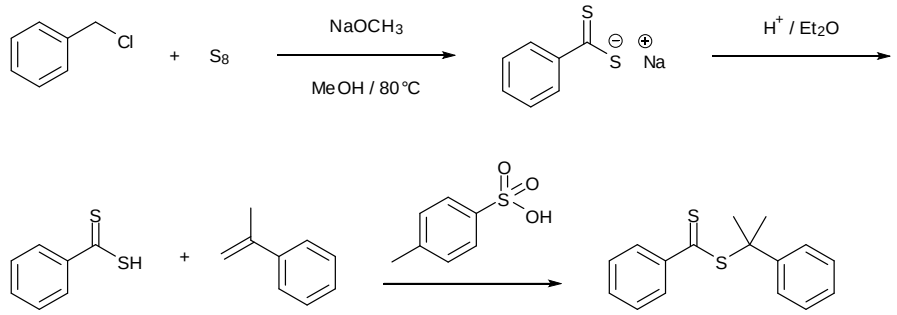

Figure 5.01. Reaction scheme for the synthesis of cumyl dithiobenzoate, a CTA for the RAFT polymerisation of styrene.

Elemental sulphur (0.89 g, 2.00 equivs, 27.8 mmol), 30% sodium methoxide solution in methanol (5.0 g, 2.00 equivs, 27.8 mmol) and 5 ml methanol were placed in a 50 ml, 2-necked, round bottomed flask equipped with a reflux condenser, magnetic stirrer and a dropping funnel. Benzyl chloride (1.76 g, 1.00 equivs, 13.9 mmol) was added slowly (dropwise) to the stirring mixture which was then heated to 80°C and left to reflux overnight. The reaction mixture was then allowed to cool to room temperature, filtered and evaporated to dryness. The resulting brown solid was dissolved in 25 ml water, transferred into a separating funnel and washed with 3 × 25 ml diethyl ether. An additional 25 ml diethyl ether was added and the contents of the separating funnel was acidified by slow addition of 32% aqueous hydrochloric acid until the brown aqueous layer turned colourless and the organic layer was deep purple. The ether layer was then dried over magnesium sulphate, filtered and evaporated to dryness to give a purple oil. The oil was dissolved in 5 ml hexane in a 25 ml flask to which was added a 20% excess of α-methylstyrene and 1% *p*-toluenesulfonic acid catalyst and the mixture left to

stir overnight. Purification was by column chromatography using hexane as the eluent to obtain the pure product in 67% yield.[1]

5.3.2 Typical experimental procedure for RAFT polymerisation of styrene

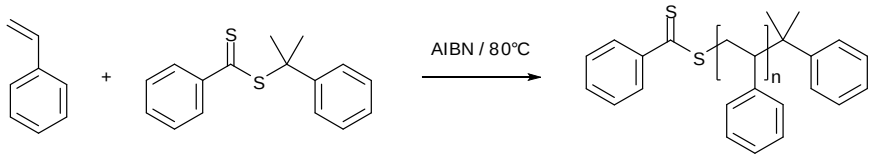

Figure 5.02. Reaction scheme for the RAFT polymerisation of styrene with cumyl dithiobenzoate.

All experiments were carried out using 2 ml (1.82 g, 17.5 mmol) styrene, and the appropriate amounts of CTA (cumyl dithiobenzoate) and initiator (AIBN). The appropriate quantity of cumyl dithiobenzoate was calculated based on the desired molecular weight assuming a certain percentage conversion using equation 1.1:

$$\mathbf{M_n = M_M \cdot x \cdot \frac{[M]_0}{[RAFT]_0} + M_{RAFT}} \qquad \mathbf{1.1}$$

Which by simple rearrangement gives equation 1.2:

$$\mathbf{[RAFT]_0 = \frac{[M]_0 \cdot M_M \cdot x}{M_n - M_{RAFT}}} \qquad \mathbf{1.2}$$

Where $\mathbf{[RAFT]_0}$ is the initial concentration of CTA, $\mathbf{[M]_0}$ is the initial concentration of monomer (styrene – worked out from density of styrene [0.909 g ml^{-1}]), $\mathbf{M_M}$ is the

molecular mass of the monomer (styrene – 104.15 g mol^{-1}, **x** is a decimal between zero and one representing the assumed percentage conversion of monomer into polymer, $\mathbf{M_n}$ is the desired molecular weight of the polymer being produced, and $\mathbf{M_{RAFT}}$ is the molecular weight of the CTA (cumyl dithiobenzoate – 272.07 g mol^{-1}).

A 1:10 molar ratio of AIBN:cumyl dithiobenzoate was used, and the appropriate amounts of cumyl dithiobenzoate and AIBN were placed in a schlenk tube containing a magnetic stirrer bar.

Example polymerisation:

Target molecular weight: 10,000 g mol^{-1}, approximate conversion 50%, 2 ml scale.

$$\mathbf{[RAFT]}_0 = \frac{8.73 \times 104.15 \times 0.5}{10000 - 272.07} = 0.04673 \text{ mol dm}^{-3} \text{ CTA}$$

Assuming 50% conversion of monomer (x = 0.5), from equation 1.2 can be used to calculate that 0.02546 g (0.09345 mmol) cumyl dithiobenzoate was required, and a tenth the molar amount (0.009345 mmol) of AIBN = 0.00153 g.

Styrene was then freshly distilled over calcium hydride from a degassed reservoir on a high vacuum line to remove any inhibitors. 2 ml styrene was then transferred into the schlenk tube and it was sealed by wiring a rubber septum onto the neck of the tube. The schlenk tube was connected to a vacuum / nitrogen line and its contents subjected to several freeze-pump-thaw cycles until thoroughly degassed. The schlenk tube was sealed under vacuum or flooded with dry nitrogen, and the reaction mixture heated to the desired temperature in an oil bath with solid state temperature control and left for 40 hours with efficient stirring. After this time the polymerisation mixture was dissolved in a minimum amount of tetrahydrofuran and precipitated into methanol (20 × volume excess of methanol over the combined volumes of polymerisation mixture and tetrahydrofuran) in order to precipitate the polymer. The polymer was then removed by vacuum filtration and dried under vacuum before being analysed by SEC and ^{1}H NMR in order to determine the average molecular weight and its distribution.

5.4 RAFT Polymerisation of *N*-vinyl pyrrolidone

5.4.1 S-malonyl N,N-diphenyldithiocarbamate (DPCM) synthesis

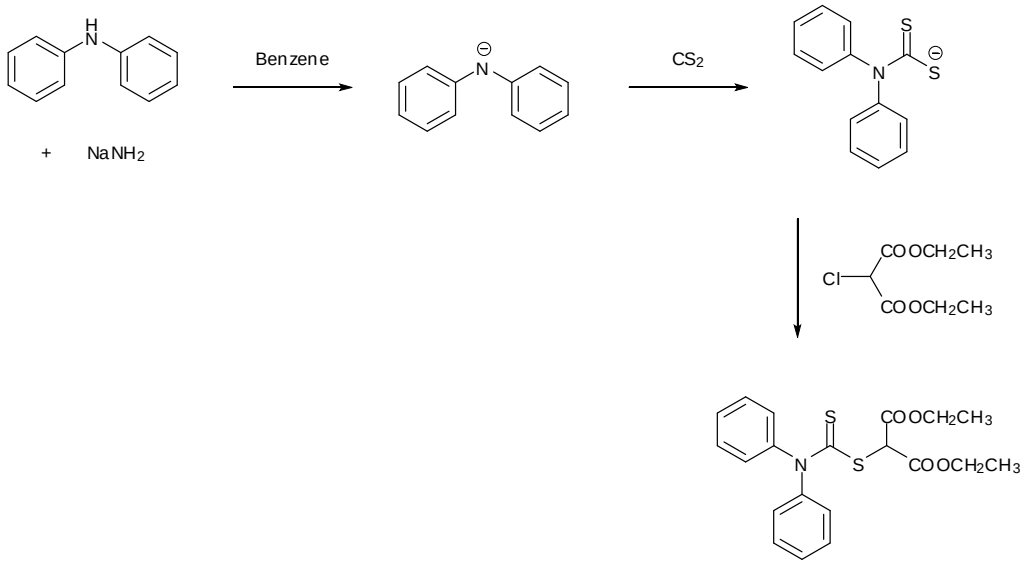

Figure 5.03. Reaction scheme for the synthesis of S-malonyl N,N-diphenyldithiocarbamate (DPCM), a CTA for the RAFT polymerisation of N-vinyl pyrrolidone.

Sodium amide (0.4854 g, 1.00 equivs, 11.82 mmol) was suspended in 20 ml benzene under a blanket of dry nitrogen in a 200 ml, 3-necked, round bottomed flask equipped with a magnetic stirrer, reflux condenser and a dropping funnel. To this was added diphenylamine (2.0000 g, 1.00 equivs, 11.82 mmol) in an additional 20 ml benzene and the mixture stirred overnight at room temperature. Carbon disulfide (1.0800 g, 1.20 equivs, 14.18 mmol) in 20 ml benzene was added followed by slow (dropwise) addition of diethyl chloromalonate (2.3003 g, 1.00 equivs, 11.82 mmol) in 20 ml benzene with efficient stirring. After 15 minutes the mixture was refluxed for 2 hours, cooled and poured into 250 ml water. The organic layer was separated, washed further with water and then dried over magnesium sulphate. Solvent was removed by vacuum distillation on a high

vacuum line leaving a yellow-brown solid which was dried further in a vacuum oven. The referenced procedure claimed that the pure product was obtained at this point, however ^{1}H NMR showed several impurities, and thus it was purified further by recrystallisation from hexane / toluene to afford the product as light yellow crystals in 8-21% yield.[2]

^{1}H NMR (400MHz, $CDCl_3$, δ, ppm) 1.30 (t, *J* 7.1 Hz, 6H, CH_2CH_3), 4.25 (q, *J* 7.1Hz, 4H, CH_2CH_3), 5.75 (s, 1H, CS(=S)C*H*), 7.42-7.46 (m, 10H, Ar*H*).

5.4.2 Typical procedure for RAFT polymerisation

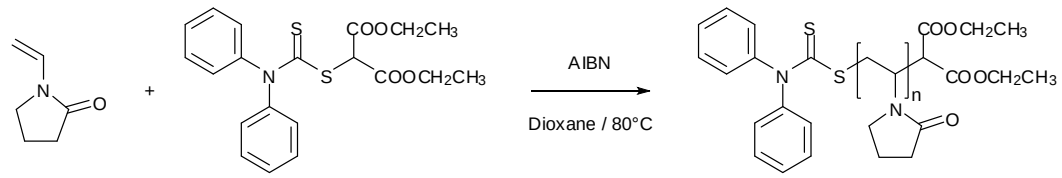

Figure 5.04. Reaction scheme for the RAFT polymerisation of N-vinyl pyrrolidone with S-malonyl N,N-diphenyldithiocarbamate (DPCM).

Initial experiments were carried out using *N*-vinyl pyrrolidone (1.00 ml, 1.045 g, 9.40 mmol), 1 ml 1,4-dioxane and the appropriate amounts of CTA (DPCM) and initiator (AIBN). The appropriate quantity of DPCM was calculated based on the desired molecular weight assuming a certain percentage conversion using equation 1.2 as previously discussed with RAFT polymerisations of styrene.

A 1:8 molar ratio of AIBN:DPCM was used, and the appropriate amounts of DPCM and AIBN were placed in a schlenk tube containing a magnetic stirrer bar.

Example polymerisation:

Target molecular weight: 10,000 g mol^{-1}, approximate conversion 80%, 1 ml NVP

$$[\mathbf{RAFT}]_0 = \frac{4.7004 \times 111.16 \times 0.8}{10000 - 403.56} = 0.04356 \text{ mol dm}^{-3} \text{ CTA}$$

Assuming 80% conversion of monomer (x = 0.8), from equation 1.2 can be used to calculate that 0.03516g (0.08712 mmol) DPCM was required, and an eighth the molar amount (0.01089mmol) of AIBN = 0.00179g).

1.00 ml *N*-vinyl pyrrolidone was then transferred into the schlenk tube, along with 1.00 ml freshly distilled 1,4-dioxane and it was sealed by wiring a rubber septum onto the neck of the tube. The schlenk tube was then connected to a vacuum / nitrogen line and its contents subjected to several freeze-evacuate-thaw cycles until thoroughly degassed. The schlenk tube was then sealed under vacuum or flooded with nitrogen, and the reaction mixture heated to 80˚C in an oil bath with solid state temperature control and left for a set amount of time (15-63 hours) with efficient stirring. After this time the polymerisation mixture was dissolved into a minimum amount of dichloromethane and precipitated into diethyl ether (20 × volume excess of diethyl ether over the combined volumes of polymerisation mixture and dichloromethane) before then being removed by vacuum filtration. The polymer was repeatedly dissolved in dichloromethane and re-precipitated into diethyl ether until pure, usually yielding a white solid. It was then dried under vacuum before being analysed by SEC and ^{1}H NMR in order to determine the average molecular weight and its distribution.[3]

5.5 G-1 Frechét-type dendritic CTA

5.5.1 Synthesis of G-1 Frechét-type dendron (G1-OH)

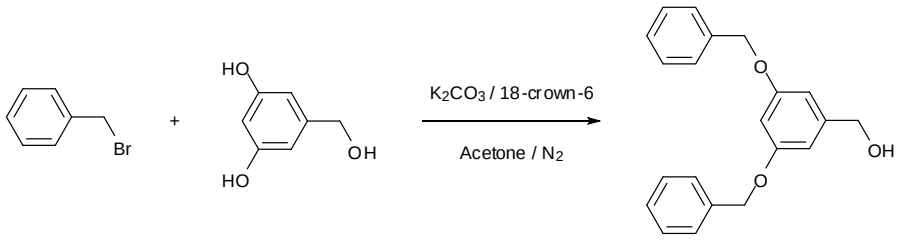

Figure 5.05. Reaction scheme for the synthesis of 3,5-dibenzyloxybenzyl alcohol.

3,5-dihydroxybenzyl alcohol (6.15 g, 1.00 equivs, 43.9 mmol), potassium carbonate (15.15 g, 2.50 equivs, 101.0 mmol) and 18-crown-6 ether (4.63 g, 0.20 equivs, 17.5 mmol) was placed in a 2-necked, 500 ml round bottomed flask equipped with a magnetic stirrer and reflux condenser and the flask flushed with dry nitrogen for 30 minutes. Benzyl bromide (15.00 g, 2.00 equivs, 87.7 mmol) was then injected into the flask, followed by cannulation of 200 ml dry acetone into the flask. The mixture was heated to gentle reflux with efficient stirring under a blanket of dry nitrogen for 48 hours. The mixture was then allowed to cool and solvent was removed by rotary evaporation. It was then partitioned between dichloromethane and water, and the aqueous layer extracted a further three times with dichloromethane. The combined organic layers were dried over magnesium sulphate, filtered and evaporated to dryness. The solid residue was recrystallised from 3:1 toluene / hexane and then dried under vacuum to a constant mass to give the final product as a white crystalline powder in 61% yield, MP=79-82˚C.[4]

^{1}H NMR (400MHz, $CDCl_3$, δ, ppm) 1.60 (s, 1H, CH_2OH), 4.65 (s, 2H, CH_2OH), 5.05 (s, 4H, Ar-CH_2O-Ar-CH_2OH), 6.55 (s, 1H, Ar*H*), 6.65 (s, 2H, Ar*H*), 7.1-7.5 (m, 10H, Ar*H*).

Elemental analysis calculated for $C_{21}H_{20}O_3$: C, 78.73; H, 6.29. Found: C, 78.97; H, 6.37.

5.5.2 Chlorination of G-1 Frechét-type dendron (G1-Cl)

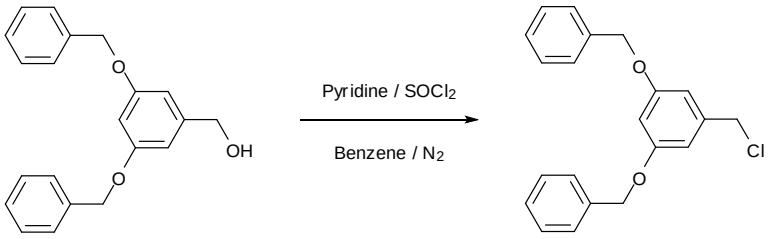

Figure 5.06. Reaction scheme for the synthesis of 3,5-dibenzyloxybenzyl chloride.

G1-OH (1.00 g, 1.00 equivs, 3.12 mmol) was dissolved in 80 ml dry benzene in a 3-necked, 250 ml round bottomed flask equipped with a magnetic stirrer, dropping funnel and reflux condenser under a blanket of dry nitrogen. To this was added anhydrous pyridine (1.97 g, 8.00 equivs, 24.96 mmol, 2.01 ml) and after 15 minutes the stirring solution was cooled to 0°C. Thionyl chloride (3.71 g, 10.00 equivs, 31.2 mmol, 2.26 ml) was then added dropwise with efficient stirring and after a further 5 minutes the ice bath removed and the reaction mixture allowed to warm to room temperature. It was then heated to gentle reflux for 24 hours. Thionyl chloride, pyridine and solvent were removed by vacuum distillation on a high vacuum line followed by distillation of dry benzene into and out of the flask twice to aziotropically remove any excess thionyl chloride. The residue was then partitioned between water and dichloromethane, and the aqueous layer was extracted with dichloromethane a further three times. The combined organic layers were dried over magnesium sulphate, filtered and evaporated to dryness. Purification was by flash chromatography eluting with dichloromethane followed by three recrystallisations from toluene / hexane (1 ml hexane added followed by

gentle heating and dropwise addition of toluene until the crude product had completely dissolved). The product was obtained as a light yellow solid in 62% yield.

^{1}H NMR (400MHz, $CDCl_3$, δ, ppm) 4.54 (s, 2H, *CH_2*Cl), 5.07 (s, 4H, Ar-*CH_2*O-Ar-CH_2Cl), 6.50 (s, 1H, Ar*H*), 6.68 (s, 2H, Ar*H*), 7.30-7.50 (m, 10H, Ar*H*).

Elemental analysis calculated for $C_{21}H_{19}ClO_2$: C, 74.44; H, 5.65; Cl, 10.46. Found: C, 73.75; H, 5.65; Cl, 10.59.

5.5.3 Synthesis of G-1 Frechét-type dendronised CTA (G1-DPCM)

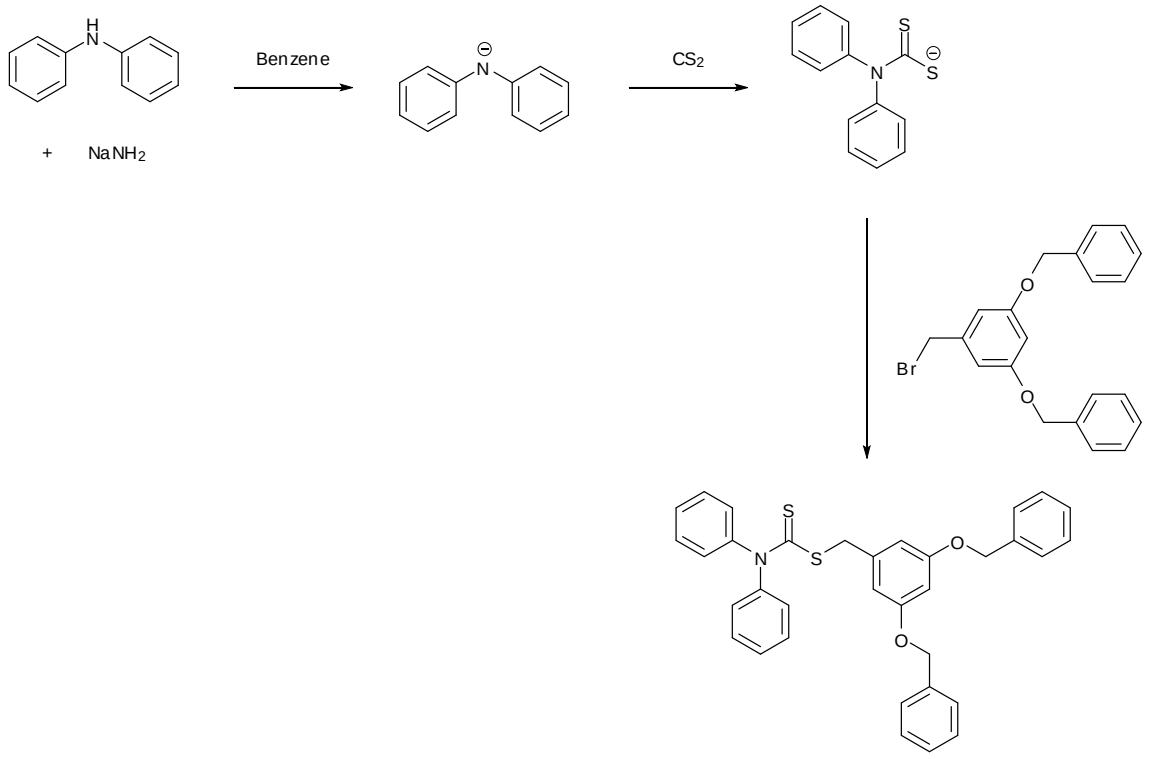

Figure 5.07. Reaction scheme for the synthesis of S-3,5-dibenzyloxybenzyl N,N-diphenyldithiocarbamate (G-1 DPCM).

95% sodium amide (0.0545 g, 1.00 equivs, 1.328 mmol) was suspended in 2.5 ml

benzene in a 3-necked, 100 ml round bottomed flask equipped with magnetic stirrer, dropping funnel and reflux condenser under a blanket of dry nitrogen. To this was added diphenylamine (0.2247 g, 1.00 equivs, 1.328 mmol) in 2.5 ml benzene and the mixture stirred overnight at room temperature. Carbon disulphide (0.1214 g, 1.20 equivs, 1.594 mmol) in 2.5 ml benzene was added followed by G1-Cl (0.4500 g, 1.00 equivs, 1.328 mmol) in 2.5 ml benzene which was slowly added dropwise to the stirring mixture. After a further 15 minutes the reaction mixture was heated to gentle reflux for 3.5 hours and then allowed to cool. The mixture was washed twice with water and then dried over magnesium sulphate. After filtration the solvent was removed by vacuum distillation on a high vacuum line. The product was obtained as a light yellow solid in 55% yield.

^{1}H NMR (400MHz, $CDCl_3$, δ, ppm) 4.44 (s, 2H, C(=S)SC*H*), 5.01 (s, 4H, Ar-*CH*$_2$O-Ar-), 6.51 (s, 1H, Ar*H*), 6.61 (s, 2H, Ar*H*), 7.30-7.44 (m, 20H, Ar*H*).

Elemental analysis calculated for $C_{34}H_{29}NO_2S_2$: C, 74.56; H, 5.34; N, 2.56; S, 11.71. Found: C, 73.82; H, 5.29; N, 2.51; S, 11.06.

5.5.4 RAFT polymerisation of N-vinyl pyrrolidone with G1-DPCM to give G1-PVP

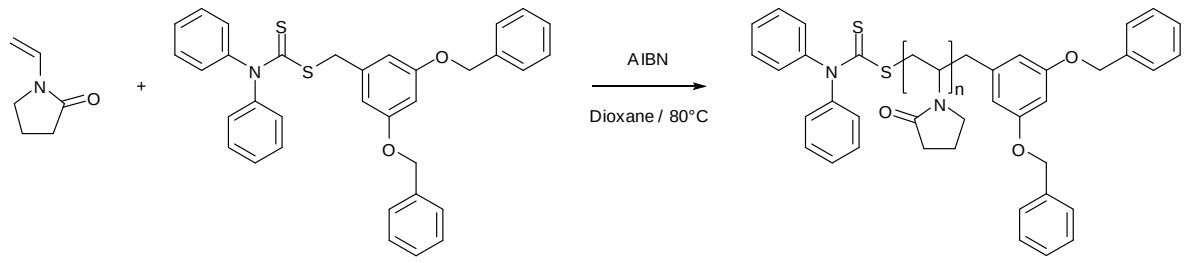

Figure 5.08. Reaction scheme for the RAFT polymerisation of N-vinyl pyrrolidone with S-3,5-dibenzyloxybenzyl N,N-diphenyldithiocarbamate (G-1 DPCM).

The polymerisation was carried out using *N*-vinyl pyrrolidone (1.00 ml, 1.045 g,

9.40 mmol), 1ml 1,4-dioxane and the appropriate amount of CTA (0.04844 g G1-DPCM, 0.088mmol) aiming for a polymer with M_n=10,000 g mol^{-1} calculated using equation 1.2 as previously discussed for styrene and *N*-vinyl pyrrolidone polymerisations.

A 1:8 molar ratio of AIBN:G1-DPCM was used, and the G1-DPCM and AIBN were placed in a schlenk tube containing a magnetic stirrer bar. 1.00 ml *N*-vinyl pyrrolidone was then transferred into the schlenk tube, along with 1 ml freshly distilled 1,4-dioxane and it was sealed by wiring a rubber septum onto the neck of the tube. The schlenk tube was then connected to a vacuum / nitrogen line and its contents subjected to several freeze-pump-thaw cycles until thoroughly degassed. The schlenk tube was then sealed under vacuum or flooded with nitrogen, and the reaction mixture heated to 80˚C in an oil bath with solid state temperature control and left for 33 hours with efficient stirring. After this time the polymerisation mixture was cooled, dissolved into a few ml dichloromethane and precipitated into diethyl ether (20 × volume excess of diethyl ether over the combined volumes of polymerisation mixture and dichloromethane) before being recovered by vacuum filtration. The polymer was then dried under vacuum and the final product was a white powder obtained in 42% yield. The polymer was analysed by SEC in order to determine the average molecular weight and its distribution, and ^{1}H NMR to verify the presence of the G-1 end group.

5.6 Di-functional and tri-functional fluorinated RAFT chain transfer agents

5.6.1 3-(perfluorooctyl)propyl bromide (PFP-Br)

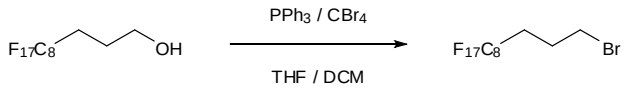

Figure 5.09. Reaction scheme for the synthesis of 3-(perfluorooctyl)propyl bromide (PFP-Br).

3-perfluorooctyl-1-propanol (75.00 g, 1.00 equivs, 0.1569 mol) and carbon tetrabromide (78.06 g, 1.50 equivs, 0.2354 mol) were dissolved in dry tetrahydrofuran / dichloromethane (40 ml / 80 ml respectively) in a 3-necked 500 ml round bottomed flask equipped with magnetic stirrer, dropping funnel and reflux condenser under a blanket of dry nitrogen. The reaction mixture was cooled to 0°C and triphenylphosphine (61.75 g, 1.50 equivs, 0.2354 mol) in dry tetrahydrofuran / dichloromethane (20 ml / 40 ml respectively) was added dropwise. The reaction mixture was then allowed to warm to room temperature and stirred for 20 hours at room temperature before being quenched with 5 ml water. Solvents were removed by rotary evaporation and the residue partitioned between dichloromethane and water. This was done in several batches in a 3 litre separating funnel and warming of the dichloromethane / water to 30-35°C was required to achieve full dissolution of the residue along with sonication in an ultrasound bath. Each organic layer was collected, washed a further two times with warm water and then all of the organic layers were combined before being dried over magnesium sulphate. After filtration solvent was removed from the filtrate by rotary evaporation and the product purified by vacuum distillation to afford PFP-Br as a colourless oil in 79% yield.[5]

^{1}H NMR (400MHz, $CDCl_3$, δ, ppm) 2.08-2.37 (m, 4H, $CH_2CH_2CH_2Br$), 3.48 (t, *J* 6.2 Hz, 2H, $CH_2CH_2CH_2Br$).

Elemental analysis calculated for $C_{11}H_6BrF_{17}$: C, 24.42; H, 1.12; Br, 14.77. Found: C, 24.21; H, 1.10; Br, 14.46.

5.6.2 3,5(di-3-(perfluorooctyl)propyloxy)benzyl alcohol (DPFPB-OH)

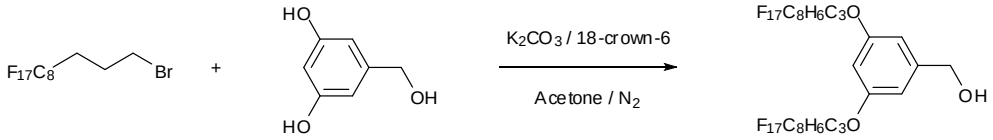

Figure 5.10. Reaction scheme for the synthesis of 3,5(di-3-(perfluorooctyl)propyloxy)benzyl alcohol (DPFPB-OH).

3,5-dihydroxybenzyl alcohol (5.52 g, 1.00 equivs, 39.4 mmol), potassium carbonate (13.80 g, 3.80 equivs, 100.2 mmol) and 18-crown-6 ether (2.10 g, 0.30 equivs, 7.94 mmol) was placed in a 3-necked 500 ml round bottomed flask equipped with magnetic stirrer, reflux condenser and a rubber septum under a blanket of dry nitrogen. PFP-Br (45.0 g, 2.11 equivs, 83.2 mmol) was then cannulated into the flask followed by 200 ml dry acetone. The reaction mixture was then heated to gentle reflux for 24 hours with efficient stirring. After being allowed to cool, solvent was removed by rotary evaporation and the residue was partitioned between ethyl acetate and water. This was done in several batches in a 3 litre separating funnel and warming of the ethyl acetate / water to ~50°C was required to achieve full dissolution of the residue along with sonication in an ultrasound bath. Each organic layer was collected, washed a further two times with warm water and then all of the organic layers were combined before being dried over magnesium sulphate. After filtration solvent was removed by rotary evaporation and the product recrystallised from ethyl acetate to afford DPFPB-OH as a white solid in 73% yield. [5]

^{1}H NMR (400MHz, $CDCl_3$, δ, ppm) 1.56 (s, 1H, -CH_2O*H*), 2.10 (m, 4H,

$CF_2CH_2\mathit{CH_2}CH_2O$), 2.31 (m, 4H, $CF_2\mathit{CH_2}CH_2CH_2O$), 4.03 (t, *J* 5.9 Hz, 4H, $CF_2CH_2CH_2\mathit{CH_2}O$), 4.64 (s, 2H, -$\mathit{CH_2}$OH), 6.37 (t, *J* 2.2 Hz, 1H, Ar*H*), 6.53 (d, *J* 2.3 Hz, 2H, Ar*H*).

Elemental analysis calculated for $C_{29}H_{18}F_{34}O_3$: C, 32.85; H, 1.71; F, 60.92. Found: C, 33.87; H, 1.87; F, 52.00.

5.6.3 3,5(di-3-(perfluorooctyl)propyloxy)benzyl bromide (DPFPB-Br)

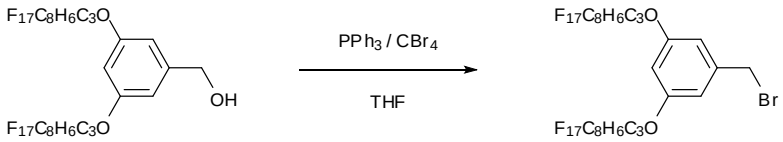

Figure 5.11. Reaction scheme for the synthesis of 3,5(di-3-(perfluorooctyl)propyloxy)benzyl bromide (DPFPB-Br).

DPFPB-OH (5.48 g, 1.00 equivs, 5.17 mmol) was dissolved in 50 ml dry tetrahydrofuran in a 2-necked 250 ml round bottomed flask equipped with magnetic stirrer and reflux condenser under a blanket of dry nitrogen. Carbon tetrabromide (3.43 g, 2.00 equivs, 10.34 mmol) was dissolved in a minimum amount of dry tetrahydrofuran and cannulated into the reaction flask. Triphenylphosphine (2.44 g, 1.80 equivs, 9.31 mmol) was added in four aliquots of 0.61 g over a 3 hour period by dissolution in a minimum amount of dry tetrahydrofuran and subsequent cannulation into the reaction vessel. The reaction was left for a further 3 hours with efficient stirring before being quenched with 5 ml water. Solvent was removed by rotary evaporation and the residue partitioned between dichloromethane and water. Warming of the dichloromethane / water to 30-35°C was required to achieve full dissolution of the residue along with sonication in an ultrasound bath. Each organic layer was collected, washed a further two times with warm water and then all of the organic layers were combined before being dried over magnesium

sulphate. After filtration solvent was removed by rotary evaporation and the product recrystallised from 4:1 ethyl acetate / methanol to give the final product as a light yellow solid in 84% yield. [5]

^{1}H NMR (400MHz, $CDCl_3$, δ, ppm) 1.98-2.09 (m, 4H, $CF_2CH_2\mathit{CH_2}CH_2O$), 2.15-2.22 (m, 4H, $CF_2\mathit{CH_2}CH_2CH_2O$), 3.95 (t, *J* 5.9 Hz, 4H, $CF_2CH_2CH_2\mathit{CH_2}O$), 4.36 (s, 2H, -$\mathit{CH_2}$Br), 6.41 (t, *J* 2.2 Hz, 1H, Ar*H*), 6.49 (d, *J* 2.2 Hz, 2H, Ar*H*).

Elemental analysis calculated for $C_{29}H_{17}BrF_{34}O_2$: C, 31.01; H, 1.53; Br, 7.11; F, 57.50. Found: C, 31.77; H, 1.48; Br, 3.67; F, 48.73.

5.6.4 Methyl-3,4,5(tri-3-(perfluorooctyl)propyloxy)benzoate (TPFPB-COOMe)

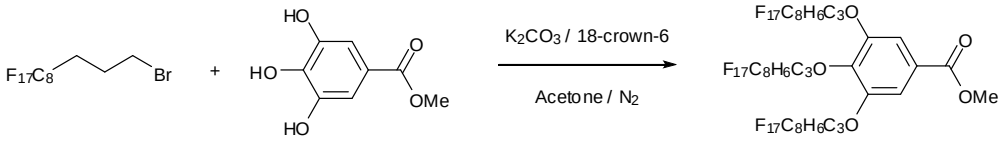

Figure 5.12. Reaction scheme for the synthesis of methyl-3,4,5(tri-3-(perfluorooctyl)propyloxy)benzoate (TPFPB-COOMe).

Methyl-3,4,5-trihydroxybenzoate (5.45 g, 1.00 equivs, 29.6 mmol), potassium carbonate (15.55 g, 3.80 equivs, 112.48 mmol) and 18-crown-6 ether (2.35 g, 0.30 equivs, 8.88 mmol) was placed in a 3-necked 500 ml round bottomed flask equipped with magnetic stirrer, reflux condenser and a rubber septum under a blanket of dry nitrogen. PFP-Br (50.29 g, 3.14 equivs, 93.0 mmol) was then cannulated into the flask followed by 150 ml dry acetone. The reaction mixture was then heated to gentle reflux for 24 hours with efficient stirring. After being allowed to cool to room temperature, solvent was removed by rotary evaporation and the residue was partitioned between ethyl acetate and water. This was done in several batches in a 3 litre separating funnel and warming of the ethyl acetate / water to ~50°C was required to achieve full dissolution of the residue along with

sonication in an ultrasound bath. Each organic layer was collected, washed a further two times with warm water and then all of the organic layers were combined before being dried over magnesium sulphate. After filtration solvent was removed by rotary evaporation and the product recrystallised from acetone to afford TPFPB-COOMe as a white solid in 91% yield. [5]

^{1}H NMR (400MHz, $CDCl_3$, δ, ppm) 2.01-2.10 (m, 2H, $CF_2CH_2\mathit{CH_2}CH_2O$), 2.10-2.20 (m, 4H, $CF_2CH_2\mathit{CH_2}CH_2O$), 2.26-2.45 (m, 6H, $CF_2\mathit{CH_2}CH_2CH_2O$), 3.92 (s, 3H, $C(=O)OCH_3$), 4.09 (t, *J* 5.9 Hz, 2H, $CF_2CH_2CH_2\mathit{CH_2}O$), 4.13 (t, *J* 5.8 Hz, 4H, $CF_2CH_2CH_2\mathit{CH_2}O$), 7.30 (s, 2H, Ar*H*).

Elemental analysis calculated for $C_{41}H_{23}F_{51}O_5$: C, 31.48; H, 1.48; F, 61.93. Found: C, 31.42; H, 1.34; F, 55.16.

5.6.5 3,4,5(tri-3-(perfluorooctyl)propyloxy)benzyl alcohol (TPFPB-OH)

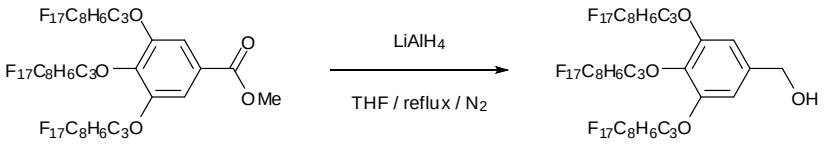

Figure 5.13. Reaction scheme for the synthesis of 3,4,5(tri-3-(perfluorooctyl)propyloxy)benzyl alcohol (TPFPB-OH).

Lithium aluminium hydride (1.54 g, 1.50 equivs, 40.56 mmol) was suspended in 90 ml dry tetrahydrofuran in a 3-necked 2 L round bottomed flask equipped with magnetic stirrer, 1 L dropping funnel and a reflux condenser under a blanket of dry nitrogen. TPFPB-COOMe (42.30 g, 1.00 equivs, 27.04 mmol) in 630 ml dry tetrahydrofuran was added dropwise and the reaction mixture then heated to gentle reflux for 12 hours. The reaction mixture was allowed to cool to room temperature before being quenched by the careful addition of 35 ml 1 M sodium hydroxide, and was then filtered. Solvent was removed by rotary evaporation and

the residue was then passed through a silica gel column using ethyl acetate as eluent. The product was then recrystallised from acetone to afford TPFPB-OH as a white solid in 86% yield. [5]

^{1}H NMR (400MHz, $CDCl_3$, δ, ppm) 1.66 (t, *J* 5.8 Hz, 1H, Ar-CH_2O*H*), 1.99-2.10 (m, 2H, CF_2CH_2*CH_2*CH_2O), 2.10-2.20 (m, 4H, CF_2CH_2*CH_2*CH_2O), 2.26-2.49 (m, 6H, CF_2*CH_2*CH_2CH_2O), 3.99 (t, *J* 5.9 Hz, 2H, $CF_2CH_2CH_2$*CH_2*O), 4.09 (t, *J* 5.9 Hz, 4H, $CF_2CH_2CH_2$*CH_2*O), 4.63 (d, *J* 5.7 Hz, 2H, Ar-*CH_2*OH), 6.60 (s, 2H, Ar*H*).

Elemental analysis calculated for $C_{40}H_{23}F_{51}O_4$: C, 31.27; H, 1.51; F, 63.06. Found: C, 31.18; H, 1.48; F, 51.76.

5.6.6 3,4,5(tri-3-(perfluorooctyl)propyloxy)benzyl bromide (TPFPB-Br)

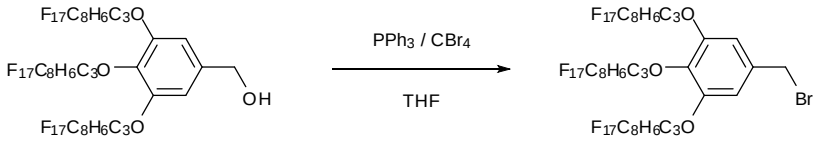

Figure 5.14. Reaction scheme for the synthesis of 3,4,5(tri-3-(perfluorooctyl)propyloxy)benzyl bromide (TPFPB-Br).

TPFPB-OH (36.42 g, 1.00 equivs, 23.70 mmol) was dissolved in 300 ml dry tetrahydrofuran in a 2-necked 1 L round bottomed flask equipped with magnetic stirrer and reflux condenser under a blanket of dry nitrogen. Carbon tetrabromide (15.72 g, 2.00 equivs, 47.40 mmol) was dissolved in a minimum amount of dry tetrahydrofuran and was then cannulated into the solution. Triphenylphosphine (12.43 g, 2.00 equivs, 47.40 mmol) was added in four aliquots of 3.11 g over a 3 hour period by dissolution in a minimum amount of dry tetrahydrofuran and subsequent cannulation into the reaction vessel. The reaction was left stirring overnight before being quenched with 10 ml water. Solvent was removed by rotary evaporation and the residue partitioned between dichloromethane and water. This

was done in several batches in a 3 litre separating funnel and warming of the dichloromethane / water to 30-35°C was required to achieve full dissolution of the residue along with sonication in an ultrasound bath. Each organic layer was collected, washed a further two times with warm water and then all of the organic layers were combined before being dried over magnesium sulphate. After filtration, solvent was removed from the filtrate by rotary evaporation and the product recrystallised from 4:1 ethyl acetate / methanol to give the final product as a white solid in 81% yield. [5]

^{1}H NMR (400MHz, $CDCl_3$, δ, ppm) 1.98-2.08 (m, 2H, $CF_2CH_2\mathit{CH_2}CH_2O$), 2.10-2.20 (m, 4H, $CF_2CH_2\mathit{CH_2}CH_2O$), 2.26-2.46 (m, 6H, $CF_2\mathit{CH_2}CH_2CH_2O$), 4.01 (t, *J* 5.8 Hz, 2H, $CF_2CH_2CH_2\mathit{CH_2}O$), 4.09 (t, *J* 5.8 Hz, 4H, $CF_2CH_2CH_2\mathit{CH_2}O$), 4.44 (s, 2H, Ar-$\mathit{CH_2}$Br), 6.63 (s, 2H, Ar*H*).

Elemental analysis calculated for $C_{40}H_{22}BrF_{51}O_3$: C, 30.04; H, 1.39; Br, 5.00; F, 60.58. Found: C, 30.28; H, 1.35; Br, 2.96; F, 59.41.

5.6.7 DPFPB-DPCM functionalised CTA

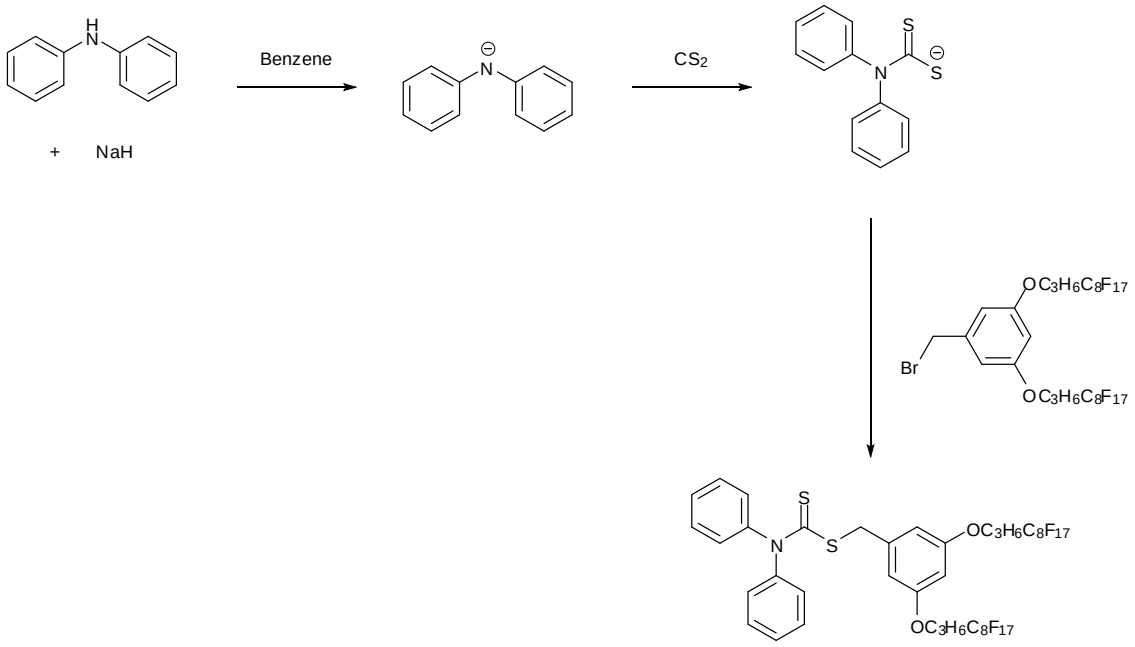

Figure 5.15. Reaction scheme for the synthesis of S-3,5(di-3-(perfluorooctyl)propyloxy)benzyl N,N-diphenyldithiocarbamate (DPFPB-DPCM).

Diphenylamine (0.7530 g, 1.00 equivs, 4.45 mmol) was placed in a 250 ml round bottomed flask, sealed and flushed with dry nitrogen. 25 ml anhydrous dimethyl sulfoxide and 12.5 ml dry tetrahydrofuran was cannulated into the flask and the solution was added by means of cannulation to a suspension of sodium hydride (0.1068 g, 1.00 equivs, 4.45 mmol) in a further 12.5 ml dry tetrahydrofuran at 0°C contained within a two-necked 500 ml round bottomed flask equipped with a magnetic stirrer, reflux condenser under a blanket of dry nitrogen. The mixture was stirred for 1.5 hours at 0°C to give a clear green solution. Carbon disulfide (0.4066 g, 1.20 equivs, 5.34 mmol, 322 µl) was then added to the solution at 0°C and the mixture stirred for a further 30 minutes to obtain an orange-yellow solution of the sodium salt of diphenyldithiocarbamate. DPFPB-Br (5.00 g, 1.00 equivs, 4.45 mmol) dissolved in a minimum amount of dry tetrahydrofuran under dry

nitrogen was then cannulated into the reaction mixture still at 0°C and then it was brought slowly up to room temperature and left to stir overnight under a blanket of dry nitrogen. The reaction mixture was then partitioned between diethyl ether and water and washed a further two times with water. The organic layer was collected, dried over magnesium sulphate, filtered and then evaporated to dryness. The residue was recrystallised several times from diethyl ether to obtain the pure product as a light yellow powder in 48% yield.

^{1}H NMR (400MHz, $CDCl_3$, δ, ppm) 2.04-2.16 (m, 4H, $CF_2CH_2\mathit{CH_2}CH_2O$), 2.22-2.41 (m, 4H, $CF_2\mathit{CH_2}CH_2CH_2O$), 4.00 (t, *J* 5.9 Hz, 4H, $CF_2CH_2CH_2\mathit{CH_2}O$), 4.44 (s, 2H, $CS(=S)C\mathit{H_2}$), 6.33 (t, *J* 2.3 Hz, 1H, Ar*H*), 6.52 (d, *J* 2.2 Hz, 2H, Ar*H*), 7.39-7.44 (m, 10H, Ar*H*).

Elemental analysis calculated for $C_{42}H_{27}F_{34}NO_2S_2$: C, 39.17; H, 2.11; N, 1.09; S, 4.98; F, 50.16. Found: C, 39.01; H, 2.00; N, 0.84; F, 40.18; S, 4.25; Br, 0.00.

5.6.8 TPFPB-DPCM functionalised CTA

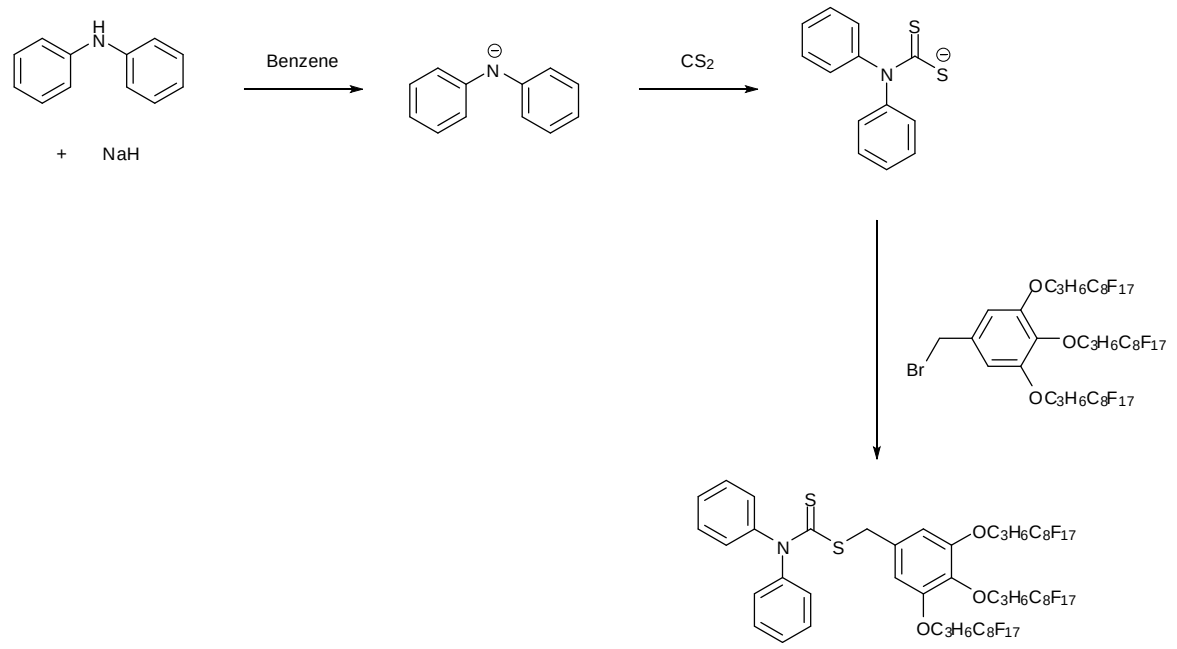

Figure 5.16. Reaction scheme for the synthesis of S-3,4,5(tri-3-(perfluorooctyl)propyloxy)benzyl N,N-diphenyldithiocarbamate (TPFPB-DPCM).

In the case of the TPFPB-DPCM, the exact same experimental procedure was followed as for DPFPB-DPCM, but using TPFPB-Br instead of DPFPB-Br.

^{1}H NMR (400MHz, $CDCl_3$, δ, ppm) 1.96-2.05 (m, 2H, $CF_2CH_2\mathit{CH_2}CH_2O$), 2.05-2.15 (m, 4H, $CF_2CH_2\mathit{CH_2}CH_2O$), 2.23-2.43 (m, 6H, $CF_2\mathit{CH_2}CH_2CH_2O$), 3.96 (t, *J* 5.9 Hz, 2H, $CF_2CH_2CH_2\mathit{CH_2}O$), 4.04 (t, *J* 5.9 Hz, 4H, $CF_2CH_2CH_2\mathit{CH_2}O$), 4.43 (s, 2H, $CS(=S)C\mathit{H_2}$), 6.58 (s, 2H, Ar*H*), 7.39-7.45 (m, 10H, Ar*H*).

Elemental analysis calculated for $C_{53}H_{32}F_{51}NO_3S_2$: C, 36.09; H, 1.83; F, 54.93; N, 0.79; S, 3.64. Found: C, 35.85; H, 1.72; N, 0.70; F, 44.97; S, 3.38; Br, 0.00.

5.7 Synthesis of low molecular weight PVP additives via the use of novel fluorinated CTAs

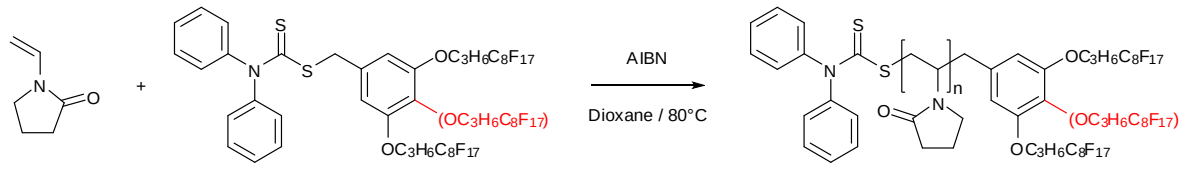

Figure 5.17. Reaction scheme for the RAFT polymerisation of N-vinyl pyrrolidone with DPFPB-DPCM and TPFPB-DPCM functionalised CTAs..

The exact same experimental procedure was used as for the RAFT polymerisation of NVP with G1-DPCM discussed earlier in this chapter, though with either of the novel fluorinated CTAs in place of G1-DPCM. The only slight variation was in the case of tri-functional polymerisations using TPFPB-DPCM, at target molecular weights of less than 10,000 g mol^{-1}. In these instances, increased amounts of CTA were used in order to make lower molecular weight polymers and this led to problems with solubility (CTA not completely dissolving in solvent), and up to 50% extra 1,4-dioxane was used in order to facilitate the complete dissolution of the CTA.

5.8 References

[1] Perrier, S.; Barner-Kowollik, C; Quinn, J. F.; Vana, P.; Davis, T. P.; *Macromolecules*, **2002**, *35*, 8300

[2] United States Patent Application 20060088487 <http://www.freepatentsonline.com/y2006/0088487.html> (15th Jan 2008)

[3] Bindu, R. L.; Borsali, R.; Devasia, R.; Gnanou, Y.; Mougin, N.; *Macromol. Symp.*, **2005**, *229*, 8

[4] Frechét, J. M. J.; Hawker, C. J.; *J. Am. Chem. Soc.*, **1990**, *112*, 7638

[5] Narrainen, A. P.; Hutchings, L. R.; Ansari, I.; Thompson, R. L.; Clarke, N.; *Macromolecules*, **2007**, *40*, 1969

Chapter 6
Concluding Remarks

6.1 Conclusions

Initial work was performed in order to gain experience with the reversible addition-fragmentation transfer (RAFT) polymerisation of *N*-vinyl pyrrolidone (NVP), using the chain transfer agent (CTA) *S*-malonyl *N,N*-diphenyldithiocarbamate (DPCM). The CTA was successfully synthesised and characterised, and used to make well defined polyvinyl pyrrolidone (PVP), the results of these RAFT polymerisations being directly comparable to those found in the literature.[1]

Following on from this work, several designs for novel, functionalised chain transfer agents suitable for the RAFT polymerisation of NVP were proposed, based upon the synthesis and structure of DPCM. The purpose of these proposed CTAs was to make well defined, end-functionalised PVP (the functionality being imparted by the CTA), with a view to incorporating end-groups containing low surface energy fluoroalkyl chains, so that these polymers could be used as efficient surface modifying additives when blended in small quantities with an unfunctionalised PVP matrix. First however, a novel first generation Frechét-type dendritic CTA (G1-DPCM, Figure 6.01) was successfully synthesised and characterised, serving as a valuable proof of concept before embarking upon the more time consuming and reasonably costly syntheses of proposed fluorinated CTAs. G1-DPCM was then successfully used to make well defined PVP bearing a first generation aryl-ether end group, via RAFT polymerisation. Results of these polymerisations were very similar to those successful RAFT polymerisations performed initially with DPCM.

Two fluorinated CTAs, the di-functional DPFPB-DPCM bearing two C_8F_{17} groups, and the tri-functional TPFPB-DPCM bearing three C_8F_{17} groups, were successfully synthesised and characterised (Figure 6.01). The synthesis of each of these materials was both technically challenging and time consuming, with most steps requiring completely anhydrous conditions and lengthy workups. These CTAs were used to perform RAFT polymerisations of NVP, and a wide range of molecular weights of both di-functional and tri-functional end-functionalised polymers were produced. Both CTAs exhibited good control over molecular

weight, though control over polydispersity was weaker than for DPCM, with polydispersity indices ranging from 1.2 to 1.6. Good degrees of end-functionalisation were achieved (typically around 80%) and these end-functionalised PVP additives were characterised by size exclusion chromatography (SEC) and ^{1}H NMR spectroscopy.

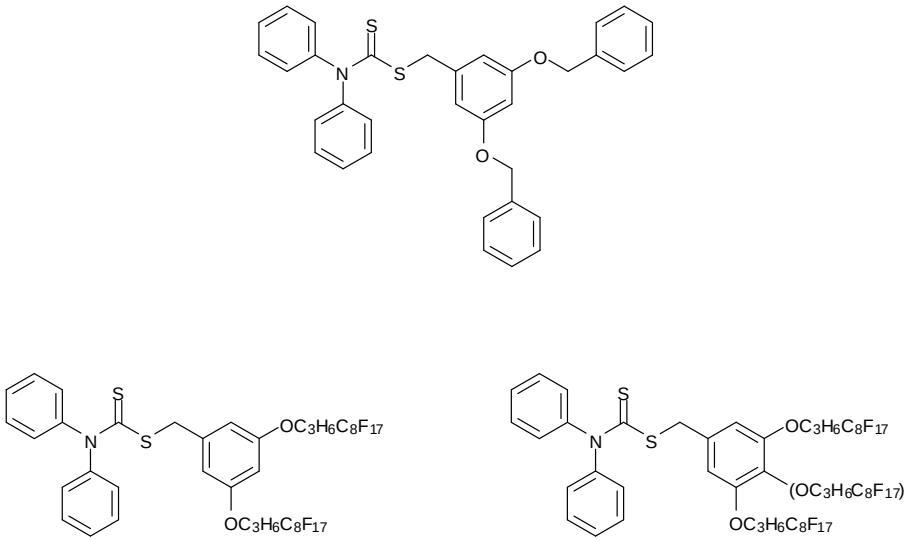

Figure 6.01. The three novel CTAs presented in this thesis: G1-DPCM (top), DPFPB-DPCM (bottom left) and TPFPB-DPCM (bottom right).

These end-functionalised PVP additives were blended with unfunctionalised PVP matrices in varying weight fractions, and spun into thin films. Contact angle measurements and ion beam analysis were then used to investigate the effects of additive concentration, additive molecular weight, matrix molecular weight, additive functionality and annealing.

First and foremost, it was successfully demonstrated that the presence of either di-functional or tri-functional PVP additive in any concentration led to a significant increase in observed contact angle at the solid-air interface, due to the spontaneous surface segregation of each additive, and the resulting fluorine

enrichment at the surface. Furthermore, it was clearly demonstrated that the surface concentration of additive increased steadily with overall additive concentration, up to a critical aggregation concentration (CAC). Upon reaching the CAC, further increases in additive concentration resulted in the spontaneous formation of aggregate structures within the polymer bulk, and no further increase in surface concentration was observed. These results were visualised predominantly with the use of contact angle measurements, and these were in good agreement with Rutherford backscattering analysis which was used to measure the concentration of fluorine atoms at the polymer surface for polymer blends containing varying weight fractions of di-functional additive.

It has also been demonstrated that additive molecular weight plays an important role in its ability to surface segregate, with lower molecular weights leading to significantly enhanced surface segregation, most notably at lower concentrations (below the CAC). Matrix molecular weight has been shown to have a far lesser effect in this regard, but the a measurable effect nonetheless, with higher molecular weight matrices leading to slightly enhanced surface segregation of additive at concentrations below that of the CAC.

Additive functionality, as expected, was shown to have a substantial effect upon surface segregation, with the tri-functional additive giving rise to significantly greater contact angles than its di-functional counterpart at all additive concentrations. The presence of a third C_8F_{17} group will further lower the surface energy of the additive thus increasing the thermodynamic drive for it to both surface segregate and form aggregates, but also leading to a greater lowering of surface energy per additive molecule than for its di-functional counterpart. The overall result is an increase in observed contact angle at all weight fractions in the case of the tri-functional additive, for example with 2.5% additive by weight, to 46° compared to the 4° observed in unfunctionalised PVP.

Finally, annealing of the polymer films was shown to have no beneficial effect in terms of surface segregation of additive. This is certainly in part due to the close proximity of the glass transition temperature of PVP, above which the films had to

be annealed, and the onset of thermal degradation of the polymer additive. This meant that the annealing temperature used in this work was confined to only 10°C above T_g, whereas in work with similar end groups attached to different polymers with higher T_gs where annealing has been shown to be of significant benefit, annealing temperatures of at least T_g + 40°C have been used.[2]

The possible effect of surface roughness and / or thermal degradation of the polymer films was investigated by atomic force microscopy (AFM) and thermogravimetric analysis (TGA) in order to explain the results obtained in the annealing study. It was found that there was little or no appreciable change in surface roughness upon annealing, and therefore this was unlikely to have any significant role in determining the observed contact angles. It is very probable that thermal degradation of the polymer additives was the cause of the results seen in the annealing study, though further work is needed in this area to reveal the precise mechanism by which this is occurring.

In addition to the thin film analysis discussed above, a brief preliminary study was conducted into the effects of incorporating these end-functionalised PVP additives into the gas diffusion layer (GDL) of a proton exchange membrane fuel cell (PEMFC). Low cost substrates (LCSs) were formulated by the application of an aqueous solution of graphite, fluoropolymer (PTFE or FEP), PVP and end-functionalised PVP additive, to a sheet of carbon fibre paper in order to cost effectively approximate the composition of a GDL. These LCSs were then subjected to simulated PEMFC operating conditions and their performance was measured in terms of water uptake and durability (tensile strength). It was found that the presence of additive had a generally beneficial effect by significantly reducing the water uptake of the LCSs, as well as making it more consistent over time – the results from the FEP-based samples were particularly promising, especially with higher concentrations of additive (20% weight fraction of overall PVP component). It is however our hypothesis that the presence of the fluoropolymer component of the formulation changes the role of the end-functionalised additive from that of a surface modifying additive. We are of the opinion that the beneficial effects seen in this case, typically at higher

concentrations of additive, are in fact not due to its ability to surface segregate, but due to it acting as a surfactant, effectively compatibilising the PVP component and the fluoropolymer component of the LCS. The effects of each additive on durability were mixed, and while overall the results from this work were promising, more work needs to be done in this area to understand precisely how the additives are behaving in this more complex system.

6.2 References

[1] Bindu, R. L.; Borsali, R.; Devasia, R.; Gnanou, Y.; Mougin, N.; *Macromol. Symp.*, **2005**, *229*, 8

[2] Hutchings, L. R.; Norazilawati, M. S.; Thompson, R. L.; *Polym. Chem.*, **2011**, *2*, 851